STUDIA

UNIVERSITATIS BABEŞ-BOLYAI

CHEMIA

2

1986

CLUJ-NAPOCA

ANUL XXXI 1986

STUDIA
UNIVERSITATIS BABEŞ-BOLYAI

CHEMIA

2

Redacţia: 3400 CLUJ-NAPOCA, str. M. Kogălniceanu, 1 ● Telefon 1 61 01

SUMAR — CONTENTS — SOMMAIRE — INHALT

STUDIA UNIV. BABEŞ—BOLYAI, CHEMIA, XXXI, 2, 1986

POLAROGRAPHIC STUDY ON THE PROTONIZATION OF 1,2-CYCLOHEXANEDIONE DIOXIME IN AQUEOUS SOLUTIONS

FERENC MÁNOK*, GABRIELLA DÉNEZSI* and CSABA VÁRHELYI*

Received: August 26, 1985

ABSTRACT. — The polarographic behaviour of 1,2-cyclohexanedione dioxime (nyoxime) has been studied in a wide pH-range (1.81—11.88) in Britton-Robinson's buffer solutions. One or two waves, in fuction of the pH-value, appear on the polarograms, the first one having a kinetic character. The rate constant of the recombination process between protons and neutral nyoxime molecule was calculated.

Introduction. The polarographic study of some weak mono-and dicarboxylic acids shows that in their polarograms two waves appear, and their relative heights vary with the pH value of the aqueous solutions [1—4]. One can presume that this phenomenon is due to the protonization of the above mentioned compounds as function of the acidity of the solutions. An analogous process takes place, probably, in the case of monoximes and dioximes either, which can be considered as very weak mono- and dibazic acids, respectively.

This peaper deals with the polarographic behaviour of the well known alycyclic α — dioxime, 1,2 — cyclohexanedione dioxime („nyoxime") in aqueous solutions, in a wide pH-range.

Results and Discussion. The polarograms of the nyoxime were taken in Britton-Robinson's buffer solutions (pH = 1.81 — 11.98). The constant ionnic strength of the solutions was ensured with sodium perchlorate. In the above experimental conditions there appear no maxima on the polarograms and that is why the use of tensioactive substances in the basis solutions was not necessary. The results of the polarographic measurements are presented in Table 1.

Some typical polarograms are presented in Figs. 1—5.

As shown in acid media only a single step appears.

At higher pH-values another wave can also be observed.

With increasing the pH-values the height of the first wave diminishes and that of the second one increases. As shown from the current intensity - pH - curves (Fig. 6.) the heights of the I and II waves become equal at pH = 6.1.

The half wave potentials of both waves are influenced from the acidity of the solutions. Their values shift towards more negative values with increasing the pH values up to pH = 8.0. Over this pH the $E_{1/2}$ — values remain unchanged.

* *University of Cluj-Napoca, Faculty of Chemical Technology, 3400 Cluj-Napoca, Romania*

Table 1

Polarographic data on nyoxime in aqueous solutions (Variation of the heights of the I and II waves with the pH value of the solutions)

pH	Wave I		Wave II	
	$-E_{1/2}$ (V)	$I_D(\mu A)$	$-E_{1/2}$ (V)	$I_D(\mu A)$
1.81	0,77	3.06	—	—
2.56	0.79	3.06	—	—
3.29	0,86	3.06	—	—
4.10	0.98	3.06	—	—
5.02	1.03	2.97	1.46	0.80
5.70	1.04	2.37	1.46	1.30
6.09	1.05	1.60	1.48	1.60
6.80	1.07	0.92	1.49	2.00
7.24	1.07	0.71	1.51	2.16
7.96	1.12	0.51	1.54	2.45
8.36	1.12	0.42	1.54	2.55
8.69	1.12	0.35	1.54	2.65
8.95	1.12	0.31	1.54	2.67
9.15	1.12	0.30	1.54	2.70
9.91	1.12	0.18	1.57	2.79
10.88	—	—	1.57	2.79
11.98	—	—	1.61	2.79

($E_{1/2}$ = half wave potential, I_D = diffusion current)

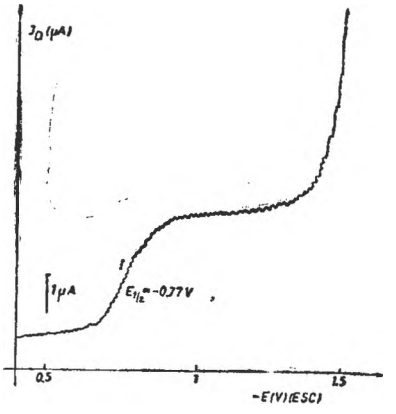

Fig. 1. Polarogram of nyoxime at pH = 1.81
[Niox. H_2] = 4×10^{-4} mole/l,
[$NaClO_4$] = 0.05 mole/l

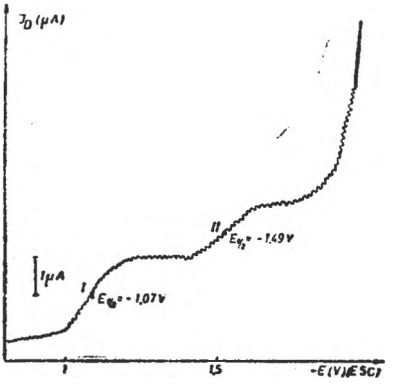

Fig. 2. Polarogram of nyoxime at pH = 6,80

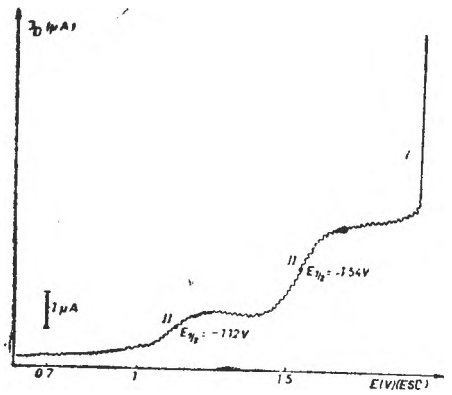

Fig. 3. Polarogram of nyoxime at pH = 7.96

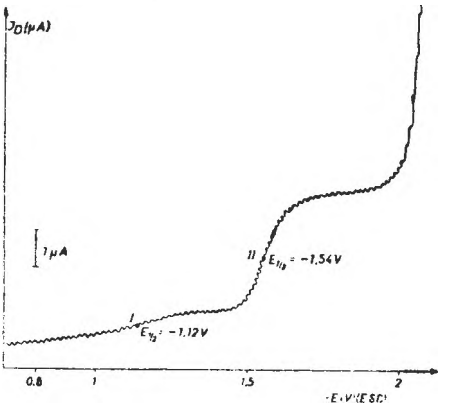

Fig. 4. Polarogram of nyoxime at pH = 8.95

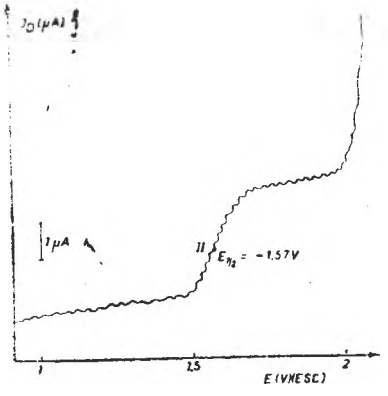

Fig. 5. Polarogram of nyoxime at pH = 9.91

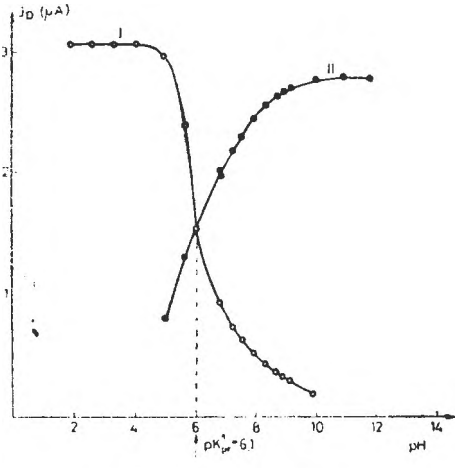

Fig. 6. I —pH diagram

The pH-value, where the heights of the first and second waves are equal, allows us to draw the conclusion, that the first step is not due to the reduction of the neutral nyoxime molecule. Otherwise the intersection of the I_D-pH curves should appear at much higher pH-values, at least at the value numerically equal to the first acidity constant of the nyoxime ($pK_a = 10.70$).

One can presume, then, that the first polarographic step corresponds to the reduction of the protonated form to nyoxime: Niox. H_3^+ and the second one to the „neutral", non dissociated nyoxime: Niox. H_2, the nyoximate anion: Niox. H^- being a polarographically inactive substance in the studied pH-range.

The first wave contains a kinetic component, which also appears at pH-values where the protonated form of the dioxime exists only in an insignificant amount. We must presume that in the solution the following equilibrium is valid :

$$\text{Niox.H}_3^+ \underset{k_r}{\overset{k_d}{\rightleftarrows}} \text{H}^+ + \text{Niox.H}_2 \tag{1}$$

where k_d is the rate constant of dissociation and k_r — the rate constant of recombination.

The caracteristic constant of the dissociation is

$$K_{dis} = \frac{[\text{H}^+][\text{Niox} \cdot H_2]}{[\text{Niox} \cdot \text{H}_3^+]} = \frac{k_d}{k_r} \tag{2}$$

The reduction of the protonated molecules perturbs this equilibrium in the vicinity of the electrode. Simultaneously, the recombination of these molecules also takes place. When the value of the rate constant of the recombination reaction is small, the heights of the polarographic waves correspond to the equilibrium concentrations of the protonated and neutral forms of the nyoxime, viz. both currents are pure diffusion currents. In this case the pH-value by equal wave heights corresponds to the real value of the dissociation constant exponent (pk_{dis}).

When the rate constant of the recombination reaction is high, two polarographis steps appear. The decrease of the more positive wave can be observed at much higher pH-values than the pk_{dis} value, and thus the nyoxime is present in the solution practically as neutral molecules. In this case the part of the current corresponding to the diffusion of the protonated molecules can be neglected and the whole current is determined by the recombination rate of the protonated molecules from the neutral nyoxime ones.

The dependence of the heights of the waves on the pH, by more positive or more negative potential values, can be written as follows:

$$\text{pH} = pk'_{dis} - \log \frac{I_{pos}}{I_{neg}} \tag{3}$$

where pk'_{dis} is the exponent of the polarographically apparent dissociation constant, I_{pos} and I_{neg} limiting current intensities of the protonated and non-protonated forms of the nyoxime. This value can be determined experimentally by measuring the pH-value at which $I_{pos} = I_{neg}$ (see the intersection of curves I and II, Fig. 6.).

Using these experimental values, the rate constant of the recombination of Niox. H_3^+ from the neutral nyoxime molecules and protons can be calculated by means of the Koutecky's relation [5] :

$$k_r = \frac{1}{t} \frac{51}{} \times 10^{(2pK' - pK)} \tag{4}$$

where t is the dropping time of mercury (in our experimental conditions: 0.35 s). On the basis of the determined pk_{dis} and pk'_{dis} values one obtains the following expression

$$k_r = \frac{1 \cdot 51}{0 \cdot 35} \times 10^{(2 \times 6.1 - 0.85)} = 9 \cdot 6 \times 10^{11}$$

This value is in agreement with those obtained for different mono- and dibazic acids.

Conclusion. On the polarograms of the nyoxime, taken in a wide pH-range (1.81—11.88) one or two waves appear as function of the pH-value, the first one having a kinetic character. The rate constant of the recombination process: $\text{Niox.H}_2 + \text{H}^+ \rightleftarrows \text{Niox. H}_3^+$ was calculated from the experimental data ($k_r = 9 \cdot 6 \times 10^{11}$).

REFERENCES

1. M. S. Wheatley, *Experientia*, **12**, 339 (1956).
2. V. Hanus, R. Brdicka, *Chem. Listy*, **44**, 291 (1950).
3. A. Ryvolova, V. Hanus, *Coll. Czech. Chem. Commun.*, **21**, 853 (1956).
4. J. Kuta, *Coll. Czech. Chem. Commun.*, **21**, 697 (1956).
5. J. Koutecky, R. Brdicka, *Coll. Czech. Chem. Commun.*, **18**, 597, 711 (1953).
6. F. Mánok, E. Kőszegi, Cs. Várhelyi, *Acta Chim. Hung.*, **116**, 51 (1984).

STUDIA UNIV. BABEŞ—BOLYAI, CHEMIA, XXXI, 2, 1986

BIOLOGICALLY ACTIVE METAL CHELATES

I. Bismuth Complexes with Pyridinic Ligands

MARIA JITARU* and GHEORGHE MARCU*

Received: October 12, 1986

ABSTRACT. — $[BiI_4]$ (HL) type complexes, with L = pyridine and -- picoline, were synthetised. Spectrophotometric, conductometric and potentiometric data, obtained in 0,1 M $NaClO_4$ solution, indicate the formation of the complexes corresponding to the ratio Bi : L = 2 : 1. It is assumed that the hexabismuthyl polycation takes up 3 molecules of L with maintenance of its octahedral structure. The complexes isolated in solid state and the solutions of the complexes at pH=7 were tested with respect to their biological activity against the EHRLICH ascinthic tumour. They were found to be active in the incipient stage of the tumour.

The chemotherapy of cancer was in practice starting from the twenties, but it came to be a success in the last quarter of this century [1—3]. The chemical treatment of cancer [4] rises problems concerning administration as well as some side efects. Some of these drugs have an increased activity when presented as metallic complexes [5—8].

Because certain types of cancer are associated with viruses, probably an anticancer medicine is an antiviral agent, though the other way round may not be true [9]. Taking into account the relation virus — cancer using metallic chelates [7], two ways occur:

— the alteration of the virus by metal complexation of its protheic parts;

— the liberation of a ligand with citostatic action in the immediate vicinity of the tumour, the metallic ion thus becoming free so as to tie itself to the virus.

To realize this, certain conditions must be imposed:

— the metallic ion must not be completely free in order not to complex with other non-viral positions which exist in the organism;

— the stability of the complex combinations used must not be too great in order to make it possible the liberation of the metal for complexation in the organism and of the ligand near the tumour;

— the kinetic stability of the coordinative compounds [10—11] must allow for realization of the coordinative links with donor atoms belonging to the virus.

By taking into account the above considerations complex compounds of some bioelements with different ligands were prepared and tested [12—16] with respect to their biological activity.

As a continuation of our previous studies [15—16] in the present paper an attempt is made to obtain and characterize some co-ordination compounds

* *University of Cluj-Napoca, Faculty of Chemical Technology, 3400 Cluj-Napoca, Romania*

of bismuth with pyridine (Py) and picoline (γ - Pic). The antiseptic action of bismuth as well as the presence of the pyridinic nucleus in numerous natural products and vitamins — B_6 — is an argument for the study of the biological activity of these compounds [17]. As far as preparation is concerned, the papers dealing with Bi-Py and Bi-γPic are outdated [18—21] and the formulas attributed to the complexes by the authors, generally, prove that no pure compounds were obtained.

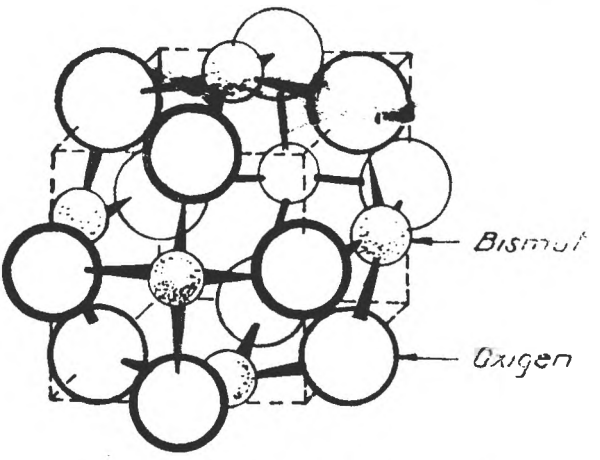

Fig. 1 Structure of $[Bi_6(OH)_{12}]^{6+}$, (23)

Since bismuth is not a typical complex generator, the psychochemical studies in both solid state and solutions are few, most of them deal with the nature of the hydrolized bismuth species co-existing in solution [22]. At a pH = 0—2 the hexabismuthyllic polycation $[Bi_6(OH)_{12}]^{6+}$ is the predominant species — log $\beta_{12,6} = 0.33$, where $\beta_{12,6}$ stands for the stability constant of the polycation and has an octahedral structure [23] having the ions of Bi situated on the sides of a cube and the OH^- on the middle of the edges (Fig. 1).

By taking into account Hume's criteria [24], Ketelar's relation [25] was chosen for the determination of the stability constant:

$$\frac{L}{d[A] - \varepsilon_A} = \frac{1}{k(\varepsilon - \varepsilon_A)[D]} + \frac{1}{\varepsilon - \varepsilon_A} \tag{1}$$

where: k = equilibrium constant for the formation of a complex; L = thickness of the layer; ε, ε_A = the molar extinction coefficients of the complex and of the acceptor, respectively; $[D]$, $[A]$ = concentration of the donor and of the acceptor, respectively; d = opticaly density.

Under the conditions in which the absorption of the hydrolized bismuth species can be neglected Eq.(1) is reduced to Hildebrand's relation:

$$\frac{L[A]}{d} = \frac{1}{K\varepsilon[D]} + \frac{1}{\varepsilon} \tag{2}$$

In order to derive the molar extinction coefficient — $\Delta\varepsilon$ and the stability constant — K — the McCconnel-Davidson method was used [26,27]:

$$\frac{[A][B]}{\Delta A_s} = \frac{[A] + [B]}{\Delta\varepsilon} + \frac{1}{\beta \cdot \Delta\varepsilon} \tag{3}$$

in which: $[A]$, $[B]$ = concentration of the metal ion and of the ligand, respectively; ΔA_s = absorption of the complex obtained by substracting the absor-

bance of the other species ; β = overall stability constant ; $\Delta\varepsilon$ = molar extinction coefficient of the complex.

Experimental. Synthesis of the complexes $[BiI_4]$ (HL) where L = C_5H_5N and C_6H_7N. To acid solutions of tetraiodbismuthate (pH = 1.5) excess ligand was added, drop by drop, under stirring to avoid resinification. The red coloured precipitate formed was filtered off after 24 hours, by washed water and dried by alcohol and ether.

Analysis : bismuth was determined by atomic absorption, halogene potentiometrically and L by elementary organic analysis (Table 1).

Table 1

Composition of the bismuth complexes

The complex	Molecular mass	%Bi		%I		% N		%C	
		theo-retic	experim.	theo-retic.	experim.	theo-retic.	experim.	theo-retic.	expe-rim.
$[BiI_4](Hpy)$	769.69	26.23	26.68 26.42	63.71	63.15 63.60	1.759	1.73 1.70	7.52	7.56 7.62
$[BiI_4](H\gamma pic)$	811.71	25.74	25.82 25.87	62.53	62.64 62.43	1.720	1.72 1.72	8.87	8.91 8.89

The study of the complexes in solution was carried out at a constant ionic strength ($NaClO_4$ 0.1 M) by means of spectrophotometric, conductometric and pH-metric methods. The choice of $NaClO_4$ as an electrolyte ensuring the constant ionic strenghth is suitable, among others, because in $NaClO_4$ the stability constant values are close to those obtained in NaCl solutions, izotonic with blood.

Since in the 240 – 265 nm spectral region where the absorption band of the complexes is situated, the ligands exhibit an important adsorbtion, ligand solutions of the same concentration were used as reference. Both systems exhibit an izosbestic point (see Fig. 2).

In the concentrations range comprised between 10^{-3} and 10^{-4} M the Lambert-Beerlaw is obeyed. Spectrophotometric measurements, visualized in Fig. 3, have been performed at the wavelength corresponding to the absorption maximum of the complex, viz. at λ = 245 nm in the case of BiPy complex and λ = 249 nm with the Bi – γ – Pic one.

In both systems $BiOClO_4$-Py and $BiOClO_4$ – γ – Pic the molar ratio method points to a combination ratio Bi : L = 2 : 1 (Fig. 3). The corrected curves 3 (for Py) and 3' (for Pic) were obtained by subtracting the absorbance of the hydrolized bismuth – curve 2 – point by poin from the experimental curves 1 and 1', respectively.

The method was applied at different wave lengths and at different bismuth concentration and in all cases the same combination ratio was found (Fig. 4). At the potentiometric titration of a $5 \cdot 10^{-4}$ M $BiOClO_4$ solution with a $5 \cdot 10^{-3}$ M ligand solution, pH was measured by means of a Radiometer type glass-electrode, by using a Radelkis OP – 208 digital pH-meter. The inflexion point of the potentiometric titration curves – 1 for Py and 1' for γ Pic – as well as the intersection of the two liniar portions of the conductometric titration curves 2 and 2' indicate the same combi-

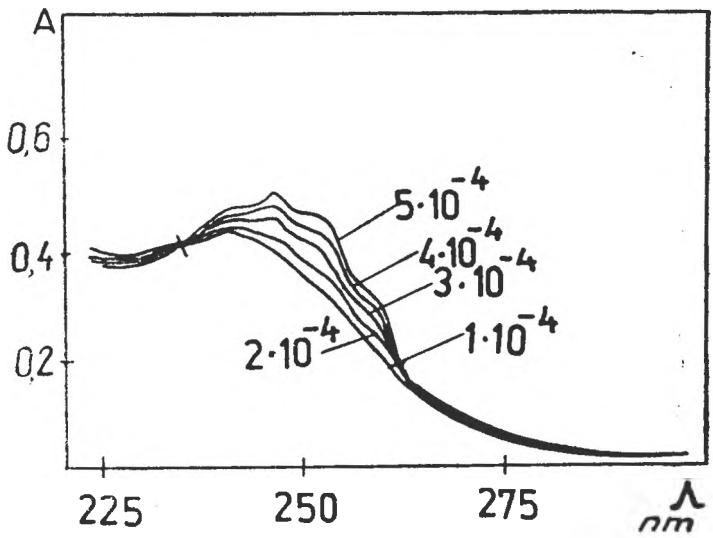

Fig. 2. Absorption curves for the complex $BiOClO_4$: Py $c_{BiOClO_4} = 5 \cdot 10^{-3}$ M, $c_{Py} = 10^{-2}$ M, ref. Py, 10^{-2} M

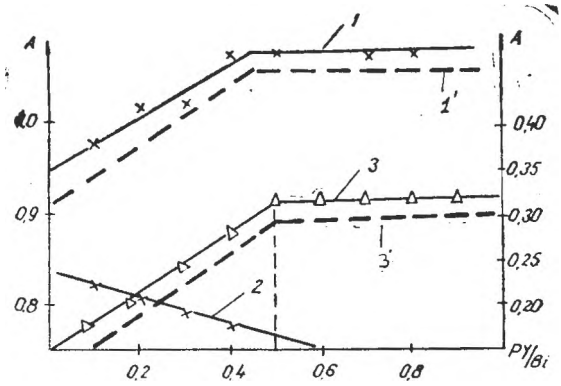

Fig. 3 The molar ratio method in the system $BiOClO_4$: Py, curves 1 and 3 $BiOClO_4$: Pic, curves 1', and 3'; $c_{BiOClO_4} = 10^{-3}$ M absorption cell of 1 cm

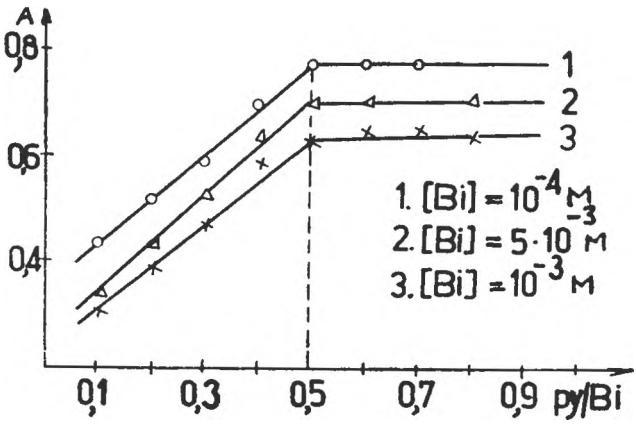

Fig. 4 The determination of the combination ratio for different concentrations of the hydrolized bismuth ion

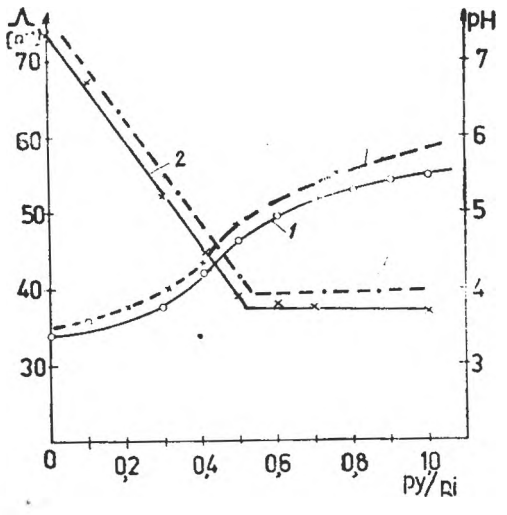

Fig. 5 Potentiometric and conductometric determination of the composition of the complexes.

nation ratio Py : Bi = 0,5 (Fig. 5). The influence of the pH on the formation and stability of the complexs Bi—I, has also been studied, since it can provide information concerning the structure, and it might be important from a biological point of view, due to the variations of the pH in the living organism. It was proved that at lower pH's, when the Bi is found entirely under the form Bi^{3+}, the formation of the complexes does not occur because the coordination capacity of the ligand to the metal ion is competed by the high concentration of the hidrogen ions. Application of Hildebrand's (Eq. (2)) and McConnel's (Eq. (3)) methods leads to the molar extinction coefifficient and stability constant values presented in Table 2. These values may be considered only as a first approach since the calculation methods used do not take into account all the equilibria occuring in the studied solutions.

Table 2

Stability constants and molar extinction coefficients of complexes III and IV

Complex	HILDEBRAND method		Mc CONNEL - DAVIDSON method	
	$K \times 10^{-2}$	$\varepsilon \times 10^{-4}$	$\beta \times 10^{-2}$	$\varepsilon \times 10^{-4}$
III — $[Bi_6(OH)_{12}py_3]^{6+}$	2.02	2.2	2.27	2.03
IV — $[Bi_6(OH)_{12}Ypic_3]^{6+}$	2.68	1.98	2.97	2.12

Interpretation of the Results. The relatively great values of the stability constants are in agreement with the observation that the presence of the ligand prevents the precipitation of the basic bismuthyl salts even at pH = 6. The molar extinction coefficients of the order of 10^4 are between the limits that characterize the charge transfer complexes, just as considered at the calculation of the stability constant by Hildebrand's method. The values obtained for the molar extinction coefficient suggest the idea that the complex generator central ion might be the hexabismuthyllic polycation whose molar extinction coefficient has a similar value. The $[Bi_6(OH)_{12}]^{6+}$ polycation can be assumed to be the most important molecular species at pH = 7.

That is in agreement with literature data [22] concerning the nature of hydrolized Bi species at pH = 5—7. X-ray diffraction patterns obtained by means of the solid isolated complex point to the maintenance of the octahedral structure of the hexabismuthyllic polycation. The organic elementary analysis

of the same complex is consistent with co-ordination of three ligand molecules by the hexabismuthyllic polycation. The very close molar extinction coefficient values suggest the idea that the basic structure of the polycation is not modified by the co-ordination of the pyridine.

Summing up the valence shell electrons and by taking into account the bonds in the polycation, it could be inferred that the ligand can be linked to the bismuth only after the breaking up of certain Bi-Bi bonds. The hexabismuthyllic polycation has 54 pairs of valence shell electrons ($N = 6 \cdot 4 + 12 \cdot 6 + 12 \cdot 8 = 108$) which occupy 30 bonding MO's, (Bi), (o), (H) and the others are distributed on non-bonding MO's of higher energy. Since the number of non-bonding M's already occupied is high enough, occupation of further non-bonding molecular orbitals by the ligand unshared electrons is highly improbable. These theoretical arguments plead for the keeping of the structure of hexabismuthyllic polycation in the complexes with pyridinic ligands at pH = 6 — 6,8. According to the above conclusions we can figure out a mechanism for the formation of the complex $[Bi_6(OH)_{12}L_3]^{6+}$ through the structure of the hexabismuthyllic polycation (Fig. 1). To maintain the polycationic frame formed out of the 6 bismuth ions, it is possible to break up at most Bi-Bi links (full lines — Fig.6). Thus, co-ordination possibilities appear for the ligand, consequently, theoretically the maximum number of ligand molecules attached to the hexabismuthyllic polycation is 3. This is in agreement with the combination ratio found above. The breaking up of the

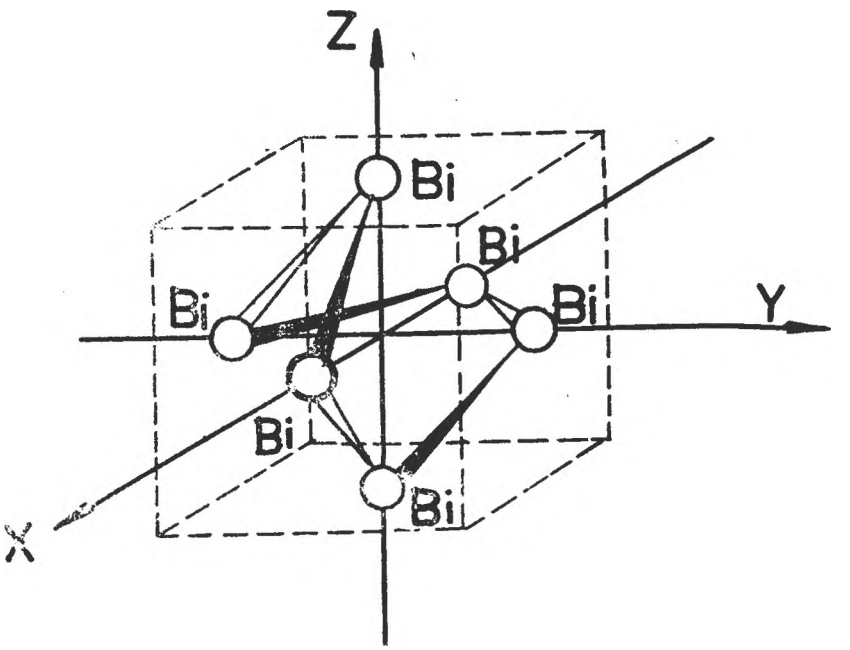

Fig. 6 The way of formation of the complex $[Bi_6(OH)_{12}L_3]^{3+}$ from the hexabismuthylic polycation

other Bi-Bi links would lead to the destruction of the polycationic frame and to the appearance of other hydrolized bismuth species.

Testing of the Biological Activity of the Complexes. Many complex compounds with antitumour activity produce a filamenting of the Escherichia coli bacillus, Brussels stem [28].

That is why the synthesized bismuth complexes as well as the solutions containing the corresponding compleses at a neutral pH were filament tested. Thus we obtained a first indication regarding the probability of an antitumour activity (Table 3). Due to the reduced solubility of the solid isolated complexes, it was necessary to disperse them in sunflower oil. The aqueous solutions of the complexes and the stable sunflower oil suspensions were inoculated subcutaneously and interperitonealy to mice previously inoculated with EHRLICH's ascithic tumour and were completely resorbed.

Table 3

Results of the filamenting test for E coli bacillus

Complex	Filamenting Test	
	026/6 Stem	Brussels Stem
$[BiI_4]$ (Hpy)	+	irrelevant
$[BiI_4]$ (Hγpic)	++	+
$[Bi_6(OH)_{12}py_3]^{6+}$	++	irrelevant
$[Bi_6(OH)_{12}\gamma pic_3]$	++	+

The evolution of the guinea pigs was surveyed in comparison with the control lot inoculated only with tumour, as well as the controls inoculated with tumour and cis- $Pt(II)(NH_3)_2Cl_2$ (Table 4).

Table 4

Results of the antitumour test

Testing conditions	Inoculation day				Nr. of mice		% healing
	EHRLICH	cis-$[Pt(NH_3)_2Cl_2]$	Complex of Bi: Sort of the complex	Complex of Bi: Day	initially	after 30 days without tumour	
EHRLICH tumour intraperitoneally	1	–	–	–	5	0	–
EHRLICH tumour subcutaneously	1	–	–	–	4	0	–
EHRLICH tumour +cis-$Pt(NH_3)_2Cl_2$	1	2	–	–	5	3	60
EHRLICH tumour	1	–	$[BiI_4](Hpy)$	2	5	1	20
intraperitoneally	1	–	$[BiI_4](H\gamma pic)$	2	5	1	20
plus bismuth	1	–	$[Bi_6(OH)_{12}py_3]^{6+}$	2	5	1	20
complexes	1	–	$[Bi_6(OH)_{12}\gamma pic_3)^{6+}$	2	5	2	40
Non-inoculated witnesses	–	–	–	–	4	4	–

The performed biological test proved that the complex solutions at a neutral pH as well as the solid isolated complexes are not inactive as to the EHRLICH ascithic tumour. We emphasize that the healing percentage is an

approximate, relative number, due primarily to the reduced number of guinea pigs and then to the one-sided testing on one type of tumour. It is necessary to test these complexes on a greater number of animals and other types of tumours.

REFERENCES

1. P. A. Platiner, *Chemotherapy of Cancer*, Elsevier, Amsterdam, 1964, p. 235
2. *Proc. 6-th National Conference*, Denver, Colorado, 1968, Lippincott Co., Philadelphia, Pa., 1970
3. L. F. L=arionov, *Chimioterapia tumorilor maligne*, Ed. Medicală, Bucureşti, 1963, p. 183
4. E. Ciorănescu, *Medicamente de sinteză*, Ed. Tehnică, Bucureşti, 1963, cap. XXIV
5. J. Schubert, *Sci. Amer.*, **214,** (5), 40 (1966)
6. A. Albert, Austr. J. Sci., **30,** (1) (1967)
7. S. Kirschner, Y. K. Wei, D. Francis, J. C. Bergman, J. Med. Chem., **9,** 369 (1966)
8. S. E. Livingstone, J. D. Nolan, A. E. Mihchelson, Inorg. Chem., **7,** 1447 (1968); **9,** 2545 (1970)
9. K. Reuss, C. Saiko, Chem. Ztg., **72,** 432 (1972)
10. J. P. Candlin, K. A. Taylor, D. T. Thomson, *Reactions of Transitions Metal Complexes*, Elsevier, Amsterdam, 1968, p. 257.
11. F. Basolo, R. G. Pearson, *Mechanisms of Inorganic Reactions*, Wiley, New York, 1958, p. 355
12. S. Kirschner, C. Drăgulescu, Ana Maurer, V. Topciu, N. Csaki, Rev. Chem. (Buc), **30,** (4), 321 (1979); **30,** (5), 428 (1979)
13. C. Drăgulescu, Maria Mracec, Z. Simon, Ana Maurer, Septimia Policec, V. Topciu, N. Csaki, Bul. st. şi tehn. Inst. Polith. „Traian Vuia", 1980
14. C. Drăgulescu, I. Havlik, Ana Maurer, Septimia Policec, V. Topciu, N. Csaki, Farmacia, (Buc), **28,** (3), 187 (1980)
15. C. Drăgulescu, Maria Jitaru, I. Havlik, Ana Maurer, Septimia Policec, V. Topciu, N. Csaki, Farmacia, (Buc), **29,** (4), 215 (1981)
16. Septimia Policec, R. Vasiliev, Ana Maurer, Maria Mracec, Maria Jitaru, V. Topciu, N. Csaki, Timişoara Medicală, **26,** (3), 29 (1981)
17. D. R. Williams, Chem. Reviews, **72,** (3), 203 (1972)
18. O. Hanser, L. Vanino, Ber., **33,** 2271 (1900)
19. L. Vanino, O. Hanser, Ber. **35,** 663 (1902)
20. A. Ch. Vournazos, Z. Anorg. Chem., **150,** 147 (1926)
21. J. J. Dick, Ana Maurer, Studii şi cerc. Şt. Chim., Baza de Cerc. Şt. Timişoara, **13,** 671 (1965)
22. A. Olin, Acta Chem. Scand., **11,** 1445 (1957); **13,** 1791 (1959)
23. H. A. Lewy, M. D. Danford, P. A. Agren, L. Chem. Phys., **31,** 1458 (1959)
24. D. N. Hume, L. Newman, J. Amer. Chem. Soc., **17, 4571 (1957)**
25. J. D. Bartlenson, R. E. Burk, H. P. Lankelman, J. Amer. Chem. Soc., **68,** 2513 (1976)
26. Mc Connel, D. Davidson, J. Amer. Chem. Soc., **72,** 3164 (1950)
27. F. J. C. Rossotti, H. Rossotti, *The Determination of Stability Constants*, Mc. Graw-Hill, 1961, p. 277
28. B. Rosemberg, L. Van Camp, Th. Krigas, Nature, **205,** 698 (1965)

STUDIA UNIV. BABEŞ—BOLYAI, CHEMIA, XXXI, 2, 1986

HETEROGEN KATALYSIERTE ZERSETZUNG ORGANISCHER HYDROPEROXIDE

III.[1] Die Zersetzung des 3,4,5-Trimethyl-Cumol-Hydroperoxide im diskontinuierlichen Reaktor[2]

LIVIU CORMOŞ*

Eingegangen am 19 November 1985

ABSTRACT. — **Decomposition of Organic Hydroperoxides in the Heterogeneous Catalysis.** *III. Decomposition of 3,4,5-Trimethyl-Cumene-Hydroperoxide in Discontinuous Reactor.* By oxidation of 3, 4, 5-trimethyl-cumene in aqueous emulsion, a new organic hydroperoxide was obtained. The yield of trimethyl-phenol obtained by decomposition of this hydroperoxide on alumino-silicate synthetics as catalyst was better than by its decomposition in H_2SO_4. The parameters of the oxidation process and the influence of the chemical composition of the catalyst in this reaction were studied.

Die Oxydation von Alkyl-Isopropylbenzolen ist von besenderem Interesse, da die entsprechenden Hydroperoxide erhalten werden, welche als Polimerisierunsinitiatoren verwendet werden, oder sich ähnlich wie Cumol-hydroperoxid zersetzen können, wobei sich Azeton und Alkyl-phenole bilden.

Sehr viele organische Hydroperoxide sind unstabil, zersetzen sich leicht, vor allem thermisch, und können nicht durch Destillation konzentriert werden [1]. Das Cumol-hydroperoxid ist bekanntlich ausreichen stabil, so dass es industriell hergestellt, konzentriert und gelagert werden kann Von dieser Tatsache ausgehend haben wir angenommen, dass die Alkyl-Isopropyl-benzene eine ähnliche Stabilität aufweisen.

In der vorliegenden Arbeit haben wir uns vorgehommen das 3, 4, 5-Trimethyl-Cumol-hydroperoxid herzustellen und in heterogener Katalyse in Azeton und 3, 4, 5-Trimethylphenol zu zersetzen.

Die stattfinden Reaktionen sind folgende:

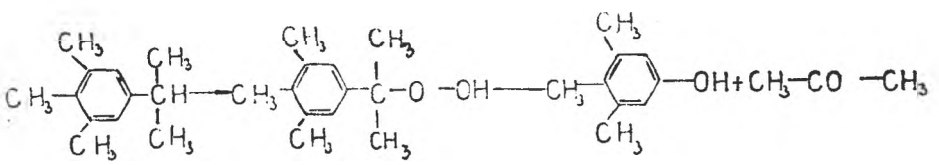

[1] Anmerking II, L. Cormos, A. Pop und V. Sbera, *Rev. Roumaine chim., 19*, 1631 (1974)

[2] Referat, vogetragen bei der Mitteilunskonferenz der Lehrkräfte und Forscher, Universitätsphase, Cluj-Napoca, 2 – 3 Nov. 1984

* *Universität Cluj-Napoca, Facultät für Chemie, 3400 Cluj-Napoca, Rumänia*

Das 3, 4, 5-Trimethyl-Cumol-hydroperoxid ist ein Hydroperoxid, in der Fachliteratur noch unbekannt [2]. Die Herstellung in dieser Weise von 3, 4, 5-Trimethylphenol ist eine neue Herstellungsmethode dieses Phenols [3].

Experimenteller Teil. Für die Oxidation wurde Trimethyl-Isopropylbenzen verwendet, das vorher durch Destillation gereinigt wurde. Es wurde die Fraktion, die im Intervall 222—223° destilliert, aufgefangen, da der in der Literatur angegebene Siedepunkt sich bei 221—223,5°C befindet [4].

Die Oxidation wurde in einer in die Literatur [5] beschriebenen Instalation duschgeführt.

Als Oxidationsmittel wurde Luft und auch reiner Sauerstoff verwendet. Die Oxidation wird in Wässriger Emulaion durchgeführt, wobei man 0,5—1 g Na_2CO_3 als Katalysator und 0,05—0,1 g Natriumstearat als Emulgator benützt. Es wurde mit 50 ml Kohlenwasserstoff und 25—100 ml distilliertes Wasser-proben gearbeitet. Die Reaktionsmasse wird bis zur gewünschten Temperatur mit Hilfe eines Thermostats, in welches der Reaktor immersiert wird, erwärmt, dann wird Luft oder Sauerstoff durchgeperlt.

Der Oxidationsprozess wurde verfolgt, indem man von Zeit zu Zeit Proben nahm und das gebildete Hydroperoxid durch die Jodometriemethode [6]. Während der ersten Versuche wurde Luft als Oxidationsmittel benützt, aber die geringe Umwandlung hat uns veranlasst die Luft durch reinen Sauerstoff zu ersetzen. In Abb.1 sind die Ergebnisse der Oxidation bei 90°C mit Luft (Kurve 2) un mit Sauerstoff (Kurve 1) dargestellt. Der Durchfluss des Oxidationsmittels ist 9,7 l/h.

Aus der Abb. 2 ist ersichtlich, dass bei der Oxidation mit Luft nach 5—6 Stunden eine Umwandlung zu 0,5—0,6 mol/l Hydroperoxid stattfindet. In derselben Zeitspenne erhält man bei Oxidation durch

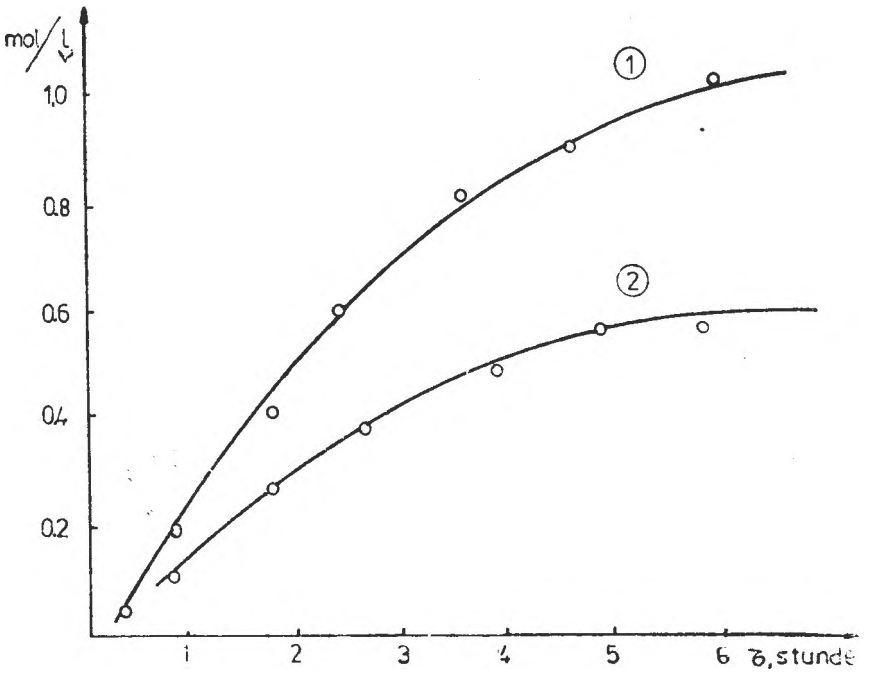

A b b. 1. Die Oxidation von Trimethylcumol bei 90°C und 9,7 l/h Durchflussmenge. Kurve 1 —Oxidation mit Sauerstoff, Kurve 2 — Oxidation mit Luft.

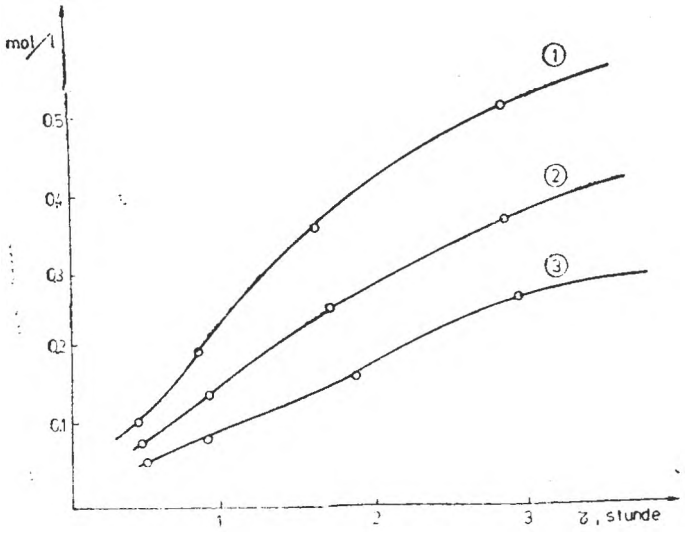

Abb. 2. Der Einfluss der Sauerstoffdurchflussmenge auf die Oxidation. Kurve 1 — 9,7 l/h, Kurve 2 — 7,68 l/h, Kurve 3—5,82 l/h.

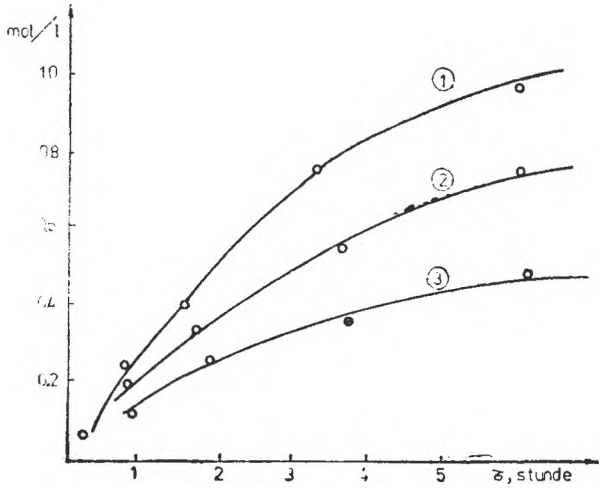

Abb. 3. Der Einfluss der Temperatur auf den Oxidationsprozess. Kurve 1 — 90°C, Kurve 2—80°C, Kurve 3 — 70°C.

Sauerstoff Umwandlungen bis zu 1 mol/l. Diesse Feststellung führte uns dazu, in allen folgenden Versuchen nur noch Sauerstoff zu verwerden.

Der Einfluss der Durchflussmenge des Oxidationsmittels auf die Oxidation ist in Abb. 2 dargestellt.

Man bemerkt, dass ein Wachstum der Sauerstoffdurchflussmenge ein Steigen der Hydroperoxidierunsgeschwindigkeit zur Folge hat.

Es wurde auch der Einfluss der Temperatur auf den Oxidationsprozess verfolt. In Abb. 3 ist ersichtlich, dass bei grosseren Temperaturen die Hydroperoxidkonzentration im Reaktionsgemisch steigt.

Das bei der Oxidation erhaltene Reaktionsgemisch bingt man in einen Scheidetrichter in dem sich die organische Schicht, die das Hydroperoxid und den unoxidierten Kohlenwasserstoff enthält, abtrennt. Durch Vakuumdestillation, kann man das gebildete Hydroperoxid isolieren Um ein reines Hydroperoxid zu erhalten, behandelt man die orga-. nische Phase mit NaOH-Lösumg Man erhält das Natriumsalz des Hydroperoxids [7], welches dann mit CO_2 zersetzt wird.

Das so erhaltene Hydroperoxid wird zu Trimethylphenol und Azeton zersetzt. Dieses stellt eine neue Herstellungsmethode des oben genannten Phenols dar. Dier ersten Versuche wurden mit verdünnter Schwefelsäure durchgeführt. Es wurde ein Abfall der Ausbeute des Trimethylphenols, wegen der sauren Verharzung eines Reaktionspdrouktteils, beobachtet. Derselbe Fall wurde von uns auch an anderen Hydroperoxide beobachtet [8]. Aus diesem Grunde wurde Zuflucht zur heterogen katalysierten zersetzung genommen. Als Katalisatoren wurden synthetische Aluminosilikate benutzt, die durch Mischausfällung aus Kieselsäure und Aluminiumnitrat [9] erhalten werden. Der erhaltene Katalysator wird bei 420° und 580°C geglüht. Es wurde mit einer Kornzummensetzung von 0,08—0,1 mm gearbeitet. Die Zersetzung wurde in einem diskontinuier lichen Reaktor ausgeführt, mit Idealmischung, ausgestattet mit Innen-und Aussenkühlung, weil die Zersetzungsreaktion stark exotherm ist.

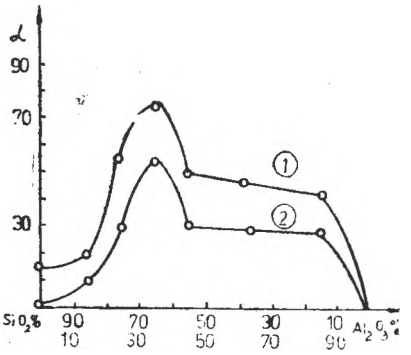

Abb. 4. Unwandlungsänderung der Zersetung des Hydroperoxids mir der chemischen Zusammensetzung des bei 420°C gelühten Katalysators. Kurve 1 — 40°C, Kurve 2 — 50°C.

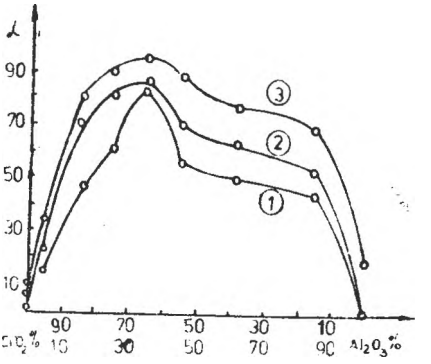

Abb. 5. Unwandlungsänderung der Zersetzung des Hydroperoxids in Funktion vond erchemischen Zusammensetung des bei 580°C geglühten Katalysators.

Es wurde mit verdünuten Hydroperoxidlösuungen gearbeitet, cca. 10% Hydroperoxid in Trimethylkumol, bei 30,40 und 50°C. Es wurde die Umwandlung des Hydroperoxids mit der chemischen Zusammensetzung des Katalysators verglichen. Die Etgebnisse sind in Abb. 4 für die bei 420°C geglühte und im Abb. 5 für die bei 580°C geglühten Systeme dargestellt.

Aus Abb. 4 und Abb. 5 ist ersichtlich, dass für ein und dasselbe katalytische System die Umwandlung mit der Zersetzungstemperatur wächst. Die Umwandlung, die nach derselben Reaktionsdauer, bei demselben Reagens/Katalysator Verhaltnis bestimmt wurde, wächst mit der Vergrösserung des Molvehältnisses Al_2O_3/SiO_2, bis dieses Verhälnis den Wert 1 : 3 erreicht, der einem Gehalt von 33—35% Al_2O_3 entspricht. Die Umwandlung verkleinert sich dann mit der Vergrösserung des Gehaltes a an Al_2O_3.

Aus der Reaktionsmasse nach der Zersetzung trennt man durch Destilation Azeton und Trimethylphenol. Die Ausbeute beträgt für Trimethylphenol 92%.

Schlussfolgerungen Es wurde durch die Oxidation in wässriger Emulsion ein neues organisches Hidroperoxid erhalten. Es wurde beobachtet, dass bei seiner Zersetzung im Idealmischungsreactor, auf synthetischem Aluminiumsilikatkatalysator, die Ausbeute fur Trimethyl-phenol grosser ist als bei der Zersetzung mit Schwefelsäure. Es wurden die Prozessparameter der Oxidation und der Einfluss der chemischen Zusammensetzung des Katalysators auf die Zersetzunsreaction untersucht.

LITERATUR

1. V. C. Toland und E. L. Nimer, Chem. Eng., **6**, 238 (1953)
2. L. Cormoş und A. Pop, *Pat. R.S.R.* nr. 73917, 21. II. 1980
3. L. Cormoş und A. Pop, *Pat. R.S.R.* nr. 70371, 13. III 1979
4. R. Raseev und S. Istrati, *„Physische Hauptkonstanten der Kohlenwaserstoffe"* vol. I., Ed. Tehnică, Bucureşti, 1964, p. 45
5. I. Vodnár, Rev. Chimie (Bucureşti), **20** (5), 291 (1969)
6. H. Hook und H. Kropf, Angew. Chem., **69**, 313 (1957)
7. B. D. Krujalov und B. I. Golovanenko, *„Gleichzeitige Herstellung des Phenols und Azeton"*, Ed. Tehnică, Moscova, 1963, p. 116
8. A. Pop und L. Cormoş, Studii şi Cercetări Chim., Acad. R.S.R., 20 (1), 95 (1972).
9. A. Pop, P. Köbl, L. Cormoş und Gh. Lengyel, Stud. Univ. Babeş-Bolyai, Chem., **12**, (2), 89 (1967)

STUDIA UNIV. BABEŞ—BOLYAI, CHEMIA, XXXI, 2, 1986

POLAROGRAPHIC STUDY OF HEXACHLORO- AND HEXABROMO-RHENATES (IV)[1]

FERENC MÁNOK*, ÁRPÁD CZÉGENI** and CSABA VÁRHELYI*

Received: 19 December, 1985

ABSTRACT. — The polarographic behaviour of $K_2[ReCl_6]$ in buffer solutions in a pH range of 2.56—9.68 and that of $K_2[ReBr_6]$ in neutral solutions has been studied. The appearance of a catalytic wave of rhenium was made evident. The nature of this wave was clarified. On the basis of this wave a sensible analytical method can be worked out for the determination of this metal.

Introduction. The various redox systems in solutions of perrhenates ($MReO_4$) were the subject of many investigations. During the reduction of ReO_4^- appear various oxidation forms of rhenium from Re^{6+} to Re^- (rhenid). The reduction at the dropping mercury electrode in various supporting electrolytes (mineral acids, neutral salts, e.g. KCl, $LaCl_3$) shows that the total reduction of ReO_4^- is a complicated eight electronic process [1,2]. Some oxidation states of this metal were also identified on the anodic polarograms of the Re^- (five anodic waves).

These complicated redox systems were also studied by coulometry, cyclic voltammetry using platinum electrodes and by means of amperometric titrations (with $K_2Cr_2O_7$) [3—5].

From the eight oxidation states of rhenium, besides the ReO_4^-, the Re^{4+} seems to be the most stable, especially in HCl and HBr media. Most of the polarographic waves of rhenium (as perrhenate) show a linear relationship between the height and the concentration of the mentioned ion and can be used for the determination of this rare element in various rocks, minerals, alloys and industrial products, using different supporting electrolytes, e.g. H_2SO_4 H_3PO_4, $HClO_4$, KCNS, EDTA, NaOH, ammonia, etc. [6—9].

The polarographic reduction of $K_2[ReCl_6]$ was studied only in neutral supporting electrolates (NaCl, $BaCl_2$, K_2SO_4). It was observed, that the half-wave potential value is not influenced by the nature of the anions present [in the supporting electrolyte.

On the other hand, the cations, exert influence on this potential value.

Results and Discussion. In the present paper the polarographic behaviour of $K_2[ReCl_6]$ and $K_2[ReBr_6]$ was studied in non buffered and buffered supporting electrolytes, respectively, in a pH range of 2.56—9.68. (Britton-Robinson buffer solutions with $NaClO_4$ for ensuring a constant ionic strength). The characteristics of the polarographic waves were determined in function of the

* *University of Cluj-Napoca, Faculty of Chemical Technology, 3400 Cluj-Napoca, Romania*
** *"Metalul Roşu" Enterprise, 3400 Cluj-Napoca, Romania*
[1] *Part of doctoral thesis*

pH-value and the concentration of the complexes. The results of these measurements are shown in Table 1.

Table 1

Polarographic data of the K_2ReCl_6 („A") and K_2ReBr_6) („B") complexes

Complex	Conc. $\times 10^{-4}$ mol/l	Supporting electrolyte	$E_{1/2}$			I_D			$I_D/C \times 10^4$		
			I	II	III	I	II	III	I	II	III
	1	"a"	0.15	0.57	—	0.12	0.24	—	—	0.24	
"A"	2	pH = 2.56				0.17	0.46	—	—	0.23	
	3					0.18	0.70	—	—	0.23	
	4					0.17	0.88	—	—	0.22	
	5					0.18	0.15	—	—	0.23	
	1	"a"	0.17	0.60	1.40	0.17	0.16	2.04		1.16	2.04
	2		0.22	0.34	4.10	0.22	0.34	4.10	—	0.17	2.05
"A"	3	pH = 3.29				0.22	0.51	6.18	—	0.17	2.06
	4					0.21	0.67	10.20	—	0.16	2.05
	5					0.21	0.85	—	—	0.17	—
	1	"a"	0.22	0.64	1.64	0.17	0.24	2.7	—	0.24	2.70
	2					0.23	0.46	5.5	—	0.23	2.75
	3	pH = 4.10				0.24	0.72	8.4	—	0.24	2.80
	4					0.23	0.96	10.3	—	0.24	2.75
	1	"a"	0.21	0.64	—	0.16	0.24	—	—	0.24	—
	2					0.22	0.46	—	—	0.23	—
"A"	3	pH = 7.24				0.21	0.72	—	—	0.24	—
	4					0.23	1.00	—	—	0.25	—
	5					0.23	1.00	—	—	0.25	
	1	"a"	0.18	0.62	—	0.15	0.24	—	—	0.24	—
	2					0.22	0.46	—	—	0.23	—
"A"	3	pH = 8.69				0.21	0.72	—	—	0.24	—
	4					0.23	1.00	—	—	0.25	—
	5					0.22	1.00	—	—	0.25	—
	2		0.20	0.61		0.15	0.24	—	—	0.27	—
"A"	4	"b"				0.22	0.52	—	—	0.26	—
	6					0.22	0.81	—	—	0.27	—
"A"	1	"c"	0.19	0.62	—	0.54	0.72	—	—	0.72	—
	1		0.92			1.70	—	—	—	—	—
"B"	2	"d"				2.0	—	—	—	—	—
	3					3.10	—	—	—	—	—

Supporting electrolyte: „a": 5 ml Britton-Robinson's buffer soln + 0.1 mol $NaClO_4$/50 ml
„b": 0.1 mol $NaClO_4$; „c": 0.1 mol $HClO_4$; „d": 0.1 mol KCl

Some characteristic polarograms are presented in Figs. 1—7.

Table 1 contains data referring to the concentrations, halfwave potentials, diffusion current intensities (I_d) and the linearity of the calibration curve.

In the case of $K_2[ReCl_6]$ appear two characteristic polarographic waves. Their $E_{1/2}$ values vary in function of the pH. The $E_{1/2}$ value of the first step between-0.15 and-0.22 V (vs. SCE) is not controlled by diffusion, because its height increases with the concentration of the complex only to a well determined value after this remaining constant. This bahaviour is characteristic for the adsorption waves. The above mentioned phenomenon appears in buffered solutions, as well as in acidic media, too (e.g. in 0.1 N $HClO_4$ solution).

The second wave presents $E_{1/2}$ value between -0.57 and and -0.64 V (vs. SCE) unaltered neither in acidic media (e.g. 0.1 n $HClO_4$). This means a signi-

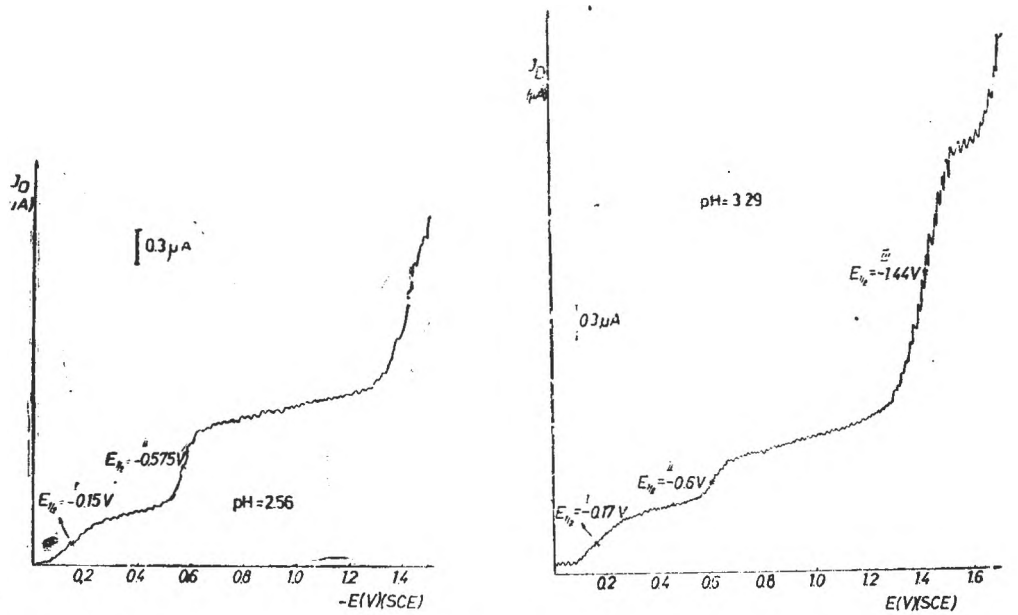

Fig. 1—2. Polarograms of $K_2[ReCl_6]$ at different pH-values in Britton—Robinson's buffer solutions

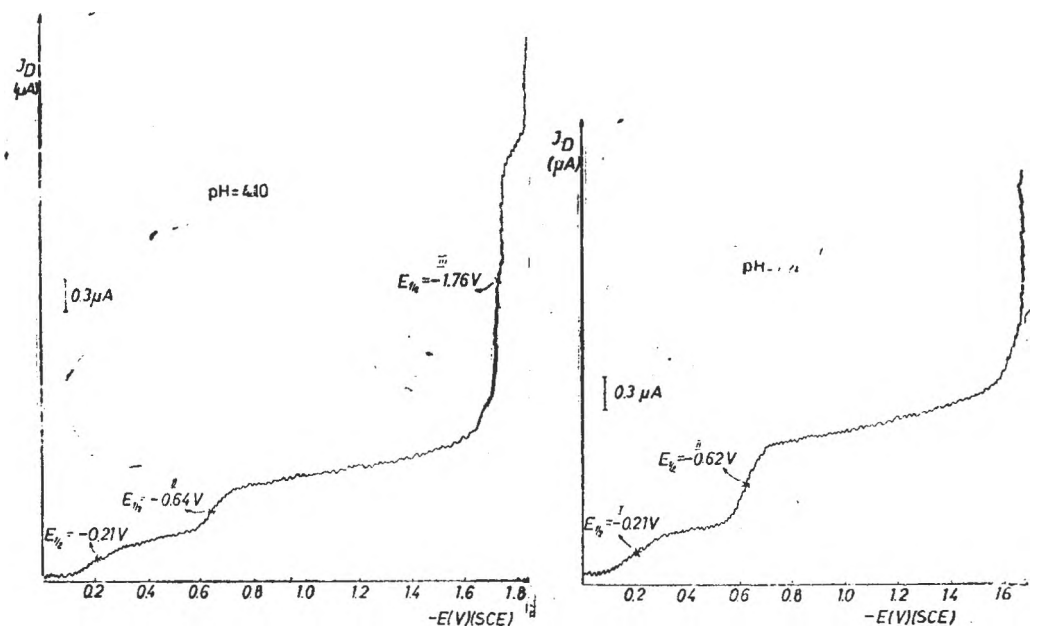

Fig. 3—4. Polarograms of $K_2[ReCl_6]$ at different pH-values in Britton—Robinson's buffer solutions

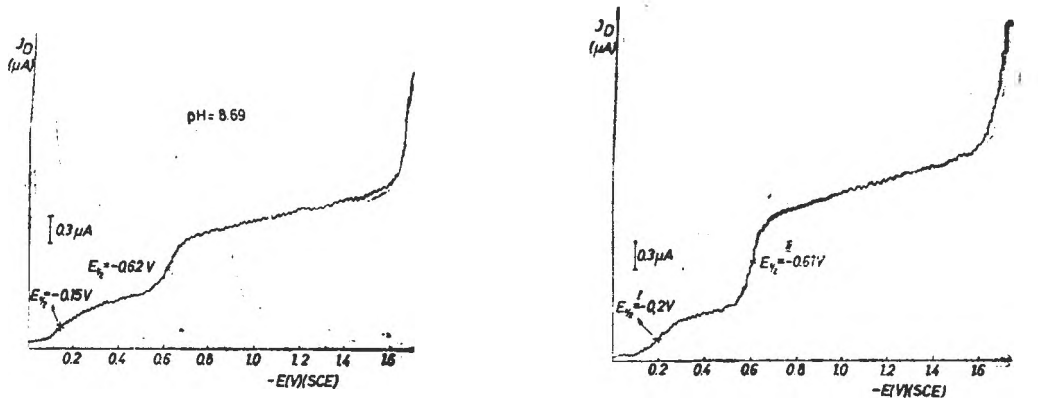

Fig. 5—6. Polarograms of $K_2[ReCl_6]$ at different pH-values in Britton—Robinson's buffer solutions

ficant inertness against substitution reactions of the $[ReCl_6]^{2-}$ in the inner coordination sphere.

The reduction of the hexachloro-complex at the dropping mercury electrode is a monoelectronic process:

$$[ReCl_6]^{2-} + e = [ReCl_6]^{3-}$$

It was observed, that in buffered solutions with pH-values: 3.29—4.10 appears a third, well formed wave ($E_{1/2} = -1.44$ V at pH = 3.29 and with $E_{1/2} = -1.64$ V at pH = 4.10, respectively.

The height of this wave is approximately 12 fold greater than that of a monoelectronic process. In order to clarify the nature of this wave the dependence of the limiting current from the head of the mercury was investigated. As shown in Fig. 8. the limiting current is independent of the head of the mercury.

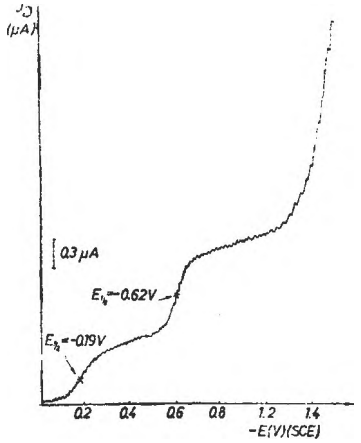

Fig. 7. Polarograms of $K_2[ReCl_6]$ at different pH-values in Britton—Robinson's buffer solutions

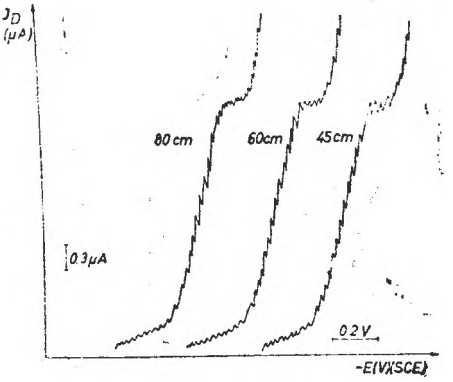

Fig. 8. The dependence of the limiting current from the head of the mercury in the case of $K_2[ReCl_6]$

This phenomenon is characteristic for catalytic currents. In this case the current can be expressed with following equation:

$$i_k = K \times h^0$$

(h^0 = height of the mercury head, K = a constant value)

On the basis of our experimental data, in agreement with earlier observations [8,9] for the explication of the nature of the catalytic wave, the following reaction scheme can be proposed:

At $E_{1/2}$ values: -1.44 V, and -1,64 V (vs. SCE) the Re(III) is reduced to Re(-1) according to the following scheme:

$Re(III) + 4e = Re(-I)$ (electrode process)

$Re(-I) + 2H^+ = Re(+I) + H_2$ (reaction in solution)

$Re(+I) + 2e = Re(-I)$ (electrode process)

The redox potential of the Re(III) — Re(—I) system is —0.23 V (vs. SCE allowing the reduction of the hydrogen ions. The catalytic wave is due to the reduction of the hydrogen ions. Since the height of the catalytic wave varies linearly with the concentration of the Re(IV), this can be the basis of a sensitive polarographic method for the determination of the above mentioned ion. The observed linearity on the calibration curve shows that these redox processes occur with a considerable rate.

The polarographic behaviour of the hexabromo-rhenate (IV) was studied in 0.1 NKCl solution. On the polarogram appears only a single step with a much more negative half wave potential, —0.92 V (vs. SCE), than that of $K_2[ReCl_6]$. This means, that the electrode process is irreversible.

The polarographic study of $K_2[ReBr_6]$ in various buffer solutions is difficult because of fast hydrolysis processes, especially at higher pH-values, when $ReO_2 \cdot nH_2O$ is precipitated.

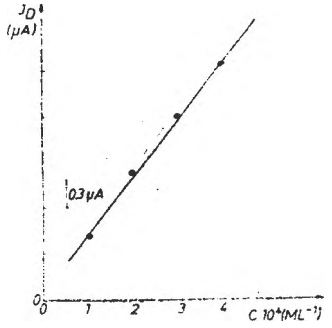

Fig. 9. Calibration curve for the catalytic wave of Re

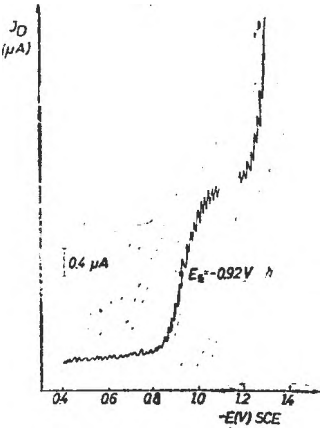

Fig. 10. Polarogram of $K_2[ReBr_6]$ in 0.1 N KCl

Experimental. $K_2[ReCl_6]$ was obtained from metallic Re with gaseous chlorine at aproximatelly 300°C in the presence of an excess (20—25%) of KCl, following the reaction:

$$Re + 2Cl_2 + 2KCl = K_2[ReCl_6]$$

The sublimed crude yellow-green product was recrystallized from warm 5% HCl.

$K_2[ReBr_6]$ was obtained by reduction of 1 g $KReO_4$ with 1—1.5 ml 50% hypophosphorous acid in the presence of 0.5 g KBr and 30—40 ml conc. HBr, by evaporation on a water bath. The separated redbrown crystalline product was filtered off, washed with 4 N HBr, acetone and ether.

The polarograms were recorded with a RADELKIS-type —OH—102 polarograph, with a TAST-Rapid —OH—9991 adapter, using a conventional polarographic cell. The oxygen was eliminated from the solutions with purified methane. The supporting electrolytes were Britton—Robinson beffers, containing $NaClO_4$ in order to ensure an ionic strength of 0.1 M.

REFERENCES

1. J. J. Lingane, *J. Amer. Chem. Soc.*, **64**, 1001, 2182 (1942).
2. C. L. Rulfs, P. J. Elving, *J. Amer. Chem. Soc.*, **73**, 3284 (1951).
3. A. Mann, C. Davidson, *J. Amer. Chem. Soc.*, **72**, 2254, 3509 (1950).
4. K. Györbiró, *Acta Chim. Acad. Sci. Hung.*, **27**, 120 (1961).
5. V. P. Spivakovskii, O. S. Dovgopol, *Zavodskaya Lab.*, **43**, 938 (1977).
6. T. Ya. Rubinskaya, M. A. Ryashentseva, V. I. Avaev, *Zhur. Analit. Khim.*, **30**, 183 (1975).
7. S. M. Basitova, R. D. Yurima, R. U. Vakholova, *Zhur. Analit. Khim.*, **34**, 935 (1979).
8. R. Geyer, *Z. anorg. Chem.*, **263**, 47 (1950).
9. Rakshit Subha, *Z. physik. Chem.* (Leipzig), **265**, 622 (1974).

STUDIA UNIV. BABEŞ—BOLYAI, CHEMIA, XXXI, 2, 1986

NEUE METALL(III)-AMIN-DERIVATE DER HEXAHALOGENO-SÄUREN DES PLATINS(IV)

CSABA VÁRHELYI* und ION GĂNESCU**

Eingegangen am 20 Dezember 1985

ABSTRACT. — New Metal(III)-Amine-Derivatives of Hexahalogeno-Acids of Platinum (IV). A number of 30 new complex salts of the hexahalogenoacids of platinum (IV): $H_2[PtCl_6]$, $H_2[PtBr_6]$ and $H_2[PtI_6]$ were obtained by double decomposition reactions with monoacido-pentamine $(Co(en)_2Cl(amine)]^{2+}$ and diacido-tetramine $([Co(amine)_4Y_2]^+$, $[Co(DH)_2(amine)_2]^+$ and $[Co(ec)(amine)_2]^+$; „en"-ethylenediamine, „DH_2"-dimethylglyoxime, „ec.H_2"-ethylenediimino-bis-acetylacetone) type cobalt (III)--amines. The products were characterized by chemical and thermal analysis.

Einleitung. Die $H_2[PtCl_6]$ — Säure und ihre Alkalisalze dienen als Ausgangssubstanzen für verschiedene Substitutionsreaktionen mit Halogenen, Pseudohalogenen (NCS^-, $NCSe^-$, N_3^-, NO_2^-) und mit neutralen Liganden, wie Amine, Phosphine, Arsine, usw. Diese Substitutionsreaktionen sind in einigen Fällen auch von Redoxprozessen ($Pt_{IV} \rightarrow Pt_{II}$ $Pt_{II} \rightarrow Pt°$) begleitet. Andere Hexahalogeno-süuren können leicht aus $H_2[PtCl_6]$ erhalten werden. Die Tendenz, komplexe Ionen mit Platin(IV) zu bilden nimmt vom Chlor nach Iod zu [1, 2].

Die $H_2[PtBr_6]$ wurde aus $H_2[PtCl_6]$ durch mehrmaliges Eindampfen mit HBr und Br_2-Mischung erhalten. $Na_2[PtI_6]$ entsteht aus der Hexachloro-säure durch Umsetzung mit überschüssiger NaI- Lösung. Diese zweibasischen, starken Komplexsäuren bilden neutrale Salze mit verschiedenen Aminen und Phosphinen ($(Amin.\ H)_2[PtX_6]$, $(Phosphin.H)_2[PtX_6]$), mit Metallen und verschiedenen Komplexbasen [3—5].

Ergebnisse und Diskussionen. Die energetischen Faktoren (Ionenpotentialwert, thermochemische Ionradien) der $[PtX_6]^{2-}$-Ionen begünstigen die Bildung von schwerlöslichen Komplexsalzen vom Typ AB, bzw. AB_2, insbesondere mit Metallaminkationen ohne hydrophyle Liganden(H_2O, OH^-, usw) mit thermochemischen Ionenradien: 2,4—2,8Å [6]. Einige Hexamine-, Monoacidopentamine und Diacidotetramine des Kobalts(III) [7,8], Chroms(III) [9, 10] und Rhodiums(III) [9, 11] sind zu diesem Zweck sehr geeignet.

In dieser Arbeit wurden 30 neue Hexahalogeno-platinate (IV) mit ein-, bzw. zweiwertigen Chelatkationen des Kobalts (III) erhalten und charakterisiert.

Die Monoacido-pentamine des Typs $[Co(en)_2X(Amin)]^{2+}$, welche, im allgemeinen, leicht lösliche Salze bilden, können aus wässrigen Lösungen mit $H_2[PtX_6]$ gefällt werden. Gut kristallisierende, charakteristische Salze bilden sich auch mit den Chelatkationen des Typs $[Co(Diox.H)_2(Amin)_2]^+$, bzw.

* *Universität Cluj-Napoca, Facultät für Chemie, 3400 Cluj-Napoca, Rümania*
** *Universität Craiova, 1100 Craiova, Rümania*

$[Co(ec)(Amin)_2]^+$ (Diox.H_2 = aliphatisches oder alycyclisches Dioximmolekül, ec. H_2 = Schiff'sche Base aus Äthylendiamin und Acetylaceton). Die erhaltenen neuen Salze sind in den Tab. 1—3 charakterisiert.

Tabelle 1

Neue Komplexsalze des Typs $[Co(Amin)_4X_2]_2$ $[PtCl_6]$

No.	Formel	Mol. Gew. ber.	Charakteristik	Analyse	Ber.	Gef.
1.	$[Co(DH)_2(NH_3)_2]_2 \cdot A$	1112,1	Goldgelbe, rhomb. Prismen	Co	10.60	10,43
				Pt	17,54	17,36
				N	15,10	15,02
				H_2O	4,85	4,70
2.	$[Co(DH)_2(m\text{-Xylidin})_2]_2 \cdot A$	1474,7	Gelbbraune hexagonale Prismen	Co	7,99	7,96
				Pt	13,23	13,09
				N	11,39	11,14
3.	$[Co(DH)_2(m\text{-Toluidin})_2]_2 \cdot A$	1418,5	Gelbbraune rhomb. Platten	Co	8,30	8,22
				Pt	13,75	13,68
				N	11,84	11,62
4.	$[Co(DH)_2(Thio)_2]_2 \cdot A$	1294,4	Goldgelbe, dünne Platten	Co	9,10	8,93
				Pt	15,07	14,90
				N	17,30	16,95
5.	$[Co(DH)_2(Pyridin)_2]_2 \cdot A$	1306,3	Gelbbraune, unregelmäss. Plättchen	Co	9,02	8,81
				Pt	14,93	14,76
				N	12,86	12,59
6.	$[Co(Pyridin)_4Cl_2]_2 \cdot A \cdot 3H_2O$	1353,2	Gelbbraune Nadeln	Co	8,70	8,61
				Pt	14,40	14,26
				N	8,27	8,19
				H_2O	4,05	4,20
7.	$[Co(ec)(\alpha\text{-Naphtylamin})_2]_2 \cdot A \cdot 3H_2O$	1596,9	Braune hexagonale Platten	Co	7,38	7,34
				Pt	12,21	12,05
				N	7,01	6,94
				H_2O	3,18	3,30
8.	$[Co(ec)(Pyridin)_2]_2 \cdot A \cdot 3H_2O$	1340,6	Sternförmige, kleine Nadeln	Co	8,79	8,51
				Pt	14,55	14,21
				N	8,35	8,19
				H_2O	3,03	3,40

(DH_2 = Dimethylglyoxim, ec. H_2 = Äthylendiimino-bis-acetylaceton, Thio = Thioharnstoff, A = $[PtCl_6]^{2-}$)

Tabelle 2

Neue Komplexsalze des Typs $[Co(Amin)_4X_2]_2$ $[PtBr_6]$, bzw. $[Co(en)_2X(Amin)]$ $[PtBr_6]$

No.	Formel	Mol. Gew. ber.	Charakteristik	Analyse	Ber.	Gef.
9.	$[Co(DH)_2(NH_3)_2]_2 \cdot B \cdot 2H_2O$	1360,8	Ziegelrote, rhomb. Prismen	Co	8,66	8,57
				Pt	14,33	14,12
				N	12,34	12,22
				H_2O	2,64	2,59
10.	$[Co(DH)_2(m\text{-Xylidin})_2]_2 \cdot B$	1741,4	Kurze, braune Prismen	Co	6,77	6,73
				Pt	11,20	11,08
				N	9,64	9,53

Tablle 2 (Fortsetzung)

No.	Formel	Mol. Gew. ber.	Charakteristik	Analyse	Ber.	Gef.
11.	$[Co(DH)_2(m\text{-Toluidin})_2]_2 \cdot B$	1685,2	Rotbraune Tafeln	Co	6,99	6,79
				Pt	11,57	11,41
				N	9,97	9,90
12.	$[Co(DH)_2(Thio)_2]_2 \cdot B$	1561,1	Gelbbraune Prismen	Co	7,55	7,30
				Pt	12,49	12,30
				N	14,35	14,09
13.	$[Co(DH)_2(Pyridin)_2]_2 \cdot B$	1573	Gelbbraune mikrokrist. Masse	Co	7,49	7,50
				Pt	12,40	12,19
				N	10,68	10,26
14.	$[Co(Pyridin)_4Cl_2]_2 \cdot B \cdot 2H_2O$	1602,9	Gelbbraune Nadeln	Co	7,35	7,19
				Pt	12,17	12,06
				N	6,99	6,91
				H_2O	2,24	2,35
15.	$[Co(ec)(\alpha\text{-Naphtylamin})_2]_2 \cdot B \cdot 2H_2O$	1845,6	Rotbraune Tafeln	Co	6,38	6,23
				Pt	10,57	10,21
				N	6,07	5,88
				H_2O	1,95	1,80
16.	$[Co(ec)(Pyridin)_2]_2 \cdot B \cdot 2H_2O$	1588,3	Gelbbraune unregelmäss. Krist.	Co	7,42	7,28
				Pt	12,28	12,11
				N	7,05	6,87
				H_2O	2,26	2,05
17.	$[Co(ec)(p\text{-Toluidin})_2]_2 \cdot B \cdot 3H_2O$	1719,5	Rotbraune unregelmäss. Krist.	Co	6,85	6,75
				Pt	11,34	11,09
				N	6,51	6,27
				H_2O	3,14	3,02
18.	$[Co(en)_2Cl(Benzylamin)] \cdot B \cdot 3H_2O$	1050,1	Braunrote unregelmäss. Krist.	Co	5,61	5,51
				Pt	18,58	18,40
				N	6,66	6,38
				H_2O	5,1	4,89
19.	$[Co(en)_2Cl(p\text{-Toluidin})] \cdot B \cdot 2H_2O$	1032,1	Gelbbraune, kleine unregelmäss. Krist.	Co	5,71	5,59
				Pt	18,90	18,72
				N	6,78	6,60
				H_2O	3,49	3,30
20.	$[Co(en)_2Cl(Anilin)] \cdot B \cdot 2H_2O$	1018	Glänzende, gelbbraune Platten	Co	5,79	5,69
				Pt	19,16	19,06
				N	6,87	6,55
				H_2O	3,53	3,40

Tabelle 3

Neue Komplexsalze des Typs $[Co(Amin)_4X_2][PtI_6]$, bzw. $[Co(en)_2X(Amin)][PtI_6]$

No.	Formel	Mol. Gew. ber.	Charakteristik	Analyse	Ber.	Gef.
21.	$[Co(DH)_2(NH_3)_2]_2 \cdot C \cdot H_2O$	1642,8	Rotbraune Nadeln	Co	7,23	7,07
				Pt	12,00	11,84
				N	10,34	10,19
				H_2O	1,11	1,20
22.	$[Co(DH)_2(m\text{-Xylidin})_2]_2 \cdot C$	2023,4	Schwarzbraune mikrokrist. Masse	Co	5,82	5,66
				Pt	9,62	9,51
				N	8,30	8,19

Tabelle 3 (Fortsetzung)

Nr.	Formel	Mol. Gew. ber.	Charakteristik	Analyse	Ber.	Gef.
23.	$[Co(DH)_2(m\text{-Toluidin})_2]_2 \cdot C$	1967	Dunkelbraune dünne Nadeln	Co	5,99	5,90
				Pt	9,92	9,67
				N	8,54	8,26
24.	$[Co(DH)_2(Thio)_2]_2 \cdot C$	1843,1	Dunkelbraune mikrokrist. Masse	Co	6,39	6,20
				Pt	10,59	10,22
				N	12,15	12,00
25.	trans-$[Co(pn)_2Cl_2]_2 \cdot C \cdot 2H_2O$	1548,7	Schwarzgraue, kurze Prismen	Co	7,61	7,41
				Pt	12,59	12,21
				N	7,23	7,06
				H_2O	2,33	2,17
26.	$[Co(en)_2Cl(Benzylamin)] \cdot C \cdot 3H_2O$	1332	Schwarzgraue, kurze Prismen	Co	4,42	4,36
				Pt	14,64	14,49
				N	5,25	5,09
				H_2O	4,05	3,70
27.	$[Co(en)_2Cl(p\text{-Toluidin})] \cdot C \cdot 2H_2O$	1314	Schwarzgraue, kleine, unregelmäss. Krist.	Co	4,48	4,42
				Pt	14,84	14,69
				N	5,33	5,19
				H_2O	2,74	2,30
28.	$[Co(ec)(\alpha\text{-Naphtylamin})_2]_2 \cdot C \cdot 2H_2O$	2127,3	Schwarzviolette unregelmäss. Krist.	Co	5,54	5,21
				N	5,26	5,08
				Pt	9,17	8,99
				H_2O	1,69	1,86
29.	$[Co(ec)(Pyridin)_2]_2 \cdot C \cdot 2H_2O$	1871,1	Dunkelbraune Sternchen	Co	6,29	6,10
				Pt	10,42	10,22
				N	5,98	5,73
				H_2O	2,08	1,90
30.	$[Co(ec)(p\text{-Toluidin})_2]_2 \cdot C \cdot 2H_2O$	1983,3	Schwarzbraune unregelmäss. Krist.	Co	5,94	5,66
				Pt	9,83	9,68
				N	5,64	5,50
				H_2O	1,81	1,78

B = $[PtBr_6]$; C = $[PtI_6]$

Die obenerwähnten Hexahalogeno-platinate (IV) sind in saurem Medium beständig und zersetzen sich leicht in Gegenwart von Alkalien. Sie sind unlöslich in apolaren organischen Lösungsmitteln und lösen sich, im allgemeinen, in DMF, DMSO und THF.

Thermogravimetrische Messungen zeigen, dass die thermische Zersetzung dieser Komplexsalze ein sehr komplizierter Prozess ist. Sie sind beständig bis 160—200 °C und zersetzen sich über diese Temperaturen ohne Bildung von stöchiometrischen Abbauzwischenprodukten. Das Endprodukt der Pyrolyse um 850—900 °C ist ein stöchiometrisches Gemisch von Co_3O_4 + Pt. Die thermische Stabilität der Hexahalogeno-platinate (IV) mit demselben Kation nimmt in der Reihe $Kat_2[PtI_6] < Kat_2[PtBr_6] < Kat_2[PtCl_6]$ zu.

Experimenteller Teil. $H_2[PtBr_6]$ wurde aus $H_2[PtCl_6]$ durch mehrmaliges Eindampfen auf dem Wasserbade mit einer Mischung von 40%-iger HBr und Br_2 erhalten. $Na_2[PtI_6]$ entsteht durch Umsetzung von $H_2[PtCl_6]$ mit NaI (Molarverhältnis 1 : 6).
Das $Na_2[PtI_6]$ zersetzt sich teilweise in wässeriger Lösung bei Verdünnung mit Ausscheidung von schwarzem PtI_4

cis-$[Co(en)_2Cl(Amin)]Cl_2$ wurde aus trans-$[Co(en)_2Cl_2]Cl$ und aus dem entsprechenden Amin, ohne Verwendung von Lösungsmittel, erhalten [12].

$[Co(DH)_2(Amin)_2]$*acetat* und $[Co(ec)(Amin)_2]$*acetat* wurden nach der klassischen Oxydationsmethode mit Luftsauerstoff aus den Komponenten erhalten [13].

Für die doppelten Umsetzungsreaktionen wurden je 0,2—0,3 mMol $H_2[PtCl_6]$, $H_2[PtBr_6]$, bzw. $Na_2[PtI_6]$ in 20—25 ml Wasser und 3—4 mMol. Komplexsalz in 30—40 ml Wasser, oder verd. Methanol verwendet. Die ausgeschiedenen kristallinen Substanzen wurden nach 15—30 Min Stehenlassen abgesaugt, mit Wasser gewaschen und an der Luft getrocknet.

Analyse. Co and Pt Bestimmung. 25—30 mg Proben wurden mit 1 ml konz. H_2SO_4 und etwa 0,1 g KNO_3 in der Hitze aufgeschlossen. Nach Abkühlen wird die Masse mit 25—30 ml Wasser aufgenommen, das schwarze Platinpulver abgetrennt, getrocknet und gewogen. Der Kobaltgehalt wurde in der Mutterlauge komplexometrisch bestimmt.

Verarbeitung der Platinrückstände. Alle Platin-haltige Lösungen werden zur Trockne eingedampft und in einem Tiegel bei 750—800°C geglüht. Der Co_3O_4 + Pt Rückstand wird mit konz. H_2SO_4 behandelt, und nach dem Aufschluss in Wasser gelöst. Das schwarze Platin wird von der $CoSO_4$ — Lösung getrennt.

LITERATUR

1. A. Gutbier, A. Rausch, J. prakt. Chem., [2], **88**, 410 (1913).
2. H. J. Schlesinger, R. E. Palmateer, J. Amer. Chem. Soc., **52**, 4316 (1930).
3. H. Reihlen, W. Hühn, Liebigs Ann. Chem., **489**, 60 (1931).
4. A. Gutbier, F. Bauriedel, C. J. Obermaier, Ber. dtsch. chem. Ges., **43**, 3230 (1910).
5. R. L. Datta, J. Amer. Chem. Soc., **35**, 1187 (1913).
6. K. B. Yatsimirski, Termohimija komplexnih soedinenii, Izdat. Akad. Nauk SSSR, Moskwa, 1961, S. 60.
7. Gmelins Handbuch der anorganischen Chemie, 8. Auflage, Kobalt, System Nummer 58, Tl. B., Verlag Chemie, GMBH, Weinheim, 1940, S. 72, 85, 87, 11—113, 118, 123, 139, 147, 162, 176, 198, 211, 216, 220—222, 233, 238, 243—245, 250, 253, 278, 288.
8. H. D. K. Drew, N. H. Pratt, J. Chem. Soc., **1937**, 510.
9. S. M. Jörgensen, J. prakt. Chem., [2], **27**, 465 (1883); **30**, 14 (1884); **31**, 81 (1885).
10. P. Pfeiffer, G. Lando, Ber. dtsch. chem. Ges., **37**, 4282 (1904).
11. J. Meyer, H. Kienitz, Z. anorg. allg. Chem., **242**, 296 (1939).
12. J. Zsakó, Cs. Várhelyi, E. J. Maxim, Rev. Chim. Minérale (Paris), **10**, 681 (1973).
13. Cs. Várhelyi, I. Gănescu, Monatsh. Chem., **109**, 83 (1978).

STUDIA UNIV. BABEŞ—BOLYAI, CHEMIA, XXXI, 2, 1986

THE REACTION BETWEEN CHROMATE AND THIOLS

I. The Oxidation of Ethanethiol

GAVRIL NIAC*, SIEGFRIED SCHÖN* and IOAN BÂLDEA**

Received: February 7, 1986

ABSTRACT. — The oxidation of ethanethiol by chromic acid proceeds via a relatively rapid and reversible formation of an intermediate chromic acid thioester

$$C_2H_5SH + HCrO_4^- \rightleftarrows C_2H_5SCrO_3^- + H_2O \qquad K$$

An equilibrium constant $K = (1.15 \pm 0.10) \times 10^3 M^{-1}$ has been determined at 25°C and 0.1 ionic strength. The visible and u.v. absorption spectrum of the thioester has been obtained.

Rate studies have been carried out on the thioester formation and redox reaction at 25°C. A third-order rate law has been deduced for the forward reaction in the equilibrium

$$rate_f = k_f^H (C_2H_5SH)(HCrO_4^-)(H^+)$$

with $k_f^H = (2.33 \pm 0.20) \times 10\ M^{-2} \cdot s^{-1}$. The mechanism of thiocompound formation is discussed. The oxidation yields Cr (III) and disulfide under conditions of a large excess of C_2H_5SH. A two term rate law has been found

$$rate_{ox} = \{k_0 + k_1(C_2H_5SH)(H^+)\}\ (C_2H_5SCrO_3^-)$$

with $k_0 = (6.5 \pm 0.7) \times 10^{-4} s^{-1}$ and $k_1 = 15 \pm 0.5\ M^{-1} \cdot s^{-1}$. The involvement of free radicals has been proved. A mechanism according to the kinetics, stoichiometry and other data has been proposed.

Introduction. In aqueous acid solutions, chromic acid oxidizes alcohols to aldehydes or ketones. It has been shown that the reactions proceed via chromic acid esters of the alcohols [1]. The best evidence for the intermediate ester formation was their extraction with nonaqueous solvents [2] and their absorption spectra [3]. It was to be expected that thiols would behave like alcohols by forming intermediate compounds during the oxidation by chromic acid. The existence of chromate-substrate transient complexes in the oxidation of inorganic [4—8] or organic [9, 10] substrates has been established. The reaction with thiosulfate starts by a rapid formation of a thioanhydride of the dichromate type, which undergoes dacay during electron transfer [4—6]. An unusually high formation constant for thiosulfato-chromate as well as spectral evidence led us to consider a Cr — S link in the complex. If during the thiol oxidation a thioester is formed, it necessarily contains a metal-sulfur bond since there is no oxygen atom in the thiol molecule. Preliminary investigations showed the formation of some chemical species at the mixing of EtSH solution with the acid solution of chromate.

* *Polytechnical Institute of Cluj-Napoca, 3400 Cluj-Napoca, Romania*
** *University of Cluj-Napoca, Faculty of Chemical Technology, 3400 Cluj-Napoca, Romania*

The subsequent redox processes of the chromate-substrate complexes have been reported and mechanisms involving Cr(IV) or Cr(V) as intermediate oxidation states of chromium have been suggested [1, 4, 7, 8, 10]. Mono-, and bi-equivalent electron transfer processes have been proposed for the rate-determining step during the reduction of Cr(VI) to Cr(III). The purpose of the present paper is to investigate the ethanethiol — chromate compound, its formation kinetics and the subseqent redox process.

Experimental. Analytical grade chemicals were used without further purification. Stock solutions of dichromate, perchloric acid and sodium perchlorate in twice distilled water were prepared and standardized. A saturated solution of ethanethiol was freshly made before each set of runs and standardized against 0.01 N solution of iodine, under the conditions of disulfide formation. Required aliquots of reagent solutions were transfered to 50 or 100 ml flasks, made up to the mark and kept in the thermostated bath at 25°C for at least 0.5 hr. prior to the initiation of a run.

Kinetic measurements were made spectrophotometrically at 450 nm by means of a zeiss VSU-1 spectrophotometer to which a thermostated cell compartment was adjusted. The intermediate formation kinetics was obtained by recording kinetic curves using a universal Zeiss G—1 B—1 recorder. The redox process was followed by reading absorption point-by-point at different time intervals of 30—120 seconds. A 1 cm path length cell was used. The initiation of the run was performed by injecting 1 ml solution of Cr(VI) containing $HClO_4$ into 4 ml solution of EtSH and $NaClO_4$ in the cell. Thermal effects due to dilution were not observed. Ionic strength was adjusted to 0.1 with sodium perchlorate.

The stoichiometry of the proces was determined by titration of the thiol excess at the end of the reaction.

The system chromate — ethanethiol was used as to initiate radical-induced polymerization of the ethylacrylate. The polymerization was performed in a conic flask provided with a decimal thermometer in order to measure the rapid increase of temperature when the reaction starts.

The absorption spectra were recorded by means of a Zeiss Specord UV—VIS spectrophotometer. Since redox reaction advanced during the plotting of the spectrum, recording vas made for small wavelenght ranges with freshly prepared solution, each range being covered three or four times.

Results. 1. *Formation Constant.* The hydrogen chromate ion colour changes from yellow to orange-red when solutions of EtSH and $HCrO_4^-$ are mixed. This is due to the formation of a new chemical species which has different absorption spectrum as compared to the reactants. By analogy with the formation of chromic acid monoesters of alcohols, we suppose that the new orange-red coloured species is a thioester. Taking into account the pK values for chromic acid and ethanethiol [11, 12], one can conclude that under acidity and concentrations used the species involved in the formation of the condensed compound are $HCrO_4^-$ and undissociated ethanethiol. The shape of the absorption spectrum suggests that only monothioester is formed. Additional support for that comes from the failure of the attempt to extract the orange-red compound into n-pentane and benzene, proving its ionic form. The condensation process takes place according to the equilibrium:

$$C_2H_5SH + HCrO_4^- \rightleftharpoons C_2H_5SCrO_3^- + H_2O \qquad K \tag{1}$$

In order to evaluate the equilibrium constant K from absorption measurements, the absorptivity coefficient of thioester should be known. Choosing a spectral range where ethanethiol is transparent, the absorption measured in an 1 cm path length cell when equilibrium was reached is given by

$$A = \varepsilon_0[(HCrO_4^-)_0 - (EtSCrO_3^-)] + \varepsilon(EtSCrO_3^-) \tag{2}$$

where $(HCrO_4^-)_0$ is the initial Cr(VI) concentration, ε_0 and ε are the absorption coefficients for $HCrO_4^-$ and $EtSCrO_3^-$ respectively. We use Et to abbreviate ethyl radical. At 450 mn, ε_0 is 208 $M^{-1}cm^{-1}$. Expressing $(EtSCrO_3^-)$ in terms of equilibrium constant K and defining observed absorption coefficient by $\varepsilon_{obs} = A/(HCrO_4^-)_0$, the equation (2) may be rearranged as follows:

$$\frac{A}{(HCrO_4^-)_0} = \varepsilon_{obs} = \varepsilon - \frac{\varepsilon_{obs} - \varepsilon_0}{(EtSH)_f} \cdot \frac{1}{K} \qquad (3)$$

$(EtSH)_f$ stands for free ethanethiol concentration. Values ε_{obs} are available from the absorption determinations at the equilibrium state for various experimental conditions used, and a plot of ε_{obs} versus $(\varepsilon_{obs} - \varepsilon_0)/(EtSH)_f$ gives ε as the intercept and K as -1/slope of the linear graph of equation (3). An objective least-squares method was used to compute molar absorptivity at 450 nm and equilibrium constant K. Some iterations have been carried out, first using $(EtSH)_f$ as total thiol concentration, next first K was used to calculate free concentration of thiol which was used again and a new and more correct K value was obtained. The convergence has been achieved after five iterations. The final values are $\varepsilon = 1490 \pm 20$ $M^{-1}cm^{-1}$ and $K = (1.15 \pm 0.10) \times 10^3$ M^{-1}. Experimental and computed data are collected in Table 1.

Table 1

Experimental and computed data for the determination of K and ε (Eq. 3) at 25°C, μ = 0.1, $(HCrO_4^-) = 4 \times 10^{-4}$.

(H^+) $\times 10^3$	$(EtSH)_f$ $\times 10^3$	Aeq.	Eobs	$(EtSH)_f$ $\times 10^3$	$\frac{\varepsilon_{obs}-\varepsilon_0}{(EtSH)_f}$	$(EtSCrO_3^-)$ $\times 10^4$
4.12	9.94	0.531	1327.5	9.586	116785	3.54
	8.52	0.535	1337.5	8.173	138199	3.47
	4.26	0.508	1270.0	3.953	268657	3.07
	2.84	0.467	1167.5	2.564	374220	2.76
	2.27	0.453	1132.5	2.014	459037	2.56
	1.70	0.425	1062.5	1.476	579126	2.29
	1.14	0.367	917.5	0.948	748418	1.88
		0.347	867.5		695675	1.88
	0.852	0.296	740.0	0.692	778786	1.60
	0.568	0.256	640.5	0.445	970787	1.23
	0.284	0.177	442.0	0.211	1110848	0.729
2.06	1.136	0.364	910.0	0.948	740506	1.88
8.24	1.136	0.346	865.0	0.948	693038	1.88

2. *Visible and u.v. Spectrum.* Absorption spectra for 3.5×10^{-2} M EtSH, solution, 4×10^{-4} M $HCrO_4^-$ solution at 4.12×10^{-3} M $HClO_4$ and ionic strength of 0.1 and their mixture respectively were recorded in the range of 240 to 540

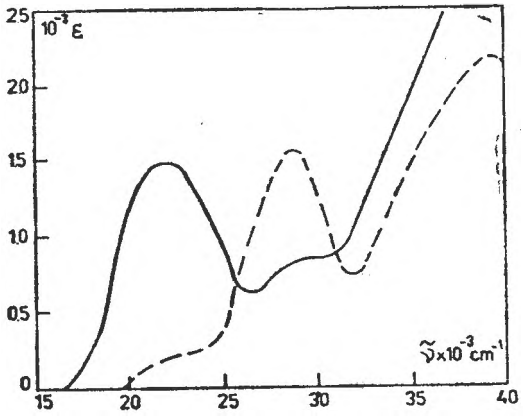

Fig. 1. Visible and u.v. spectra for $HCrO_4^-$ (— — —) and $EtSCrO_3^-$ (—)

nm. Significant difference between spectra was observed. Under the large excess of thiol, the equilibrium (1) was almost completely shifted to the right, 97% of Cr(VI) being involved as thioester. Therefore we could calculate absorption coefficients as a function of wavelength. Figure 1 presents spectra of thioester and acid chromate ion.

The peak at 28750 cm^{-1} in hydrogen chromate ion spectrum is now located at 22200 cm^{-1} in $EtSCrO_3^-$, while the spectrum of chromic ester of EtOH exhibits a peak at 27950 cm^{-1}.

3. *Kinetics of Thioester Formation.* The formation of inrermediate compound occurs within 6—30 seconds, in the range of thiol concenthation of 1.14×10^{-3} to 9.94×10^{-3} and hydrogen ion concentration of 4.12×10^{-3} M; it undergoes a redox decay within 15—20 minutes. As a conceqence, it was possible to record the formation of thioester following the increase of absorbance ingoring the subsequent redox process. Under ethanethiol excess, the graphs of ln $(A_{eq}-A)$ as a function of time were linear. A_{eq} represents the absorption at equilibrium and A the absorption at time t. Accurate first-order plots up to 90—95% completion have been obtained. Table 2 presents first-order rate constants k_{obs} at different hydrogen ion and thiol concentrations as mean of 3—4 individual experiments. Second-

Table 2

The effect of (EtSH) and (H^+) on the thioester formation at $\mu = 0.1$ and $(HCrO_4^-) = 4 \times 10^{-4}$.

(H^+) $\times10^3$	(EtSH) $\times10^3$	k_{obs} s^{-1}	k_2 $M^{-1}.s^{-1}$
2.06	1.136	0.0904	51.4
4.12	1.136	0.198	113.0
	1.704	0.237	102.0
	2.272	0.321	111.0
	2.84	0.336	97.2
	4.26	0.533	109.2
8.24	1.136	0.373	214.4
	1.704	0.501	215.8

order rate constants which include hydrogen ion concentration were calculated from the observed rate constant k_{obs}, as $k_2 = k_{obs}/\{(EtSH) + K^{-1}\}$. They are given in the fourth column of Table 2, showing no significant dependence on thiol concentration at constant acidity, but a linear dependence on acid concentration. When second-order rate constants are divided by hydrogen ion concentration, value close to $(2.33 \pm 0.20) \times 10^4$ $M^{-2}s^{-1}$ are obtained. Therefore the reaction of $EtSCrO_3^-$ complex formation obeys a third-order rate law, first-order in each $HCrO_4^-$ ion, EtSH and H^+ ion. The thioester formation is catalyzed by hydrogenion as expected, and the rate can be written as

$$\frac{d(EtSCrO_3^-)}{dt} = \text{rate}_f = k_f^H (EtSH)(HCrO_3^-)(H^+) \qquad (4)$$

4. *Kinetics of Redox Reaction.* The formation of ethanethiol — chromate intermediate took place much faster than its decomposition under experimental conditions used in the study, which permitted to simplify the treatment of data by taking into account only the decay of intermediate, considered to be formed instantaneously. On the other hand, all kinetical measurements were carried out using a large excess of ethanethiol, which ensured that all amount of Cr(VI) be involved as thioester. Under these circumstances, we followed only the disappearance of $EtSCrO_3^-$ as a function of time.

Pseudo-first-order rate constants were derived from the plots of $\ln(A - A_\infty)$ against time. The linearity was respected to more than 90% completion. The first-order rate constants k'_{obs} were dependent on thiol and hydrogen ion concentration. Table 3 contains their values as a function of thiol concentration. A plot of k'_{obs} versus EtSH concentration gave a straight line which did not pass through origin. Such a dependence suggested the occurence of two parallel processes, one of zero- and the other of first-order on thiol concentration. On this basis the following rate law at constant hydrogen ion concentration can be written:

$$-\frac{d(EtSCrO_3^-)}{dt} = \text{rate}'_{ox} = \{k_0 + k'_1(EtSH)\}(EtSCrO_3^-) \qquad (5)$$

The specific rate (least-square calculated) are $k_0 = (6.2 \pm 0.5) \times 10^{-4}$ s^{-1} and $k'_1 = 0.18 \pm 0.02$ $M^{-1}s^{-1}$.

The effect of hydrogen ion concentration is shown in Figure 2, as determined at constant EtSH concentration in the range of $(H^+) = 2.5 \times 10^{-3}$ to 3.69×10^{-2}. Three to six individual runs were carried out for each set of experimental conditions. The line in Figure 2 does not pass through origin. Again, the influence of acid concentration on the rate can be written as

$$-\frac{d(EtSCrO_3^-)}{dt} = \text{rate}'_{ox} = \{k_0 + k''_1 (H^+)\}(EtSCrO_3^-) \qquad (6)$$

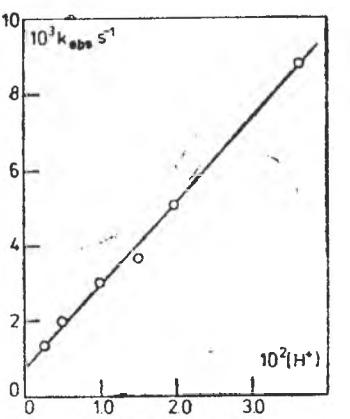

Fig. 2. Dependence of first-order rate constant k_{obs} (s^{-1}) on the hydrogen ion concentration at the oxidation of EtSH.

Table 3

Dependence of first-order rate constant for the redox process on (EtSH) at 25°C, $\mu = 0.1$ and $(H^+) = 1 \times 10^{-3}$.

(EtSH) $\times 10^2$	$10^3 k'_{obs}$ s^{-1}	mean	$\frac{k'_{obs}}{(EtSH)}$ $M^{-1} s^{-1}$
0 49	1 59	1 56	0.319
	1 52		
	1 56		
	1 55		
0 73	1 98	1 93	0 264
	1 93		
	1 87		
	1 92		
	1 93		
1 22	2.91	2 87	0 235
	2.85		
	2 85		
1 46	3 17	3 14	0 215
	3 19		
	3 18		
	3 09		
	3 15		
2 20	4.80	4 72	0 214
	4 73		
	4 65		
	4 72		

with $k_0 = (6.8 \pm 0.6) \times 10^{-4}\ s^{-1}$ and $k_1'' = 0.21 \pm 0.005\ M^{-1}s^{-1}$. The values of k_0 derived from both the thiol and the acid concentration dependence are close together within the limits of experimental errors. On this basis one can conclude a genuine monomolecular decomposition of thioester. The monomolecular rate constant may be taken as a mean of the two intercepts $k_0 = 6.5 \pm \pm 0.9) \times 10^{-4} s^{-1}$. Concerning the second term in the rate equations (5) and (6), one can see that the process of first order with respect to thiol concentration is of first order with respect to hydrogen ion concentration. The overall rate law showing the influence of both EtSH and H^+ concentrations has the form:

$$-\frac{d(EtSCrO_3^-)}{dt} = \text{rate}_{ox} = \{k_0 + k_1(EtSH)(H^+)\}\ (EtSCrO_3^-) \qquad (7)$$

The third-order rate constant k_1 can be derived from either k_1' or k_1''. The best experimental value of $15 \pm 0.5\ M^{-2}s^{-1}$, which is less affected by experimental errors has been taken into consideration.

5. *Stoichiometry.* The stoichiometry of the redox reaction was found to be 3 EtSH : 1 Cr(VI) under the conditions of ethanethiol excess. Values close to 3 : 1 were determined by titration of substante excess after the oxidation by chromate went to completion for seven experimental conditions.

6. *Free Radical Identification.* If a one-equivalent electron transfer process occurs, some free radicals must be involved. In order to prove this, the system chromate-ethanethiol in acid media was used to initiate radical-induced polymerization of ethylacrylate. The rapid increase of temperature when monomer is added to the mixture is consistent with the presence of free radicals [13]. Thermal effect of radical reactions is cumulative and can be noticed despite of the fact that small quantity of polymer has been found. The increase of temparature was 2.4—3.8°C in three different experiments, while no temperature effects were observed when only acid chromate and monomer or thiol, acid and monomer were shaken in the flask. This result proves the presence of free radicals during the redox reaction.

Discussion. The high formation constant of $1.15 \times 10^3\ M^{-1}$ as compared to $6.9\ M^{-1}$ for ethyl chromate formation, in which a Cr—O link is involved, agrees with our previuos conclusion concerning thiosulfato-chromate complex, where a sulfur bridge has been supposed [4]. Formation constants for thiosulfato-and sulfato- chromate were 1.24×10^4 and $4.1 M^{-1}$ [14] respectively. The shift towards lower wavenumbers of the second peak of the hydrogen chromate ion when an oxygen atom is replaced by atoms of lower electronegativity provides additional evidence for a Cr—S bond. These peaks are considered as charge-transfer transitions from ligand to the central atom. This is illustrated in Table 4.

The formation of thioester by condensation of hydrogen chromate and ethanethiol is catalyzed by hydrogen ion. The intervention of H^+ in the mechanism of the formation of similar condensed Cr(VI) compounds is argued in the literature. Haight, Beattie and coworkers [5, 7, 18, 19] have assumed that the first step is a diffusion-controlled formation of five-coordinated Cr(VI) compound. In this complex the substrate incoming the condensed product is weakly bonded to chromium (VI). It follows a proton transfer either from the substrate or from an acid in solution, as rate-determining step. The water molecule coordinated to chromium, subsequently leaves the compound in a rapid step.

$$HX + HOCrO_3^- \underset{k_{-0}}{\overset{k_0}{\rightleftharpoons}} \underset{H}{X} \ldots \underset{OH}{CrO_3^-} \underset{k_{-1}}{\overset{k_1(HA)}{\rightleftharpoons}} X - \underset{OH_2}{CrO_6^-} \underset{k_{-2}}{\overset{k_2}{\rightleftharpoons}} XCrO_3^- + H_2O \qquad (8)$$

Haim [20] has given an alternative and kinetically indistinguishable mechanism, in which the proton was attached to hydrogen chromate, the rate-determining step is the departure of a water molecule during the attack of the nucleophile

$$\begin{aligned} HOCrO_3^- + H &\rightleftharpoons H_2OCrO_3 \quad \text{fast} \\ X^- + H_2OCrO_3 &\rightarrow XCrO_3^- + H_2O \end{aligned} \qquad (9)$$

Both the associative pathway given by Lin and Beattie [7] and the dissociative pathway given by Haim have taken into account the relative insensitivity of third-order rate constant to the nature of HX, while the equilibrium constants

Table 4

Position of the second absorption peak of Chromium(VI) condensed compounds of C_{3v} symmetry and their formation constants.

Species	λnm	$\tilde{\nu}cm^{-1}$	$K M^{-1}$	Ref.
$HOCrO_3^-$	350	28750	-	3,11
$AcOCrO_3^-$	347	28850	4.5	3
$O_3SOCrO_3^{2-}$	350	28750	4.1	14
$HO_3POCrO_3^{2-}$	350	28750	2.9	15
$CH_3OCrO_3^-$	356	28100	4.7	3
$C_2H_5OCrO_3^-$	358	27950	6.9	3
$ClCrO_3^-$	358	27950	17.0 10.2	14 16
$(SCN)CrO_3^-$	380	26300	9,2 220[a]	17 7
$O_3SSCrO_3^{2-}$	394	25400	1.24×10^4 1.1×10^4	4 5
$CySCrO_3^-$[b]	426	23530	1.48×10^3	Next paper
$CH_2SCrO_3^-$ COOH	425	23800	1.09×10^3	To be published
$C_2H_5SCrO_3^-$	450	22200	1.15×10^3	This paper

a) units M^{-1} b) CySH stands or cysteine.

varied three orders of magnitude. The value of k_f^H of 2.33×10^4 $M^{-2}s^{-1}$ for the reaction between ethanethiol and chromate fits within one order of magnitude the k_f^H values for reactions between $HCrO_4^-$ ion and several anions ($HCrO_4^-$ $H_2PO_4^-$, $H_2PO_3^-$, $S_2O_3^{2-}$, SCN^-) listed by Muirhead, Haight and Beattie [5]. The lower value determined in this study could be ascribed to the lack of charge of thiol molecule, which influences the nucleophilic strength of sulfur atom. It seems reasonable to admit that the protons intervention occurs in a rapid preequilibrium and that breaking of $Cr-OH_2$ bond at the attack of nucleophile is the rate-determining step.

The stoichiometry of 3 : 1 shows that each reducing molecule donates one electron to chromium and the final product is disulfide. The result has been expected since thiols which do not have carbonyl groups in α or β positions with respect to the —SH group, are oxidized only to disulfide by stronger oxidizing agents as Ce(IV), hydrogen peroxide and $S_2O_8^{2-}$ [21].

The observations concerning the formation of $EtSCrO_3^-$, kinetics and stoichiometry of redox reaction as well as the involvment of free radicals suggest the following steps accounting for redox process :

$$\begin{aligned} &EtSH + HCrO_4^- \rightleftharpoons EtSCrO_3^- + H_2O \qquad \text{fast} \quad K \\ &EtSCrO_3^- \rightarrow EtS^{\bullet} + Cr(V) \qquad\qquad\qquad\quad k_0 \\ &EtSCrO_3^- + EtSH + H^+ \rightarrow EtSSEt + Cr(IV) \quad k_1 \end{aligned} \tag{10}$$

The one-equivalent oxidation process is an intramolecular electron transfer from sulfur to chromium accompanied by the breaking of Cr—S bond and formation of Cr(V) and free radicals $EtS^{\bullet}$. The two-equivalent oxidation process occurs through a nucleophilic attack of the second thiol molecule on the condensed compound with direct production of Cr(IV) and disulfide. Free radicals, Cr(V) and Cr(IV) are rapidly consumed in subsequent steps which could be :

$$\begin{aligned} &EtSH + Cr(V) \rightleftharpoons EtSCr(V) + H_2O \qquad \text{fast} \quad K' \\ &EtSH + EtSCr(V)\ (+H^+) \rightarrow EtSSEt + Cr(III) \\ &EtSH + Cr(IV) \rightarrow Cr(III) + EtS^{\bullet} \\ &EtS^{\bullet} + EtS^{\bullet} \rightarrow EtSSEt \end{aligned} \tag{11}$$

Cr(V) is an anionic species [22] namely hypochromic weak acid H_3CrO_4 which could condense with thiol, under thiol excess, like chromic acid itself, yielding a new thioester. Subsequently, this could undergo the attack of a second reducing molecule, producing Cr(III) and disulfide. Cr(IV) species is considered a cationic one [23] which could react in an one-equivalent oxidation step, giving Cr(III) and free radicals. Thiol free radicals combine together to form disulfide. Similar elementary steps have been reported in different inorganic or organic substrates oxidation by chromate. The involvment of Cr(V) was proposed by Srinivasan and Roček [10] in the oxidation of oxalic acid. The direct formation of Cr(IV) was demonstrated in the oxidation of secondary alcohols [11]. The elementary steps of two-equivalent processes given above were also suggested in the oxidation of thiosulfate [4] iodide [24] and thiocyanide [25] with direct formation of a dimer of a radical, *e.g.* I_2, $O_3S—SS—SO_3^{2-}$. It is worth mentioning the particular behaviour of ethanethiol as compaed to the other thiocompounds in the reaction with chromate. It consists in the presence of a one-equivalent monomolecular decomposition of thioester ; such a step has not been found in the oxidation of thiosulfate.

REFERENCES

1. F. H. Westheimer and N. Nicolaides, J. Amer. Chem. Soc., **71**, 25 (1949) ; F. H. Westheimer, Chem. Rev., **45**, 419 (1949).
2. H. H. Zeiss and D. A. Pease, J. Amer. Chem. Soc., **78**, 3182 (1956) ; A. C. Chaterji and S. K. Mucherjee, Z. Physik. Chem., **228**, 159 (1965).
3. U. Kläning and M. C. R. Symons, J. Chem. Soc., **1961**, 3204.
4. I. Bâldea and G. Niac, Inorg. Chem., **7**, 1232 (1968) ; idem, **9**, 110 (1970).
5. K. A. Muirhead, G. P. Haight and J. K. Beattie, J. Amer. Chem. Soc., **94**, 3006 (1972).

6. M. I. Edmonds, K. E. Howlett and B. L. Wedzicha, J. Chem. Soc., **1970 A,** 2866.
7. C. T. Lin and J. K. Beattie, J. Amer. Chem. Soc., **94,** 3011 (1972).
8. K. K. Sengupta and J. K. Chaklader, J. Chem. Soc., Dalton Trans., **1974,** 222.
9. I. Baldea and S. Schön, Studia Univ. Babeş-Bolyai, Chemia, **18 (1),** 47 (1973).
10. V. Srinivasan and J. Roček, J. Amer. Chem. Soc., **96,** 127 (1974).
11. J. Y. Tong and E. L. King, J. Amer. Chem. Soc., **75,** 6180 (1953).
12. M. M. Kreevoy, E. T. Harper, R. L. Duvall, H. S. Wilgus and L. T. Ditsh, J. Amer. Chem. Soc., **82,** 4899 (1960).
13. O. Marek and M. Tomka, „Acrilovie Polymeri" Izd. Khim., 1966, p. 80.
14. G. P. Haight, P. C. Richardson and N. H. Coburn, Inorg. Chem., **3,** 1777 (1964).
15. F. Holloway, J. Amer. Chem. Soc., **74,** 224 (1952).
16. O. Lukkari, Suomen Kemistilehti, **B 35,** 91 (1962); idem, **B 38,** 121 (1965).
17. G. Niac, I. Baldea and M. Lungu, Studia Univ. Babeş-Bolyai, Chemia, **14 (2),** 83 (1969).
18. S. A. Frennesson, J. K. Beattie and G. P. Haight, J. Amer. Chem. Soc., **90,** 6018 (1968).
19. S. A. Frennesson, J. K. Beattie and G. P. Haight, Acta Chem. Scand., **23,** 3277 (1969).
20. A. Haim, Inorg. Chem., **11,** 3147 (1972).
21. J. Hill and A. Mcauley, J. Chem. Soc., **1968 A,** 156; idem, **1968 A,** 2405; I. Pascal and D. S. Tarbell, J. Amer. Chem. Soc., **79,** 6015 (1957); L. S. Levit, J. Org. Chem., **20,** 1293 (1959).
22. J. H. Espenson, Accounts Chem. Rev., **3,** 347 (1970).
23. E, Huss and W. Klem, Angew. Chem., **66,** 468 (1954); K. A. Wilhelmi, O. Jonsson and E. Lagervall Acta Chem. Scand., **23,** 1074 (1969).
24. K. E. Howlett and S. Sarsfield, J. Chem. Soc., **1968 A,** 683.
25. K. A. Muirhead and G. P. Haight, Inorg. Chem., **12,** 1116 (1973).

STUDIA UNIV. BABEŞ—BOLYAI, CHEMIA, XXXI, 2, 1986

THE REACTION BETWEEN CHROMATE AND THIOLS

II. The Oxidation of Cysteine

IOAN BÂLDEA* and GAVRIL NIAC**

Received: February 7, 1986

ABSTRACT. — Rate studies have been carried out on the condensed compound formation and redox reaction of cysteine with chromate by spectrofhotometrical means in acid solutions. The oxidation starts by a relatively rapid equilibrium $CySH + HCrO_4^- \rightleftarrows CySCrO_3^- + H_2O$, when thioester is formed. The equilibrium constant is determined and the spectrum of condensed compound is given. The formation of $CySCrO_3^-$ obeys the rate law

$$\text{rate}_f = \left\{k_f^0 + k_f^H(H^+)\right\}(CySH)(HCrO_3^-)$$

with $k_f^0 = 2.1 \pm 0.15\ M^{-1} \cdot s^{-1}$ and $k_f^H = (1.40 \pm 0.12) \times 10^2 M^{-2} \cdot s^{-1}$.

The redox process yielding disulfide and Cr(III) proceeds by two parallel ways, folowing the rate law

$$\text{rate}_{ox} = \{k_2 + k_3(H^+)\}(CySH)(CySCrO_3)$$

with $k_2 = (7.7 \pm 0.3) \times 10^{-2} M^{-1} \cdot s^{-1}$ and $k_3 = 0.7 \pm 0.2\ M^{-2} \cdot s^{-1}$ at 25 C and $\mu = 0.22$. Both, the substitution on hydrogen chromate and subsequent redox process mechanisms are discussed. Activation parameters for redox reaction are given.

Introduction. The formation of chromate-substrate complexes as intermediates during the oxidation of various organic and inorganic reducing agents has been estabilished [1—8]. We have presented spectral evidence for the existence of transient species of Cr(VI)-thiosulfate [1], Cr(VI) — thiocyanide [2] Cr(VI)—t—$C_{12}H_{25}SH$ [3], Cr(VI)—EtSH [4] complexes. Howlett *et al* [5], Haight, Beattie and coworkers [6—8] have confirmed the formation of this kind of condensed compounds. Third-order rate laws, first-order with respect to each hydrogen chromate, substrate and hydrogen ion have been obtained for the formation of these intermediates. Rate constants of the same order of magnitude ($10^5\ M^{-2} \cdot s^{-1}$) have been determined for these processes, except for the case of EtSH—Cr(VI) system [4], where a rate constant one order of magnitude smaller has been found. Two mechanisms for the substitution on $HOCrO_3^-$ were suggested. To get more information about the role of the substrate nature, cysteine has been chosen as thiol substrate to react with chromate.

The subsequent electron-transfer reactions occur within a period of 10—100 times longer than the intermediate formation. In the case of thiosulfate and

* *University of Cluj-Napoca, Faculty of Chemical Technology, 3400 Cluj-Napoca, Romania*
** *Polytechnical Institute of Cluj-Napoca, 3400 Cluj-Napoca, Romania*

ethanethiol oxidations, second-order terms with respect to the reducing agent have been found, suggesting transition states where two substrate molecules were bound. Sulfur-sulfur bondings are formed during the oxidation. Cysteine is expected to react like thiosulfate, because of its similar behaviour in reaction with iodine [9, 10]. The present study also extends the investigation on chromate oxidation of cysteine.

Experimental. Chemicals were of analytical grade purity and used without further purifications. Stock solutions were prepared in twice distilled water and diluted to the required concentration of each kinetic run. Cysteine solutions were freshly prepared before each set of experiments using crystalline CySH · HCl · H_2O. Since the equilibrium constant for chlorochromate formation is much smaller than those for thiochromate complexes, we have assumed that the presence of HCl in the solution does not affect the studied equilibrium and kinetics [11]. Therefore hydrogen chloride was used as a source of protons. Some experiments were carried out with perchloric acid in the kinetic study of intermediate formation. Data were superimposed with those in the hydrochloric acid media. Cysteine solution were standardized by means of the reaction with Fe(III) [12]. A known excess of Fe^{3+} was added to cysteine solution. After the reaction was accomplished, ferric ion concentration was determined photometrically in the presence of sulfosalicylic acid in acetate buffered solution. The same procedures were used to determine the stoichiometry of the reaction. The Fe^{3+} solution was added to reaction mixture after Cr(VI) was entirely reduced. Cr(III) did not interfere with the photometrical measurements.

The reaction was initiated by injecting oxidant solution into reducing agent solution in a silica cell with a pathlength of 1 cm. The formation of condensed compound between cysteine and chromate occurs within 0.5—1.5 minutes in the investigated concentration range, while the redox process occurs within 20—150 minutes. The experimental procedure to follow the two kinetic processes is described in a previous paper [4]. A relative large excess of cysteine was used in both the condensed compound formation and disappearance by redox reaction. That ensured a simple treatment of data and a constant stoichiometry.

The absorption spectrum for transient species was recorded using a Zeiss Specord UV—VIS spectrophotometer. Recordings were made for small wavelength range, with freshly prepared mixtures to avoid decomposition by redox reaction. Each range was covered four or five times.

Some attempts were made in order to determine if free radicals were involved in the process. Thus, the cysteine-chromate system was used to initiate radical induced polymerization of ethylacrylate.

Results and Discussion. 1. *The Formation of $CySCrO_3^-$. Equilibrium and Kinetics.* The formation of a condensed compound containing sulfur-chromium bond as transient species is belived to occur. A change of colour from yellow to red-orange took place rapidly when acid solution of chromate was mixed with cysteine solution.

The spectra of stoichiometric mixture of reactants (3.33×10^{-4} M) in 1×10^{-2} M H^+ and mixture with a large excess of cysteine (1.2×10^{-2} M) were recorded, and compared to spectrum of $HOCrO_3^-$ ion. Important differences between them were noticed. The molar absorptivities as a function of wavenumber were calculated considering that all Cr(VI) was bound as thioester according to the equilibrium

$$CySH + HOCrO_3^- \rightleftharpoons CySCrO_3^- + H_2O \qquad (1)$$

completely shifted to the right under the large excess of cysteine. CySH is the abbreviation for $HOOC—CH(NH_3^+)—CH_2—SH$. The spectra of the complex and of $HOCrO_4^-$ ion respectively, are presented in Figure 1. Molar absorptivities were in a good agreement with those calculated from the recorded spectrum when 1 : 1 ratio was used. Similar to the $CrS_2O_6^{2-}$, $EtSCrO_3^-$ and $(SCN)CrO_3^-$ comple-

xes, in which charge transfer maxima occur at lower energy (380—450 nm) as compared to oxygen-bridged condensed compound as $CrSO_7^{2-}$ or $ROCrO_3^-$ (350 nm), cysteine-chromate complex exhibits a red shift of absorption bands. The peak at 28,750 cm^{-1} in $HOCrO_3^-$ ion is now located at 23,700 cm^{-1} in $CySCrO_3^-$ and corresponds to a charge transfer transition from sulfur to chromium.

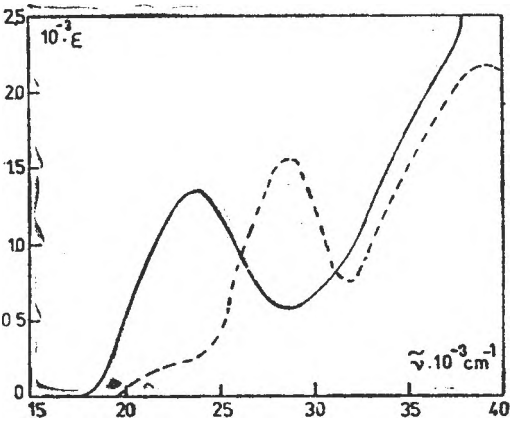

Fig. 1. Absorption spectra of $CySCrO_3^-$ (—) and $HCrO_4^-$ (— —)

To evaluate the equilibrium constant for cysteine-chromate complex formation from absorbance meansurements at 420 nm, a similar procedure to that described previously [4] was used. Absorbance values at equilibrium under various experimental conditions are presented in Table 1. Absorption coefficients $\varepsilon_{obs} = (A_{eq}/HCrO_4^-)_0$ measured at various (H^+) and

Table 1

Absorbance values at equilibrium and observed molar absorption coefficient at 25 °C and $(HOCrO_3^-) = 4 \times 10^{-4}$.

μ	(H^+) $\times 10^2$	$(CySH)$ $\times 10^3$	A_{eq}	ε_{obs} $M^{-1} \cdot cm^{-1}$
0,15	1,80	19.8	0,533	1332.5
	1,52	9.9	0.538	13450
	1.50	9 06	0 520	1300.0
	1.18	8 97	0 523	1307 5
	1.07	1 21	0 350	875 0
			0.350	875 0
	1 00	0 448	0.235	587 5
			0 240	600.5
			0.250	625.5
		0.224	0 180	450 0
			0 180	450 0
0 22	1.27	3 74	0 475	1187 5
	1.14	2 24	0 415	1037 5
	108	1.50	0 409	1022 5
	106	0 748	0.268	670 0
	077	3 76	0.468	1170 0

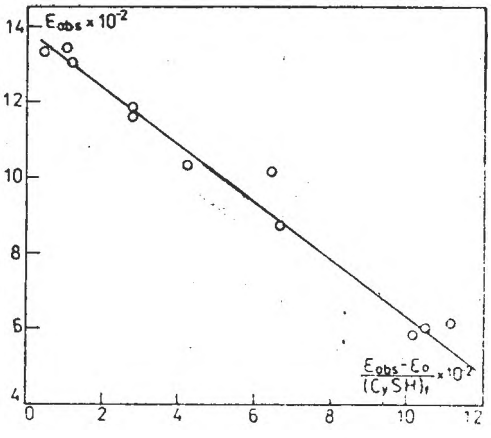

Fig. 2. Linear dependence of ε_{obs} on $(\varepsilon_{obs} - \varepsilon_0)\ (CySH)_f^{-1}$ (eq. 2)

(CySH) are related to the formation constant K by the expression (2)

$$\varepsilon_{obs} = \varepsilon - \frac{1}{K} \cdot \frac{\varepsilon_{obs} - \varepsilon_0}{(CySH)_f} \qquad (2)$$

where $(CySH)_f$ is the free concentration of cysteine, ε and ε_0 the absorption coefficients for complex and $HCrO_4^-$ ion at 420 nm. By plotting ε_{obs} against $(\varepsilon_{obs} - \varepsilon_f)\ (CySH)_f^{-1}$, K and ε values were obtained. An iterative procedure, using an objective least-squares method gave $K = (1.48 \pm 0.15) \times 10^3\ M^{-1}$ and $\varepsilon = 1380 \pm 20\ M^{-1}\ cm^{-1}$. Figure 2 shows a good fit of data to linear expression (2). Again, the large value of formation constant is consistent with a sulfur-bridged complex. The oxygen-bridged compounds as sulfatochromate [11], phosphatochromate [13] and chromic esters [14] exhibit formation constants between 2 and 7 M^{-1}.

Under the conditions of a large cysteine excess, a first-order dependence with respect to $HCrO_4^-$ ion was obtained for the binding of cysteine to chromate process. Plots of $\ln(A_{eq} - A)$ versus time gave straight lines over at least 80—85% of reaction. A_{eq} and A represent the absorbance at equilibrium and at time t respectively. The slopes of lines were the apparent first-order rate constants k_{obs}. Second-order rate constants for the forward reaction in equilibrum (1) k_f were calculated taking into account that

$$k_{obs} = k_f\ (CySH) + k_r = k_f[(CySH) + K^{-1}] \qquad (3)$$

These values are presented in Table 2 as dependant of (H^+). Free acidity was derived from both the mineral acid and cysteine chlorhydrate concentrations. The first acid dissociation constant K_{a1} is 1.3×10^{-2} M and attributed to carboxyl group in cysteine. Thiol and $-NH_3^+$ groups are weaker acids [15] (pK of 10 and 8.6). The reaction order with respect to the hydrogen-ion concentration is about 0.7, showing two concurrent processes, one independent and the other linear dependent on (H^+). A linear dependence has been obtained by plotting k_f against (H^+), as shown in Figure 3. Therefore, the following rate law can be written for the forward reaction in the equilibrium (1):

$$\frac{d(CySCrO_3^-)}{dt} = rate_f = \{k_f^0 + k_f^H\ (H^+)\}\ (CySH)(HCrO_3^-) \qquad (4)$$

The rate constants k_f^4 and k_f^H as calculated (least-squares) from the intercept and the slope at 25°C and $\mu = 0.22$ are $2.1 \pm 0.15\ M^{-1} \cdot s^{-1}$ and $(1.40 \pm \pm 0.12) \times 10^2 M^{-2} \cdot s^{-1}$ respectively.

The existence of a pathway zero-order in acidity is in disagreement with the mechanism proposed by Haight, Beatie and coworkers [6, 7], in which the acid catalysed proton transfer in a pentacoordinate substrate—Cr(VI) inter-

Table 2

Dependence of k_f on (H^+) for the reaction of cysteine-chromate complex at 25°C, $\mu = 0.22$ and $(HCrO_4^-) = 4 \times 10^{-4}$.

(H^+) $\times 10^2$	$(CySH)$ $\times 10^2$	K'_{obs} s^{-1}	K_f $M^{-1}.s^{-1}$
0 22	0 254	0 0078	2 425
0 39	0 504	0 0148	2 258
0 68	1.01	0 0322	2 988
0 77	0 376	0 0127	2.860
		0 0121	2 728
0 90	1 51	0 0522	3 499
1 14	0.224	0.0120	3 850
1 27	0.374	0 0150	3 397
	0 376	0 0170	3 833
		0 0160	3 607
		0.0160	3 607
1 50	0.748	0 0360	4 414
1 54	1 12	0 0520	4 100
1 64	1 50	0 0644	4 108
1 77	1 87	0 0851	4 392
1 92	2 245	0 108	4 670
2.27	0.376	0 0230	5 185
		0 0250	5 636
		0 0230	5 185

mediate is considered as rate-determining step. An alternative mechanism has been proposed by Haim [16] in which the dissociation of a water molecule from the pentacoordinate Cr(VI) intermediate has been postulated as rate-determining

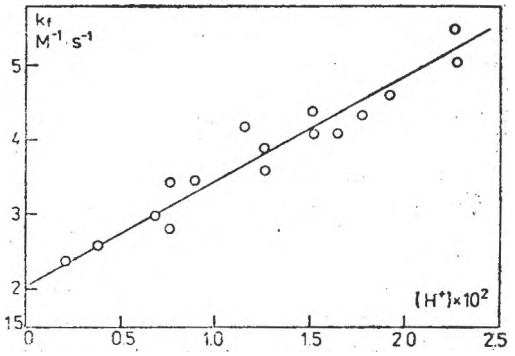

Fig. 3. Dependence of the second-order rate constant k_f for the formation of condensed compund on hydrogen ion concentration.

step. Both mechanisms have considered the fact that k_f^H was relatively independent, within one order of magnitude, on the nature of the substrate. We are inclined to consider a mecanism of Haim type to be operative for cysteine — chromate system, provided that, besides the dissociative character of the activation, the association itself yielding pentacoordinate Cr(VI) with a Cr—S bond should have a contribution to global activation energy. The following sequence could be responsible for the above given kinetics:

$$H^+ + HOCrO_3^- \rightleftharpoons H_2OCrO_3 \quad K_{ass} \text{ fast} \tag{5}$$

zero-order in acidity

$$CySH \rightleftharpoons CyS^- + H^+ \quad K_{diss} \text{ fast} \tag{6}$$

$$CyS^- + H_2OCrO_3 \rightarrow CySCrO_3^- + H_2O \quad k_f^0 \tag{7}$$

first-order in acidity

$$CySH + H_2OCrO_3 \rightarrow CySCrO_3^- + H_2O + H^+ \quad k_f^H \tag{8}$$

Third-order rate constant k_f^H ranges three orders of magnitude below the previously determined ones. Such a difference cannot be explained only by steric effects. In the case of chromate-thioglycolic acid, where an undissociated (or slightly dissociated) carboxyl group is sited in α-position to thiol group, a rate constant of $2.47 \times 10^3\ M^{-2} \cdot s^{-1}$ has been found [17]. The value is ten times greater than that obtained in the cysteine-chromate system, where an ammonium group of a relative small volume is in α-position to thiol. The presence of a positive charge at the function in α-position to thiol modifies the electronic density on sulfur atom and, therefore, the nucleophilic character at this reaction site. As a consequence, both the acid dissociation of —SH and the association with Cr(VI) yielding pentacoordinate activated state are influenced.

2. *Stoechiometry of Redox Reaction.* The stoichiometry of the redox process was obtained by determination of unreacted cysteine after the completion of the reaction. In all the cases when cysteine excess was used, ratios close to 3 CySH : 1 Cr(VI) were found. This ratio is consistent with the oxidation to cystine. In the situation of chromate excess, further oxidation of cystine took place. These conditions were not investigated kinetically.

3. *Kinetics and Mechanism of Redox Reaction.* Experimental conditions for redox reaction were chosen such that cysteine was always in a large excess (up to 80 fold excess). This ensured that only formation of cystine took place, and all amount of Cr(VI) existed as thioester; the absorption of the solution was proportional to cysteine-chromate complex concentration. Under such circumstances, the oxidation reaction followed a first-order dependence on thioester or total Cr(VI) concentration. The graphs of $\ln(A - A_\infty)$ versus time were linear over 90% completion at $(H^+) = 10^{-2}$ and over 95—98% at $(H^+) = 4 \times 10^{-2}$.

To determine the reaction order with respect to cysteine, various cysteine concentration were used at constant acidity. As shown in Figure 4, a linear relationship was observed, by plotting first order rate constants k'_{obs} against (CySH). The line passes through origin indicating a first order dependence on cysteine concentration and no monomolecular decomposition of thioester in this range of concentration. Thus, a second-order rate law, first-order in both the condensed compound and cysteine could be deduced at constant acid con-

centration. The effect of (H^+) on the rate was studied at constant cysteine concentration of 1.58×10^{-2}, in the range of $(H^+) = 0.01 - 0.1$. A fractional order between zero and one has been found. A linear relationship was obtained when experimental second-order rate constants were plotted versus hydrogen-ion concentration. As shown in Figure 5, the lines intercepted the ordinate

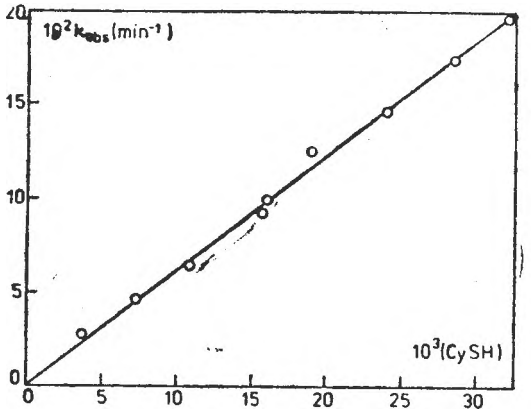

Fig. 4. Dependence of first-order rate constant for the oxidation on cysteine concentration.

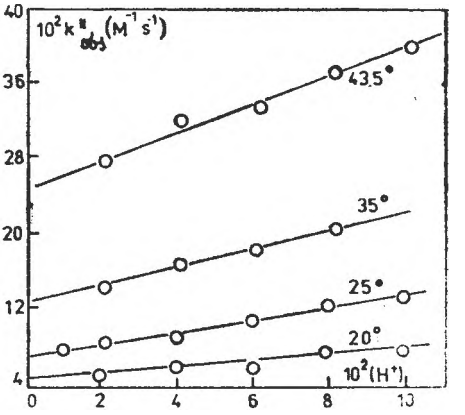

Fig. 5. The effect of acidity and temperature on second-order rate constant for the oxidation. k''_{obs} was calculated from k'_{obs} by dividing by (CySH).

at values differnt from zero. This indicated the existence of two parallel processes, zero and first order with respect to hydrogen ion concentration. Thus, the overall rate law can be written as:

$$-\frac{d(\mathrm{CySCrO_3^-})}{dt} = [k_2 + k_3(H^+)](\mathrm{CySCrO_3^-})(\mathrm{CySH}) \qquad (9)$$

In order to study the effect of temperature on k_2 and k_3, experiments were made in the temperature range of 20—43.5°C. Figure 5 presents the dependence of second-order rate constants on acidity and four different temperatures. Each point on the graph represents the mean value of 3—4 individual runs, which do not differ more than 5%. Second-order k_2 and third-order k_3 rate constants were derived from the intercepts and the slopes of the lines, respectively. Table 3 lists these values. Activation parameters (least square calculated) are:

for k_2 $\Delta H^{\neq} = 51.0 \pm 2.1$ kJ/mol; $\Delta S^{\neq} = -96.2 \pm 21$ J/mol. K

for k_3 $\Delta H^{\neq} = 43.9 \pm 2.0$ kJ/mol; $\Delta S^{\neq} = -100 \pm 25$ J/mol.K

The following mechanism is consistent with the equilibrium formation of thioester, stoichiometry and kinetical observations:

$$\mathrm{HCrO_4^-} + \mathrm{CySH} \rightleftharpoons \mathrm{CySCrO_3^-} + \mathrm{H_2O} \quad K$$

$$\mathrm{CySCrO_3^-} + \mathrm{CySH} \rightarrow \mathrm{CySSCy} + \mathrm{Cr(VI)} \quad k_2' \qquad (10)$$

$$\mathrm{CySCrO_3^-} + \mathrm{CySH} + \mathrm{H^+} \rightarrow \mathrm{CySSCy} + \mathrm{Cr(VI)} \quad k_3 \qquad (11)$$

Table 3

The effect of temperature upon second- and third- order rate constants in the redox process.

Temp °C	$10^2 \cdot k_2$ $M^{-1} \cdot s^{-1}$	k_3 $M^{-2} \cdot s^{-1}$
20.0	5.0 ± 0.2	0.38 ± 0.02
25.0	7.7 ± 0.3	0.70 ± 0.02
35.0	13.2 ± 0.2	1.17 ± 0.04
43.5	26.3 ± 0.4	1.63 ± 0.07

CySSCy stands for cystine. After a reletively rapid equilibrium, two bi-equivalent electron transfer processes follow, yielding Cr(IV) and disulfide. Condensed compound of "esteric" type is formed prior the electron transfer process. Cr(IV) formed in (10) and (11) may react rapidly either with a new cysteine molecule to form Cr(III) and cysteine free radical, or with Cr(VI) to form Cr(V), another active species which acts as a bi-equivalent oxidant. Under the cysteine excess conditions, the first alternative seems to be operative.

The involvment of free cysteine radical, which combines to yield cystine, was proved by the induced polymerization of ethylacrylate with this redox system.

The rate law deduced from the mechanism and stoichiometry is:

$$-\frac{d(CySCrO_3^-)}{dt} = \frac{K}{3}[k_2 + k_3(H^+)]\frac{(CySH)^2}{1 + K(CySH)}(HCrO_4^-) \qquad (12)$$

Under the cysteine excess $K(CySH) \gg 1$, and the expression (12) becomes simpler and in agreement with empirical rate law.

The oxidation of cysteine by chromate is similar to the oxidation of thiosulfate. In both cases S—S bondings are directly formed [1]. Activation parameters are larger as compared to thiosulfate oxidation. On the basis of large negative entropies, we consider the activated complex as containing two cysteine molecule and a pentacoordinate chromium (VI); after the electron transfer, one from each organic molecule, Cr(IV) and cystine are formed.

REFERENCES

1. I. Baldea and G. Niac, Inorg. Chem., **7**, 1232 (1968); idem, **9**, 110 (1970).
2. I. Baldea and S. Schön, Studia Univ. Babeş-Bolyai, Chemia, **18 (1)**, 47 (1973).
3. G. Niac, I. Baldea and M. Lungu, Studia Univ. Babeş-Bolyai, Chemia **14 (2)**, 83 (1969).
4. G. Niac, S. Schön and I. Baldea, Previous paper in this issue.
5. M. I. Edmonds, K. E. Howlett and B. L. Wedzicha, J. Chem. Soc., **1970 A**, 2866.
6. K. A. Muirhead, G. P. Haight and J. K. Beattie, J. Amer. Chem. Soc., **94**, 3006 (1972)
7. C. T. Lin and J. K. Beattie, J. Amer. Chem. Soc., **94**, 3011 (1972).
8. K. A. Muirhead and G. P. Haight, Inorg. Chem., **12**, 1116 (1973).
9. A. D. Awtrey and R. E. Connick, J. Amer. Chem. Soc., **73**, 1341 (1951); idem, **73**, 4546 (1951).
10. J. P. Danehy and M. Y. Oester, J. Org. Chem., **32**, 1491 (1967).
11. G. P. Haight, P. C. Richardson and N. H. Coburn, Inorg. Chem., **3**, 1777 (1964).
12. D. L. Leusing, I. P. Mislan and R. J. Goll, J. Phys. Chem., **64**, 1070 (1960).
13. F. Holloway, J. Amer. Chem. Soc., **74**, 224 (1952).
14. U. Kläning and M. C. R. Symons, J. Chem. Soc., **1961**, 3204.
15. R. E. Benesch and R. Benesch, J. Amer. Chem. Soc., **77**, 5877 (1955); A. Albert Biochem J., **50**, 690 (1952).
16. A. Haim, Inorg. Chem., **11**, 3147 (1972).
17. I. Baldea To be published.

STUDIA UNIV. BABEŞ—BOLYAI, CHEMIA, XXXI, 2, 1986

CONDENSATION PRODUCTS OF 3-FORMYL—10-METHYL—PHENOTHIAZINE WITH NITROGEN COMPOUNDS

MIRCEA DIUDEA* and VALER FĂRCĂŞAN**

Received: April 9, 1986

ABSTRACT. — Some new condensation products of 3-formyl-10-methyl-phenothiazine (I) with nitrogen compounds, namely IX ... XVI and VII_j, were prepared and their IR and UV—VIS spectra registered. The microbiostatic activity of I, VI, IX...XVI was also tested.

Some condensation products of 3—formyl—10—methyl-phenothiazine (I) with nitrogen compounds are known, namely II, $III_{a...f}$[1], IV [2], V [3], VI and $VII_{a...i}$[4].

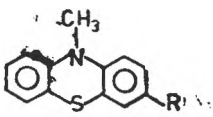

I) R: CHO ; II) R: CH=N–NH–C(=S)–NH$_2$

III)$_{a...f}$ R: CH=N–NH–C(=S)–N(C(=O)–CH–R′)

a) R′ = H ; b) R′: C_2H_5 ; c) R′: $(CH_3)_2CH$

d) R′: $CH_3(CH_2)_3$– ; e) R′: $CH_3(-CH_2)_{13}$ f) R′: $CH_3(CH_2)_{15}$

IV) R: CH=N–OH ; V) R: CH=N–NH–C(=O)–NH$_2$;

VI) R: CH=N–C_6H_5 ; IX) R: –CH=N–C_6H_4OH (2)

X) R: CH=N–C_6H_4OH (3) ; XI) R: CH=N–C_6H_4OH (4)

XII) R: CH=N–$C_6H_4CO_2C_2H_5$ (4) XIII) R: CH=N–NH–(OH, N, N, CH_3)

* *Chemico-Pharmaceutical Research Institute, 3400 Cluj-Napoca, Romania*

** *University of Cluj-Napoca, Faculty of Chemical Technology, 3400 Cluj-Napoca, Romania*

The tuberculostatic activity of certain thiosemicarbazones with thiazolinic nucleus derived from 3—formyl—10—methyl—phenothiazine ($III_{a...f}$)/ [1], as well as the anticarcinogenic action of some arylhydrazones [5] stimulated us to react 3—formyl—10—methyl—phenothiazine (I) with compounds containing the anilino- or hydrazino-groups, in the view to obtain new biological active substances.

From the starting compounds the thiocarbazide as dihydrate (VIII) was prepared by an original method.

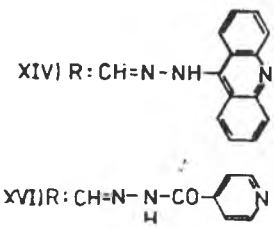

XIV) R: CH=N-NH-

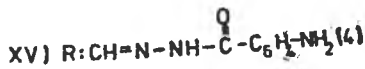

XV) R: CH=N-NH-C(=O)-C_6H_4-NH_2(4)

XVI) R: CH=N-N(H)-CO-

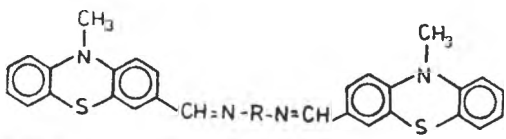

VII) a ... j : a) R: -$(CH_2)_2$-; b) R: -$(CH_2)_3$-;

c) R: -$(CH_2)_6$- d) R: -$(CH_2)_{10}$-; e) R:  ;

f) R:  ; g) R: 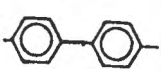 ;

h) R: 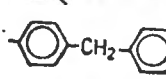 ; i) R: -CH_2-CH_2-S-CH_2-CH_2-

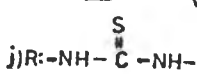

j) R: -NH-C(=S)-NH-

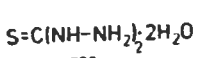

S=C(NH-NH_2)$_2$·2H_2O

VIII

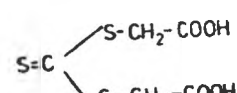

XXV

The new condensation products, listed in Table 1 (IX ... XVI, VII_j), were obtained by reacting the nitrogen compounds XVII ... XXIV and VIII, with I, in the conditions described in the experimental section.

To observe that some of them are derivatives of well known substances (e.g. XX, XXIV) used in clinical medicine.

Table 1

Condensation products of 3-formyl-10-methyl-phenothiazine (I)

Substance	Starting nitrogen compound	Yield	Melting point °C	Formula (Molecular weight)	Analysis (Calcd./Found) N %	Spectra a) IR (1/λ ; cm^{-1}) b) UV-VIS [$\lambda_{max;nm}$;($\varepsilon_{max} \cdot 10^{-4}$)]
I.						a) C=O 1765 b) 237.6 (1.82); 257.7 (1.47); 269.5 (1.66); 285.7 (1.89); 381.7 (0.57)
VI.	——	——	——		——	a) C=N 1625 b) 239.7 (1.35); 271.7 (2.00); 289.0 (2.04); 313.7 (1.35) 382.3 (1.08)
IX	2-Aminophenol XVII	52.7	147	$C_{20}H_{16}N_2OS$ (332.41)	8.42 8.23	a) C=N 1630 b) 240.4 (2.21) 273.2 (2.07) 286.9 (2.11) 320.8 (1.07) 390.6 (1.57)
X.	3-Aminophenol XVIII.	48.5	162	$C_{20}H_{16}N_2OS$ (332.41)	8.42 8.41	a) C=N 1630 b) 240.4 (1.40); 258.4 (1.13) 286.5 (1.00) 312.2 (0.66); 394.6 (0.40)
XI.	4-Aminophenol XIX	64.6	217	$C_{20}H_{16}N_2OS$ (332.41)	8.42 8.14	a) C=N 1625 b) 238.7 (2.12) 271.0 (1.99) 287.4 (1.99) 324.7 (1.41) 384.6 (1.66)
XII.	Ethyl-4-amino-benzoate (XX)	62.5	124	$C_{23}H_{20}N_2O_2S$ (388.49)	7.21 7.53	a) C=N 1625 C=O 1710 b) 248.4 (2.34); 256.0 (2.29); 275.3 (2.24); 297.6 (2.68); 393.1 (1.12)
XIII.	2-Hydrazino-4-methyl-6-hydroxy-pyrimidine (XXI) *	63.8	166	$C_{19}H_{17}N_5OS$ (363.44)	19.27 19.29	a) C=N 1618 C=O 1680 b) 227.8 (1.84); 240.1 (1.93); 269.4 (1.93); 280.6 (2.05); 313.9 (1.99); 375.9 (1.52);
XIV.	9-Hydrazino-acridine (XXII)	49.1	208	$C_{27}H_{20}N_4S$ (432.55)	12.95 12.61	a) C=N 1620 b) 235.4 (3.00); 247.4 (2.38); 286.7 (1.61); 320.5 (0.88); 448.8 (1.62)
XV.	4-Amino-benzhydrazide (XXIII)	61.2	248	$C_{21}H_{18}N_4OS$ (374.47)	14.96 15.07	a) C=N 1630 C=O 1650 b) 223.2 (2.35); 241.2 (2.25); 266.0 (2.05); 317.9 (4.10); 371.7 (2.25)
XVI.	Isonicotin hydrazide (dihydrate) (XXIV)	58.6	234	$C_{20}H_{16}N_4OS$ (360.44)	15.55 15.43	a) C=N 1605 C=O 1680 b) 243.3 (1.82); 265.7 (1.80); 294.1 (2.29); 384.6 (1.34)
VII.	Thiocarbon-hydrazide (dihidrate) (VIII.)	56.1	265	$C_{29}H_{24}N_6S_3$ (552.72)	15.20 15.51	a) C=N 1630

* The spectrum was also registered by Canquil and Casadevall [6]

Table 2

Microbiostatic activity of compounds I, VI, IX-XVI

Compound	Diameter of the zone of complete inhibition (in mm)				
	organisme				
	SA [a]	SH [b]	BS [c]	EC [d]	PA [e]
I	20	—	18	—	—
VI	20	—	—	—	—
IX	18	—	20	—	12
X	20	—	—	10	14
XI	22	12	18	10	14
XII	18	—	—	—	—
XIII	20	—	—	—	16
XIV	16	10	—	—	16
XV	16	—	—	10	—
XVI	16	—	—	—	10

a) SA = Staphylococus aureus
b) SH = Staphylococus haemolyticus
c) BS = Bacilus subtilis
d) EC = Escherichia coli
e) PA = Pseudomonas aeruginosa
f) The compound was considered inactive when the diameter of the inhibition zone was smaller than 10 mm.

The new compounds were characterised by IR and electronic spectra.

In the IR spectra of all derivatives the $\nu_{C=N}$ band (1605 — 1630 cm^{-1}) is present. The spectra of compounds XII, XIII, XV and XVI also show the $\nu_{C=O}$ band situated at higher frequencies as compared with the $\nu_{C=N}$ one.

If the UV—VIS spectra of the condensation products VI, IX... XVI are compared with that of the starting substance I, a red shift of the first band, situated in the 370—450 nm region, may be observed excepting XIII and XV. By the acridine derivative (XVI) this shift is unexpectedly marked, taking into account the same band in the spectra of the parent compounds I and XXIII [7] or in those of the other condensation products specified in Table 1.

The microbiostatic activity of I, VI, IX ... XVI was measured by the diffusion test procedure against five Gram-positive and Gram-negative bacteria. The data are listed in Table 2.

3-Formyl-10-methyl-phenothiazine (I) inhibits the growth of Staphylococus aureus and Bacillus subtilis. All the condensation products prepared by us exhibit nearly the same activity against Staphylococus aureus but only two, IX and XI, also against Bacillus subtilis. In two cases, VI and XII, the blocking of the formyl group of I results in the lowering of the bacteriostatic activity. If in the Schiff's base VI a hydroxyl group was introduced, the activity increased as more as we pass from the ortho- (IX) to the para-derivative (XI). Moreover the last one, XI, shows the largest spectrum among the compounds tested by us.

Experimental. The melting points were determined in glass capillaries and are uncorrected. For the recording of the IR spectra in KBr pellets a double beam spectrophotometer Carl Zeiss Jena (type UR — 10) was used. The electronic spectra were recorded in methanol on a double-beam spectrophotometer „SPEKORD" Carl Zeiss Jena.

3-Formyl-10-methyl-phenothiazine (I), was prepared by the Bodea *et al.* [8] procedure with the following amendament: the crude reaction product was extracted with chloroform and to the solution ligroine was stepwise added until a resinous impurity precipitates. After filtering, the light-yellow solution was concentrated and thus I, m.p. 87 °C was obtained. (Lit [1] m.p. 89 °C).

Thiocarbazide dihydrate (VIII). To a solution of 125 g thiocarbonyl-bis-thioglycollic acid (XXV) in 1000 ml butanole, 100 ml 80% hydrazine hydrate were added under stirring, for ten min. The reaction is exothermic. From the warm mixture the aqueous layer was separated and cooled. Thus VIII precipitated as white needles. After recrystallization from water, 27 g (34.4%) pure substance were obtained. M.p. 123°C. (Lit. [9] for the anhydrous substance m.p. 168°C). IR 600, 780, 945, 1020, 1150, 1300, 1545, 1670, 3220, 3285 cm^{-1}. $CH_{10}N_4O_2S$ (142.18). Calcd. N% 39.41. Found 40.11.

Condensation products of 3-formyl-10-methyl-phenothiazine. (General method). A mixture of 1 part I and 3 parts amino- or hydrozino-derivative (VIII, XVII ... XXIV) in 15 ... 25 ml absolute ethanol was boiled for two hours and hot filtered. By cooling the solution the reaction products precipitated as yellow crystalls excepting XIV which is orange. The crude products were recrystalized from ethanol or acetone-water, in some cases in the presence of charcoal.

Acknowledgments. The authors are grateful to Dr. V. Chiorean (IMF Cluj-Napoca) for the testing of the biological activity and to Dr. Jana Rusu (ICCF Cluj-Napoca) for the recording of the UV—VIS spectra.

REFERENCES

1. N. P. Buu — Hoi, N. Hoan, J. Chem. Soc., **1951,** 1834.
2. A. Burger, A. C. Schmalz, J. Org. Chem., **19,** 1841 (1954).
3. G. Cauquil, A. Casadevall, Bull. Soc. chim. France, **1955,** 768.
4. W. Kremers, J. W. Steele, Canad. J. Chem., **45,** 745 (1967).
5. S. Takeuchi, C. Higashikaze; A. Kawabata, S. Esumi, K. Sasaki, S. Kawabata, T. Saida, Y. Inoue, T. Yamamoto, Jpn. Kokai Tokkyo Koho, 80 45, 657. Chem. Abstr., **93,** 210257k (1980).
6. G. Cauquil, A. Casadevall, Bull. Soc. chim. France, **1955,** 1061.
7. A. Albert, J. Chem. Soc., **1965,** 4653.
8. C. Bodea, V. Fărcăşan, I. Oprean, Rev. Roumaine Chim., **10,** 1103 (1965).
9. R. Stolle, P. E. Bowles, Ber. dtsch. chem. Ges., **41** 1099 (1908).

STUDIA UNIV. BABEŞ—BOLYAI, CHEMIA, XXXI, 2, 1986

ISO—K_x AND ISO-CONVERSION DIAGRAMS FOR THE HYDROGENATION OF CARBON MONOXIDE

JÁNOS ZSAKÓ* and MÁRTA FEKETE*

Received: April 14, 1986

ABSTRACT. — Standard free energy changes are calculated for a number of 40 reactions occurring in the conditions of the Fischer-Tropsch synthesis. *log P vs T* curves are constructed corresponding to $K_x = 1$ and to different equilibrium conversion values for temperatures comprized between 298 and 1000 K. Correlations between iso-K_x and isoconversion curves are discussed, as well as the usefulness of these diagrams.

Introduction. The Fischer—Tropsch synthesis is the main tool of the transformation of coal into hydrocarbons. Consequently, the thermodynamics of the reactions occuring under the conditions of catalytic hydrogenation of carbon monoxide are extensively discussed in many papers [1]. Generally heats, standard free energies, equilibrium constants are calculated for a grea. number of possible reactions, in a large temperature interval, comprized bett ween 0 and 900°C. The diagrams and tables of this type yield very usefu- pieces of information, but they are not able to give a direct and clear picl ture of the possible equilibria. Since the majority of the reactions involved- occur with a variation of the number of moles, the equilibrium conversions, depend very much on the pressure. Therefore, isoconversion diagrams have been constructed for several reactions, by plotting the pressure at which a given conversion, e.g. 80%, is attained, as a function of the temperature.

In order to obtain a clearer picture of the thermodynamics of the above mentioned hydrogenation reactions, in the present paper calculations are performed, by using literature data for a number of 40 reactions.

Theoretical. The equilibrium constant $K_\varphi(T)$ of a reaction in a homogeneous gaseous phase, at the temperature T, can be given by means of the equilibrium fugacities, φ_i, of the components and it is related to the standard free energy change of the reaction, ΔG^0_T, by the usual definition

$$-\Delta G^0_T = RT \ln K_\varphi(T) \tag{1}$$

Since under the conditions of the Fischer—Tropsch synthesis, the upper limits of pressure and temperature are of 30 to 40 atm and 400°C, in the expression of the equilibrium constants, as a first approximation, instead of the fugacities, the partial pressures, P_i, can be used, which are related to the overall pressure P by the relation $P_i = x_i P$, where x_i stands for the molar fraction of the component i.

* *University of Cluj-Napoca, Faculty of Chemical Technology, 3400 Cluj-Napoca, Romania*

Consequently, Eq. (1) can be written in the following form:

$$-\Delta G_T^0 = RT \ln K_x(T) + \Delta\nu RT \ln P \tag{2}$$

where $K_x(T)$ and $\Delta\nu$ stand for the equilibrium constant expressed by means of the molar fractions, and for the variation of the number of moles in the reaction, respectively.

Let us express $\log P$ from Eq. (2):

$$\log P = -\frac{\Delta G_T^0}{2.303\Delta\nu RT} - \frac{\log K_x}{\Delta\nu} \tag{3}$$

Eq. (3) allows us to calculate the pressure at which K_x attains a wanted value. For $K_x = 1$ one has:

$$\log P = -\frac{\Delta G_T^0}{2.303\,\Delta\nu\, RT} \tag{4}$$

By using Eq. (4), $\log P$ *vs.* T diagrams can be constructed for $K_x = 1$. Other iso—K_x diagrams may be obtained by using Eq. (3). In order to construct an iso-conversion curve of the reaction, one must calculate the K_x value, ensuring the wanted conversion, and use the same Eq. (3). Thus, in the case of a given reaction, an iso—K_x curve is also an iso-conversion curve, by presuming that the starting system is a stoichiometric mixture of the reagents. But if one wants to compare different reactions, the curves constructed for the same K_x, will not correspond to the same conversion. Therefore, the diagrams constructed for the same equilibrium conversion of a stoichiometric mixture, are more relevant, than the diagrams, corresponding to the same K_x value.

Calculation of ΔG_T^0. Three main types of reactions were considered, leading by hydrogenation of carbon monoxide to the formation of paraffins, monoolefins and alcohols, respectively. Each of them can produce either water (marked A), or carbon dioxide (marked B). The stoichiometric equations of the reactions and the variations of the number of moles are the following:

$$(2n+1)H_2 + nCO = C_nH_{2n+2} + n\,H_2O; \quad \Delta\nu = -2n \tag{IA}$$

$$(n+1)\,H_2 + 2nCO = C_nH_{2n+2} + nCO_2; \quad \Delta\nu = -2n \tag{IB}$$

$$2n\,H_2 + n\,CO = C_nH_{2n} + n\,H_2O; \quad \Delta\nu = -2n+1 \tag{IIA}$$

$$nH_2 + 2n\,CO = C_nH_{2n} + n\,CO_2; \quad \Delta\nu = -2n+1 \tag{IIB}$$

$$2n\,H_2 + n\,CO = C_nH_{2n+1}\,OH + (n-1)\,H_2O; \quad \Delta\nu = -2n \tag{IIIA}$$

$$(n+1)\,H_2 + (2n-1)\,CO = C_nH_{2n+1}OH + (n-1)\,CO_2; \quad \Delta\nu = -2n \tag{IIIB}$$

By taking the difference between the stoichiometric equations of the A type and B type reactions, one obtains the equation of the water gas reaction:

$$H_2O + CO = H_2 + CO_2 \tag{IV}$$

More exactly:

$$(IB) - (IA) = (IIB) - (IIA) = n(IV)$$

$$\text{and } (IIIB) - (IIIA) = (n-1)(IV)$$

Thus, by calculating ΔG_T^0 for the reactions (IA), IIA), (IIIA) and (IV), the standard free energy changes of B type reactions are obtained as:

$$\Delta G_{T,IB}^0 = \Delta G_{T,IA}^0 + n\Delta G_{T,IV}^0, \quad \Delta G_{T,IIB}^0 = \Delta G_{T,IIA}^0 + n\Delta G_{T,IV}^0$$
$$\text{and} \quad \Delta G_{T,IIIB}^0 = \Delta G_{T,IIIA}^0 + (n-1)\Delta G_{T,IV}^0 \tag{5}$$

Obviously, for $n = 1$, reactions (IIIA) and (IIIB) are identical.

The calculation of ΔG_T^0 has been performed by using the usual relation:

$$\Delta G_T^0 = \Delta H_{298}^0 + \int_{298}^{T} \Delta\Sigma\nu C_P dT - T\Delta S_{298}^0 - T\int_{298}^{T} \frac{\Delta\Sigma\nu C_P}{T} dT \tag{6}$$

where ΔH_{298}^0 and ΔS_{298}^0 stand for the standard heat and standard entropy change of the reaction, respectively, and $\Delta\Sigma\nu C_P$ means the sum of the isobar molar heats of the products, multiplied each of them by its stoichiometric coefficient, minus the same sum for the reagents. ΔH_{298}^0 and ΔS_{298}^0 values were calculated by using tabulated standard formation enthalpy and standard entropy values for the compounds involved [2]. For the molar heats tabulated polynominals were used [2].

Calculations have bean performed for $T = 298$, 400, 500, 600, 700, 800 900 and 1000 K.

$K_x = 1$ diagrams. The *log P vs. T* diagrams were constructed by using calculated ΔG_T^0 values and Eq. (4).

The thermodynamic characteristics of isomers are different and consequently, also the P values, coresponding to $K_x = 1$, are different. As seen from Table 1, these differences are not important at all. Therefore, the *log P vs. T* plots are performed only for a single isomer, viz. for the normal one.

Table 1

log P values (P in atm), ensuring $K_x = 1$ for reactions (IIA) and (IIB), leading to the formation of C_4H_8 isomers

Isomer	IIA			IIB		
	298 K	600 K	1000 K	298 K	600 K	1000 K
Buthene-1	−7.37	−0.61	2.17	−10.24	−1.42	2.15
cis-Buthene-2	−7.49	−0.63	2.20	−10.36	−1.44	2.18
trans-Buthene-2	−7.56	−0.66	2.18	−10.44	−1.47	2.16
2-Methyl-Propane	−7.64	−0.69	2.17	−10.51	−1.50	2.14

The temperature dependence of $\Delta G^0_{T,IV}$ is of capital importance for the general features of the diagrams of A and B type reactions. As seen from Table 2, the free energy variation of reaction IV is negative, up to about 1000 K, where it becomes vanishingly small. Consequently, at this temperature both ΔG^0_T values and P values corresponding to $K_x = 1$, will have practically the same value for B type reactions as for the A type ones.

Table 2

Standard free energy variation of reaction (IV)

T, K	298	400	500	600	700	800	900	1000
ΔG^0_T, kJ	−28.7	−24.4	−20.4	−16.4	−12.4	−8.5	−4.7	−0.8

Some illustrative examples of $K_x = 1$ curves are presented in Figs. 1—4. In these figures, the curves give the P values at which K becomes equal to unity. Since reactions (I) — (III) occur with diminution of the number of moles, in all cases K_x increases with increasing P, i.e. above the before mentioned curves one has $K_x > 1$, below them $K_x < 1$.

As seen, in all the temperature range considered, K_x values of B type reactions are higher than the K_x values of the analogous A type reactions, at the same pressure. From Fig. 1 it is obvious, that the formation of paraffins is more favourable from thermodynamic point of view, than the formation of mono-

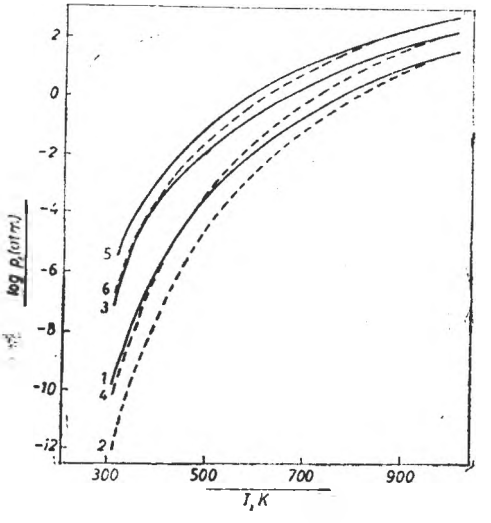

Fig. 1. $K_x = 1$ diagrams for $n = 2$.
1,2—C_2H_6; 2,3—C_2H_4; 5,6—C_2H_5OH;
Type of reaction: full lines — A; dashed lines — B.

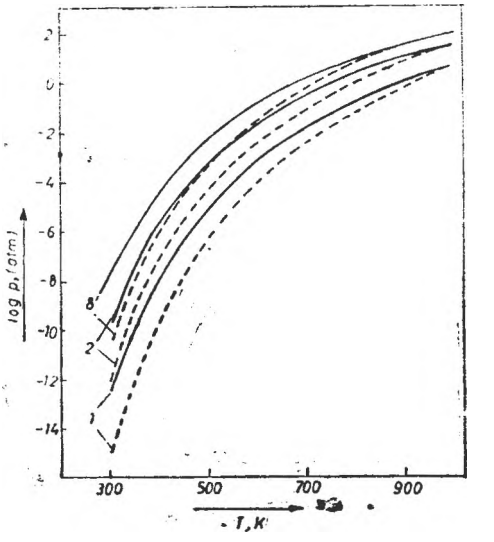

Fig. 2. $K_x = 1$ diagrams for reactions (IA) and (IB).
1 — CH_4; 2 — C_2H_6; 8 — C_8H_{18}.

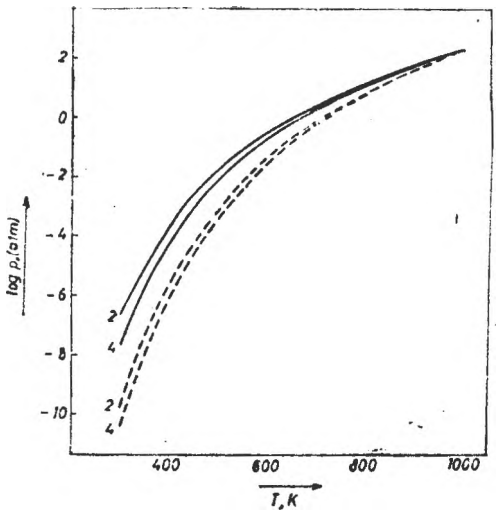

Fig. 3. $K_x = 1$ diagrams for reactions (IIA) and (IIB).
2 — C_2H_4; 4 — C_4H_8.
Type of reactions: as in Fig. 1.

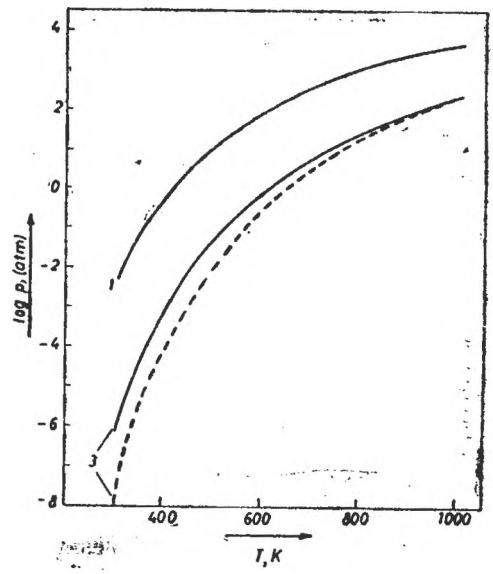

Fig. 4. $K_x = 1$ diagrams for reactions(IIIA) and (IIIB).
1 — CH_3OH; 3 — C_3H_7OH.
Type of reactions: as in Fig. 1.

olefins, and the latter is more favourable than the formation of alcohols, containing the same number of C-atoms. This means, that at the same P and T, and for the same n value, one has:

$$K_{x,I} > K_{x,II} > K_{x,III}$$

Figs. 2—4 show that with increasing number of C-atoms increases the P value, necessary to ensure $K_x = 1$, i.e. at the same P and T, the K_x value decreases with increasing n. At small n-values K_x decreases rapidly, but at higher n-values the length of the hydrocarbon chain has practically no influence.

Iso conversion curves. By using a stoichiometric mixture of the reagents as starting system, the equilibrium conversion, $\bar{\alpha}$, will be a unique function of the equilibrium constant K_x. By comparing the same reaction, e.g. (IA), corresponding to different n values, a given conversion corresponds to very different K_x values, depending on n. Some illustrative examples are given in Fig. 5, for reaction (IA). As seen, for extreme conversions, like 0.01 or 0.9, the K_x for the formation of C_8H_{18} differs with over 10 orders of magnitudes from the K_x value of the CH_4 formation. Differences are less in the case of medium conversions, as $\bar{\alpha} = 0.5$.

By taking into account Eqs. (3) and (4), one can see, that isoconversion curves can be obtained from the $K_x = 1$ curves, by using a correction:

$$\Delta \log P = -\frac{\log K_x}{\Delta v} \tag{7}$$

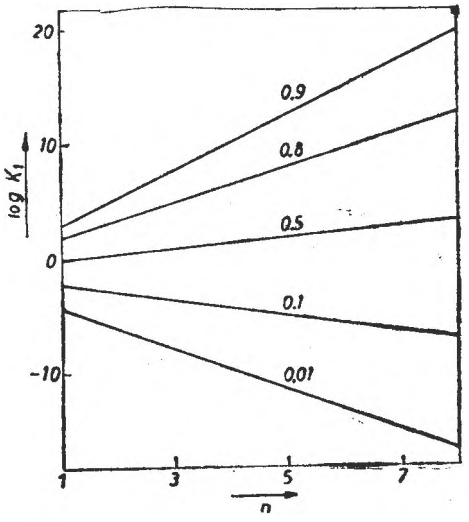

Fig. 5. K_x value of reaction (IA), ensuring a given conversion, as a function of the number of C-atoms.
The figures indicate the $\bar{\alpha}$ values.

depending on the type of the reaction, on n and on $\bar{\alpha}$. The graphical plot of the correction (7) is given in Fig. 6 for reactions (IA) and (IB) as function of n. As seen, in the case of CH_4 the increase of $\bar{\alpha}$ from 0.01 po to 0.9, needs a much larger increase of P than with C_6H_{14}. This is also illustrated by Fig. 7.

Figure 6 shows the correction (7) to be rather small in the case of $\bar{\alpha} = 0.5$, especially for $n = 1$. Generally, the isoconversion curves for $\bar{\alpha} = 0.5$ do not differ very much from the corresponding $K_x = 1$ curves. As seen from Table 3, the *log P* values corresponding to $K_x = 1$ and to $\bar{\alpha}=0.5$ are rather close to each other, since the equilibrium conversion corresponding to $K_x = 1$ is not very far from 0.5, as seen from the last line of Table 3.

In Fig. 8 several isoconversion curves are presented for $n = 1$. As seen, in the

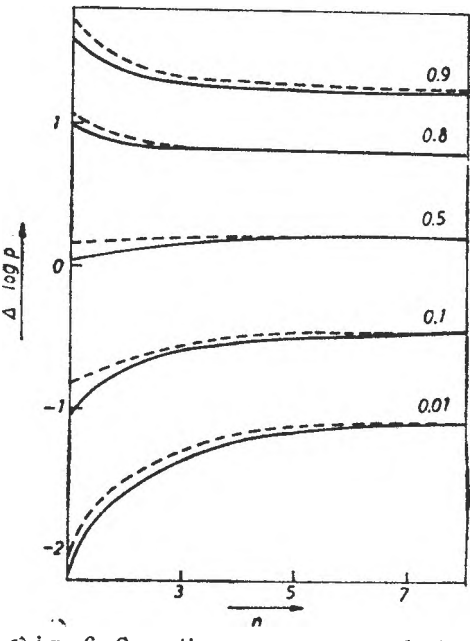

Fig. 6. Corrections necessary to obtain iso-conversion curves from $K_x = 1$ diagrams in the case of reactions (IA) and (IB). The figures indicate the $\bar{\alpha}$ value. Type of reaction: as in Fig. 1.

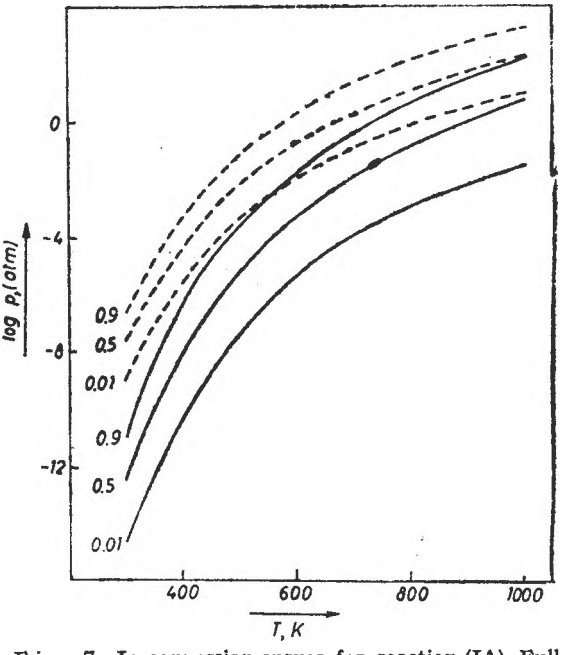

Fig. 7. Isoconversion curves for reaction (IA). Full line: formation of CH_4. Dashed line: formation of C_6H_{14}. Figures indicate the $\bar{\alpha}$ value.

Table 3

log P values (*P* in atm), ensuring $K_x = 1$ and $\bar{\alpha} = 0.5$, respectively, in reaction (IA)

T, K	CH_4		CH_6		C_8H_{18}	
	$K_x = 1$	$\bar{\alpha} = 0.5$	$K_x = 1$	$\bar{\alpha} = 0.5$	$K_x = 1$	$\bar{\alpha} = 0.5$
298	−12.48	−12.41	−9.47	−9.34	−7.84	−7.61
600	−3.17	−3.10	−1.62	−1.50	−0.75	−0.53
1000	0.69	0.75	1.62	1.75	2.14	2.37
$\bar{\alpha}$	0.473		0.429		0.338	

most common conditions of the Fischer-Tropsch synthesis, one has for reaction (IA) and (IB) the conversion $\bar{\alpha} > 0.9$ and for reaction (III) the conversio $\bar{\alpha} < 0.01$, i.e. the methanol formation is completely avoided.

Although in the Fischer-Tropsch synthesis the main problem is to find the appropriate catalyst, the knowledge of the thermodynamics of the possible reactions is of capital importance and especially the iso-conversion curves can be very useful. For their construction it is necessary to solve equations of higher order, viz. this order is equal to $3n + 1$ in the case of reactions (I) and $3n$ with reactions (II) and (III). The construction of $K_x = 1$ diagrams is very easy, nevertheless, they can give also very valuable information.

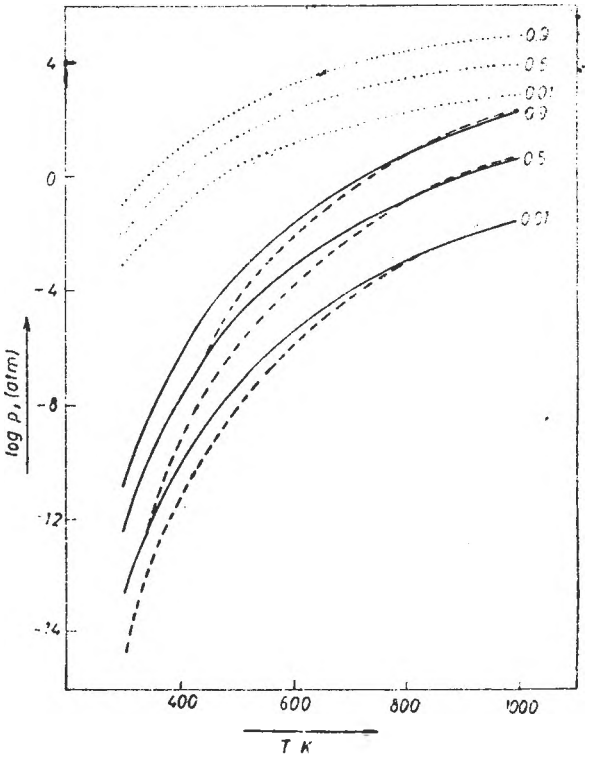

Fig. 8. Isoconversion curves for $n = 1$. Reaction: full line — (IA); dashed line — (IB); dotted line — (III). Figures indicate the $\bar{\alpha}$ value.

REFERENCES

1. R. B. Anderson, in *„Catalysis"*, vol. IV. Edited by Emmett, P. H., Reinhold Publ. Corp. New York, 1956.
2. *„Kratkii spravochnik fiziko-khimicheskih velichin"*, Edited by Mishchenko, K. P. and Ravdel, A. A., Izd. Khimia, Moscow—Leningrad, 1965, p. 8—25.

STUDIA UNIV. BABEŞ—BOLYAI, CHEMIA, XXXI, 2, 1986

OHMIC CHARACTERISTICS OF ATP-ASE IONOPHORES MODIFIED BLM

ŞT. HOBAI*, L. ONICIU** and C. LITEANU**

Received: October 8, 1986

ABSTRACT. — A sephadex gel filtration of a tryptic digestion product of sarcoplasmic reticulum, incorporated in oxidized cholesterol BLM showed similar ohmic properties with those described in many previous papers. The shapes of conductance-concentration and conductance-pH characteristics suggested the fact that in ATP-ase fragments there is at least a site for Ca^{2+} having the properties of a weak acid which by association with Ca^{2+} produces a conformational change of protein, determining the ionophoric activity.

Fifteen years ago [1] a protein of about 100 kDa, (Ca, Mg) — ATP-ase, was isolated from sarcoplasmic reticulum (SR). This enzyme, called „calcium pump", plays an important part in the muscle relaxation, the calcium influx in SR, against concentration gradient, being the result of a cycle in which (Ca, Mg) — ATP-ase passes through different energetic states as a consequence of phosphorylation with ATP [2].

S h a m o o, M a c L e n n a n, *et al.* [3] studied the permeability for calcium and other cations of solubilized (Ca, Mg) — ATP-ase modified BLM. Also, the Ca^{2+}-ionophoric activity of some fragments resulted from its triptych digestion was studied [4, 5, 6, 7] (for review see 7). It was suggested that the structure able to transport selectively by Ca^{2+} through membranes is a subunit of the enzyme representing about the fifth part of it [8] or even less [6]. From these data S h a m o o *et al.* proposed molecular models for the active transport of Ca^{2+} into SR [9] and a spatial arrangement of (Ca, Mg) — ATP-ase in the SR bilayer [10].

In our paper, on the basis of data obtained from ohmic measurements, we tried to bring new contribution concerning the ionophoric activity mechanism of some fragments obtained in triptych digestion of SR.

Materials and Methods. The BLM-forming solution consisted of oxidized cholesterol in n-octane and was obtained by boiling a cholesterol (BDH) 4% solution in n-octane (Riedel—Haen) under O_2 current [11].

In a relon block with two secant cylindrical pits, one of them having the lateral walls made of glass, a cylindric teflon cup was introduced in one of the pits. The cup fits exactly in the pit and in the wall has an orifice with 1 mm diameter directed to the next pit. After filling the system with an electrolyte, a calomel electrode was introuced in each compartment. Some tens of microlitres of BLM-forming solution were spread on the cup orifice. Due to London-Van der Waals forces the membrane spontaneously became thinner as a result of the solvent and lipid molecules elimination, tending to a bilayer state. For the observation of the „black film" a beam of light was directed upon the orifice from a 24 V bulb, which may be observed by a microscope after the reflexion on the already formed membrane.

* *Medical and Pharmaceutical Institute, 38 G. Marinescu str., 4300 Tg. Mureş, Romania*
** *University of Cluj-Napoca, Faculty of Chemical Technology 3400 Cluj-Napoca, Romania*

In the electrical circuit for BLM conductance measurements the voltage applied by a potentiometer was measured by a milivoltmeter (MV-84 Prăcitronic). The current through the BLM was measured by a high impedance current amplifier (picoamperometer K-201) in series with the membrane. The triphasic system: aqueous solution/BLM/aqueous solution was thermostated and screened by a Faraday cage.

The ATP-ase ionophores preparation consisted in the first step of the SR vesicles (R_1-washed) isolation [1]. R_1-washed having 6,1 U as specific enzymatic activity (Lowry method for protein determination, bovine serum albumine as standard; colorimetric method for phosphate determination, ATP as enzymatic reaction substrate) was left overnight to freeze. In the second step the triptych digestion of R_1-washed was performed using the method described by Stewart and MacLennan [12] in which the following weight ratios were chosen: trypsin/protein = 1/25 and trypsin/trypsin inhibitor = 1/4 using pig pancreatic trypsin (Merck) and soybean trypsin inhibitor (Cell. Biol. Pathol. Inst. Bucharest). During the last step natrium deoxycholate (DOC) (Riedel—Haen) was added to the inhibited sample in an up to 1% concentration. The solution was passed through a sephadex column G-100 (medium). The elution was made with 1% DOC solution (pH = 8.0) and two protein fractions were obtained. The second fraction was retained and after dialysis against TRIS—Cl 10 mM at 4°C (pH = 8.0) it was liophylised. The resulting flakes were preserved in refrigerator having in view further study of ionophoric activity.

Results and Discussions. After injection of the BLM's-forming solution in the electrochemical cell containing the buffer solution: TRIS—Cl 5 mM, $CaCl_2$ 5 mM (pH = 7.5) (symmetrical cell), a 50 mV potential was applied by means of the potentiometer. The cell conductance was measured for several minutes. The same procedure was performed in the presence of 10 μg ionophoric protein/ml buffer solution. The average curves of the conductance variation in time are shown in Fig. 1. The vertical bars between arrows show the intervals of variance of the conductance values. The number of BLM tested is written between paranthese. There is a difference of more than one order of magnitude between the unmodified BLM cell conductivity and those of modified BLM. Since the conductance of calomel electrodes and aqueous solutions are much greater than those of the cell, it results that the measurements are performed under clamp-voltage conditions.

The current-voltage characteristics of the symmetrical cells containing different salts are shown in Fig. 2. They are traced by the points which rep-

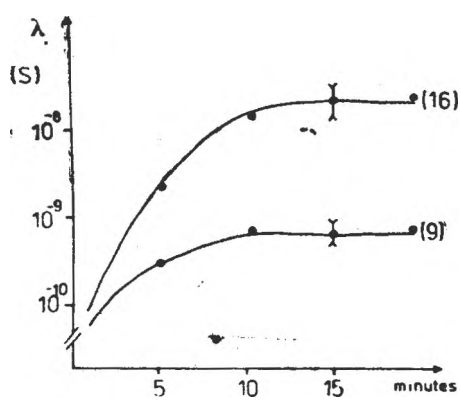

Fig. 1. Conductance-time curves.

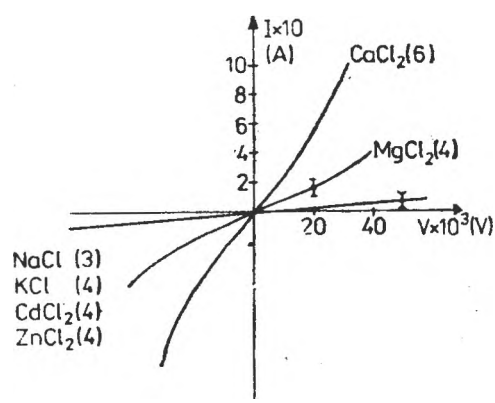

Fig. 2. Current-voltage characteristics (symmetrical cell).

resent the averages of the individual values. The vertical bars between the horizontal segments represent the double values of the standard deviations. The values of the slopes in origin estimate the conductances at zero voltage. The conductivities sequence: $BaCl_2 > CaCl_2 > MgCl_2 > NaCl$, KCl, $CdCl_2$, $ZnCl_2$ is identical with that found under biionic conditions [3].

Fig. 3 shows the inhibitor effect produced by $CdCl_2$ upon BLM conductivity if this salt was added after BLM formation. These data are consistent with those obtained in the study of a well-defined fragment of (Ca, Mg) — ATP-ase [4].

Fig. 4 represents the current-voltage characteristic of a cell with $CaCl_2$ concentration gradient. The concentrations ratio of the two compartments $c''/c' = 1/2$. The abscissa intercept gives the value of the potential difference at zero current. The compartment containing the most diluted solution had the more pozitive potential, the potential difference being much below that generated by a cation-selective membrane at the same concentration difference. The potential difference grew in a subnernstian manner with the concentration ratios. From the point of view of the electro-diffusion model it follows that these BLM's are more permeable for cations (Ca^{2+}) than for anions (Cl^-) and between the two permeabilities there is only a small difference.

An apparent contradiction results from the fact that these BLM's had a great conductivity for alkaline-earth chlorides without being permeable for other metal chlorides.

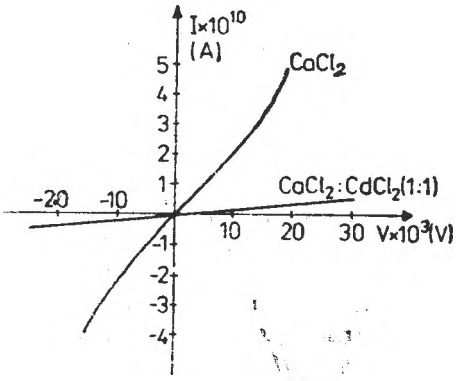

Fig. 3. The effect of added $CdCl_2$ upon Ca^{2+}-ionophoric activity.

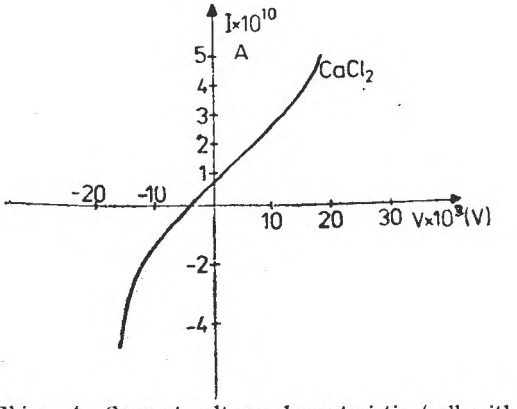

Fig. 4. Current-voltage characteristic (cell with concentration gradient).

The symmetrical cell conductances were also measured, the cell containing $CaCl_2$ at different concentrations and the same BLM (Fig. 5). A point of inflexion is remarked at 10^{-3} M $CaCl_2$. A curve of similar shape was reported in the study of the ionophoric activity of succinylated (Ca, Mg) — ATP-ase [3]. It suggests the fact that in ATP-ase fragments there is at least a site for Ca^{2+} which should play an important part in their ionophoric activity. The Ca^{2+}

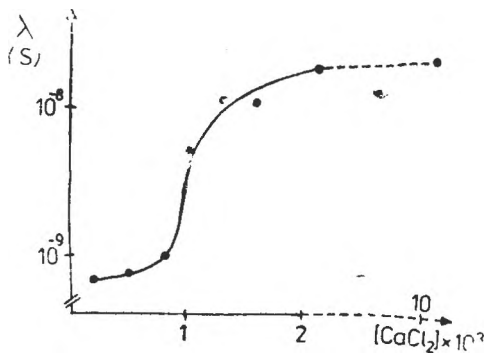

Fig. 5. Conductance — $CaCl_2$ concentration characteristics.

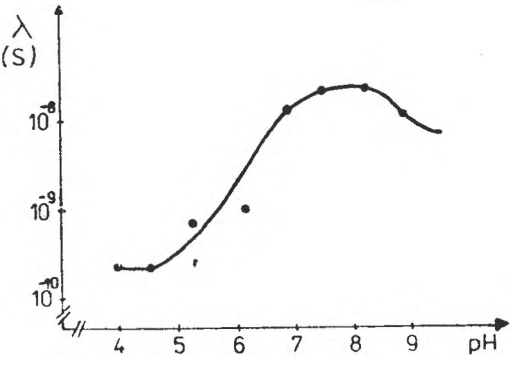

Fig. 6. Conductance — pH characteristic.

association constant can be graphically estimated as being approximately 10^3 M^{-1}.

In Fig. 6 the growth of BLM conductance with pH (up to pH = 8) is noticeable, it suggests the fact that the site has the properties of a weak acid.

The inhibitor effect of Cd^{2+} suggests a „poisoning" of the site. By accepting the presence of a site at which by association of Ca^{2+} a conformational modification occurs determining an ionophoric activity, the above mentioned contradiction disappears.

REFERENCES

1. D. H. MacLennan, *J. Biol. Chem.*, **245**, 4508 (1970).
2. L. De Meis, and A. L. Vianna, *Annu. Rev. Biochem.*, **48**, 275 (1979).
3. A. E. Shamoo, and D. H. MacLennan, *Proc. Nat. Acad. Sci. USA*, **71**, 3522 (1974).
4. A. E. Shamoo, *J. Membr. Biol.*, **43**, 227 (1978).
5. J. J. Abramson, and A. E. Shamoo, *J. Membr. Biol.*, **44**, 233 (1978).
6. T. R. Herrmann, and A. E. Shamoo, *Biochim. Biophys. Acta*, **732**, 647 (1983).
7. A. E. Shamoo, and T. R. Herrmann, *USSR—Adv. Mod. Biol.*, *91*, 350 (1971).
8. A. E. Shamoo, T. E. Ryan, P. S. Stewart, and D. H. MacLennan, *J. Biol. Chem.*, **251**, 4147 (1976).
9. A. E. Shamoo, and D. A. Goldstein, *Biochim. Biophys. Acta*, **472**, 13 (1977).
10. T. R. Herrmann, and A. E. Shamoo, Isolation and Use of Ionophores for Studying Ion Transport across Natural Membranes, in *„Membranes and Transport"*, A. N. Martonosi, ed., Plenum Press, New York and London, (1982).
11. H. T. Tien, S. Carbone and E. A. Davidowicz, *Nature (London)*, **212**, 719 (1966).
12. S. P. Stewart, and D. H. MacLennan, *J. Biol. Chem.*, **249**, 985 (1974).

STUDIA UNIV. BABEŞ—BOLYAI, CHEMIA, XXXI, 2, 1986

INFRARED SPECTROSCOPIC INVESTIGATION OF THE ADSORPTION PRODUCTS OF 8-HYDROXYQUINOLINE ONTO MALACHITE

GABRIELA OPREA* and EMIL CHIFU**

Received: October 15, 1986

ABSTRACT. — The compounds formed during flotation with 8-hydroxyquinoline (oxyne) at the surface of malachite have been studied by infrared spectroscopy.

By using the potassium bromide pelleting technique the infrared spectra were run for natural malachite, 8-hydroxyquinoline, copper (II) oxynate, as well as for malachite treated with a solution of 8-hydroxyquinoline.

By comparing the obtained spectra the conclusion is drawn that the compound formed at the surface of malachite is copper oxynate.

Introduction. The solid-gas interface has been largely subjected to experimental studies by infrared spectroscopy [1—3]. The solid-liquid interface, however, is more difficult to investigate, especially when the liquid is an aqueous solution of reagents, as used in flotation processes.

The methods employed in studying the solid-liquid adsorption processes by infrared spectroscopy are similar to those applied to the solid-gas interface. The work of Little *et al.* [1] summarizes several experimental results and techniques in the infrared spectroscopy of adsorbed species, and Rochester [4] makes a re-examination of the methods, giving new examples and explanations.

Infrared spectroscopic determinations have also been used for surveying the formation of certain species at the surface of minerals during adsorption of various reagents, and there are many reports on this subject [5—14].

The chelation agents, organic reagents acting as precipitants in solution, are lately used in the processes of separation by flotation of ores as well. These reagents are suited to ores containig oxidated minerals and they work as collectors or activators [11—14].

In our investigations and experiments we were interested in the collector properties exerted by some chelation reagents during the flotation of oxidated Cu(II), Pb(II), and Zn(II) minerals.

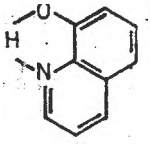

(I)

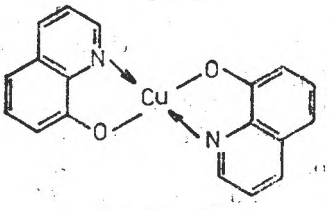

(II)

* *Lycée of Natural Sciences, 4800 Baia-Mare, Romania*
** *University of Cluj-Napoca, Faculty of Chemical Technology, 3400 Cluj-Napoca, Romania*

One of these studied reagents, namely 8-hydroxyquinoline (structure I) or oxyne, performs important copper recoveries in the flotation of malachite — $Cu_2(OH)_2CO_3$ — and it proves a good collector.

In solution, 8-hydroxyquinoline forms insoluble, stable chelate compounds with many metals, copper included, and these compounds have (II)-type structures.

In the present work we report some results obtained by an infrared spectroscopic investigation, on compounds formed at the surface of malachite in the course of flotation with 8-hydroxyquinoline (oxyne).

Experimental. The recording of infrared spectra was performed by a UR 20, Carl Zeiss Jena, double beam spectrometer; KBr, NaCl, and LiF prisms; resolution 0.6—2000 cm^{-1}; region 400—5000 cm^{-1}.

We assumed that copper oxynate was formed at the surface of malachite treated with the chelation reagent. This complex was prepared as follows: 150 cm^3 of 0.1 M aqueous $Cu(NO_3)_2 \cdot 3H_2O$ was treated with 100 cm^3 of 0.3 M oxyne in acetic acid at pH = 2.5; the yellow precipitate formed was filtered through a G_4 crucible under vacuum, washed with 10% acetic acid, then with water; after that it was dessicated at 110°C for one hour.

The mineral was ground in an agate mortar up to the granulation of $\approx 2\mu$. 100 mg of malachite thus prepared was treated with 25 cm^3 acetone solution of 8-hydroxyquinoline, stirred for 5 minutes, then filtered through a filter crucible, washed and dried in air.

Using the potassium bromide pelleting technique, we recorded the infrared spectra in the region 400—1700 cm^{-1} for: malachite (Fig. 1a); 8-hydroxyquinoline (Fig. 1b); copper oxynate (Fig. 1c); and malachite after the treatment with acetone solution of oxyne (Fig. 1d).

The spectrum in Fig. 1d, run on malachite after the treatment with the chelation agent, exhibits a number of supplementary bands as compared to the spectrum of malachite (Fig. 1a). Some of the bands belonging to copper oxynate can be noticed: 1600—1580 — 1505 — 1470 — 1390 — 1330 — 1240 — 528 cm^{-1}, what proves the formation of this complex at the surface of malachite treated with 8-hydroxyquinoline.

A very strong band arises at 1290 cm^{-1} in the spectrum of malachite. It is shifted both against copper oxynate, where it is found at 1285 cm^{-1}, and against 8-hydroxyquinoline, where it is situated at 1293 cm^{-1}. A similar phenomenon is also noticed in the 745 cm^{-1} band of the malachite spectrum. It is very strong at 740 cm^{-1} in the complex, and at 742 cm^{-1} in 8-hydroxyquinoline. The bands at 778 and 802 cm^{-1} from the copper oxynate do not arise in the malachite spectrum; instead, a band arises at 788 cm^{-1}, while in 8-hydroxyquinoline it is situated at 780 cm^{-1}.

There are, however, numerous bands of oxyne which are absent in the case of malachite: 1515 — 1415 — 1385 — 1230 — 1215 — 1180 — 712 cm^{-1}.

Conclusions. The infrared spectra studied in the present work give evidence of the formation of copper oxynate at the surface of malachite during the flotation process in which 8-hydroxyquinoline is used as a collector. This evidence is supported by the numerous bands belonging to copper oxynate in the infrared spectrum of malachite treated with 8-hydroxyquinoline.

Yet, a reduced number of bands in the spectrum of malachite treated with the chelation agent is shifted both against their positions in the spectrum of the complex, and against those in the spectrum of the reagent. We suggest, in this case, the possible formation of some more compounds at the surface of malachite, with stoechiometric compositions other than that of the copper oxynate. It must also be taken into account that the reagent fixed onto the mineral surface in the flotation process is in a much smaller concentration and more unequally distributed than in the pure complex. A similar phenomenon has also been found by other authors [15] when treating malachite with salicyl-

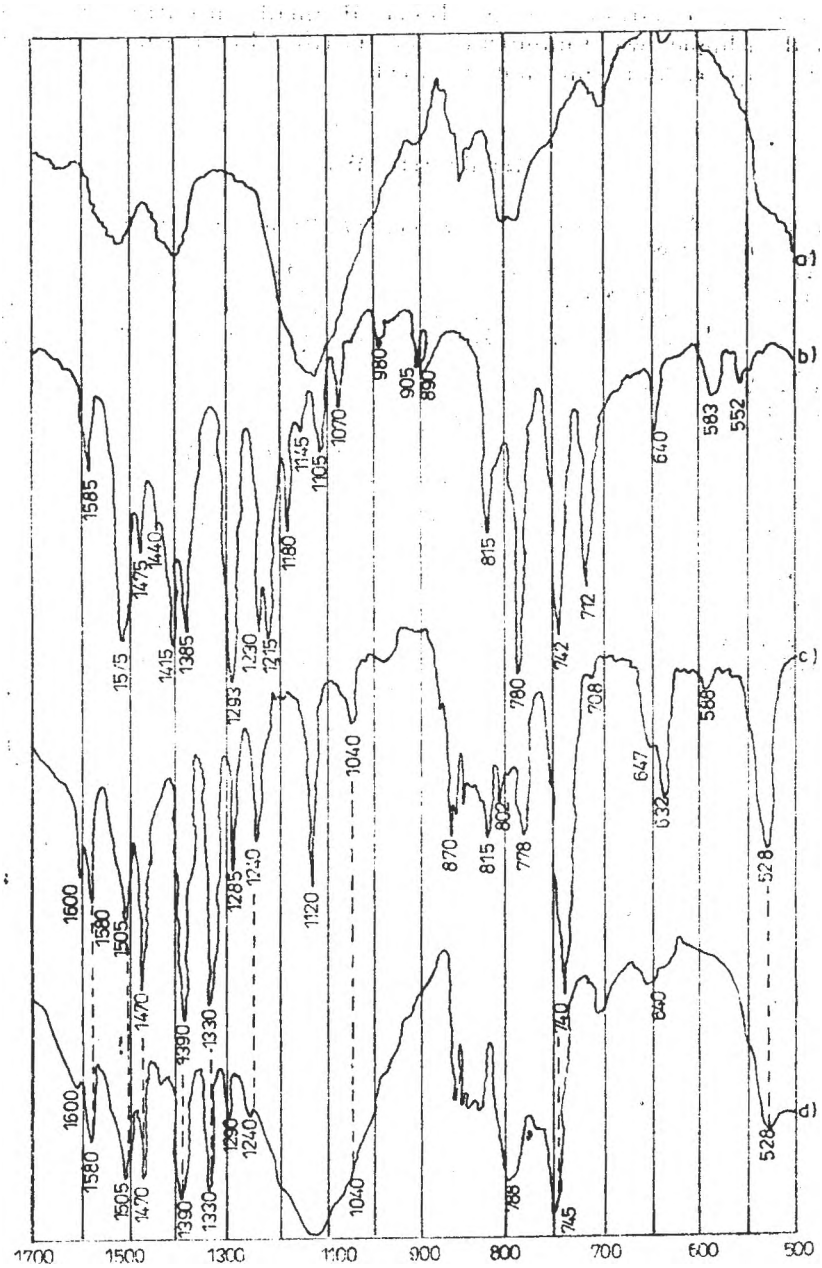

Fig. 1. Infrared spectra indicating the adsorption of oxyne onto malachite. a) malachite in KBr; b) 8-hydroxyquinoline in KBr; c) copper oxynate; d) malachite after treatment with acetone solution of oxyne.

aldoxyme solutions of various concentrations : at small concentrations there were bands shifted to higher wave numbers, some ascribed to the Cu(II) monosalicyl-aldoxymate complex, and some not ascribed.

REFERENCES

1. L. H. Little, A. V. Kiselev, V. I. Lygin, *Infrared spectra of adsorbed species*, Academic Press, London, 1966.
2. M. L. Hair, *Infrared spectroscopy in surface chemistry*, Marcel Dekker, New York, 1967.
3. M. R. Basilia, Appl. Spectroscopy Rev., **1**, 289 (1968).
4. C. H. Rochester, Powder Technology, **13**, 157 (1976).
5. V. M. Lovel, L. A. Goold, N. P. Finkelstein, Internat. J. Mineral Process., **1**, 183 (1974).
6. A. S. Peck, E. Milton, 7th Internat. Miner. Process. Congr. New York Publ. Gordon and Breach, **1**, 259 (1964).
7. R. G. Grendler, J. Phys. Chem., **66**, 879 (1962).
8. J. Leja, L. H. Little, G. W. Poling, Trans. Inst. Min. and Met., **72**, 407 (1963).
9. G. W. Poling, M. C. Fuerstenau, (Ed) Flotation — A. M. Gaudin Memorial Volume, **1**, 334, AIME (1976).
10. J. Mielczarski, P. Novak, J. W. Strojek, A. Pomianowski, 13th Internat. Miner. Process. Congress, Warszawa 61 (1979).
11. S. Raghavan, D. W. Fuerstenau, J. Colloid Interface Sci., **50**, 319 (1975).
12. L. Evrard, J. De Cuyper, 11th Internat. Miner. Process. Congress, Cagliari 35 (1975).
13. G. Rinelli, A. M. Marabini, V. Aless, Symposium A. M. Gaudin Flotation, **1**, 549, AIME New York (1976).
14. I. A. Goldsmith, S. D. Ross, Spectrochim. Acta, **24 A**, 2131 (1968).
15. G. Barberi, J. L. Cecile, Industrie minérale-Métalurgie, Août-Septembre, 109 (1979).

STUDIA UNIV. BABEŞ—BOLYAI, CHEMIA, XXXI, 2, 1986

THE ELLIPSOMETRIC STUDY OF POLYMER FILMS ON METALS

SIMION JITIAN* and EMIL CHIFU**

Received: October 10, 1986

ABSTRACT. — We present herein the results obtained through the ellipsometric study of the polystyrene and poly(methylmethacrylate) films on steel, copper and nickel surfaces. There have been obtained the thicknesses and refractive indices for the polymer films which were supposed to be transparent, based on the optical constants of the metals that have been obtained through ellipsometric measurements as well. The polymer films have been obtained from polymer solutions in trichloromethane or benzene, deposited on centrifuged metallic surfaces following the evaporation of the solvent.

Introduction. When a radiation is reflected on the interface between two media of different optical constants, as shows in Figure 1, there is a change in the radiation polarization that can be expressed by means of the ellipsometric parameters Δ and ψ. For an optical absorbing medium, the refractive index is a complex value as such:

$$\tilde{n} = \bar{n} - ik \qquad (1)$$

where $\bar{n}$ and $\bar{k}$ are the optical constants (Drude). $\bar{n}$ expresses the radiation phase propagation through the respective medium and $\bar{k}$ the radiation absorption in the medium.

The ellipsometry is one of the methods of finding out the optical constants $\bar{n}$ and $\bar{k}$ of an optical absorbing medium on the basis of the measured ellipsometric parameters Δ and ψ. The fundamental ellipsometric relationship that relates the ellipsometric parameters Δ and ψ to the medium optical constants $\bar{n}$ and $\bar{k}$ is:

$$\tan\psi \cdot e^{i\Delta} = \tilde{\rho} = \frac{\tilde{r}_p}{\tilde{r}_s} =$$

$$= \frac{\tilde{n}\cos\varphi_0 - n_0\cos\tilde{\varphi}}{\tilde{n}\cos\varphi_0 + n_0\cos\tilde{\varphi}} \cdot \frac{n_0\cos\varphi_0 + \tilde{n}\cos\tilde{\varphi}}{n_0\cos\varphi_0 - \tilde{n}\cos\tilde{\varphi}} \qquad (2)$$

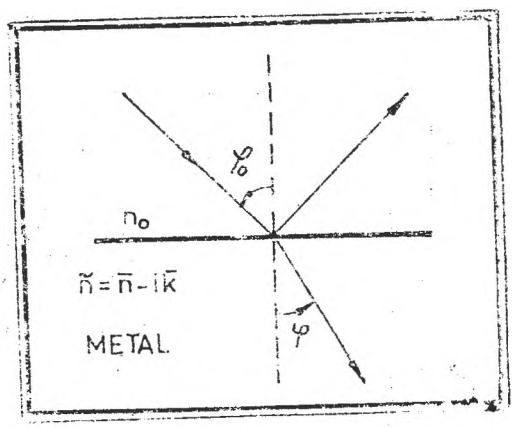

Fig. 1. Radiation reflection on the interface between air and an optical absorbing homogeneous and isotropic medium.

* "Traian Vuia" Polytechnic Institute — I. S. Hunedoara, 2750 Hunedoara, Romania
** University of Cluj-Napoca, Faculty of Chemical Technology, 3400 Cluj-Napoca, Romania

where: n_0 is the refractive index of the incidence medium; φ_0 is the angle of incidence to the surface; $\tilde{r}_p$ and $\tilde{r}_s$ are the Fresnel complex reflection coefficients corresponding to the radiation components polarized parallel to the plane of incidence and normal to the plane of incidence, respectively; $\tilde{\varphi}$ is the complex refraction angle defined by Snellius's law:

$$n_0 \sin \varphi_0 = \tilde{n} \sin \tilde{\varphi} \tag{3}$$

Δ expresses the difference between the phases of the two radiation components after reflection:

$$\Delta = \delta_p - \delta_s ;$$

$\tan \psi$ represents the ratio of the amplitudes of the two radiation components after the reflection.

The general form of the fundamental ellipsometric relationship:

$$\tan \psi \cdot e^{i\Delta} = f(n_0, \varphi_0, \bar{n}, \bar{k}) \tag{4}$$

shows the possibility of obtaining the optical constant of a material after a sole ellipsometric measurement by solving the set of equations $(1 \div 3)$.

In case there is a surface covered with a surface film, as shown in Figure 2, the fundamental ellipsometric equation is as such:

$$\tan \psi \cdot e^{i\Delta} = \tilde{\rho} = \frac{\tilde{r}_{p1} + \tilde{r}_{p2} \cdot e^{i2\tilde{D}}}{1 + \tilde{r}_{p1} \cdot \tilde{r}_{p2} \cdot e^{i2\tilde{D}}} \cdot \frac{1 + \tilde{r}_{s1} \cdot \tilde{r}_{s2} \cdot e^{-i2\tilde{D}}}{\tilde{r}_{s1} + \tilde{r}_{s2} \cdot e^{-i2\tilde{D}}} \tag{5}$$

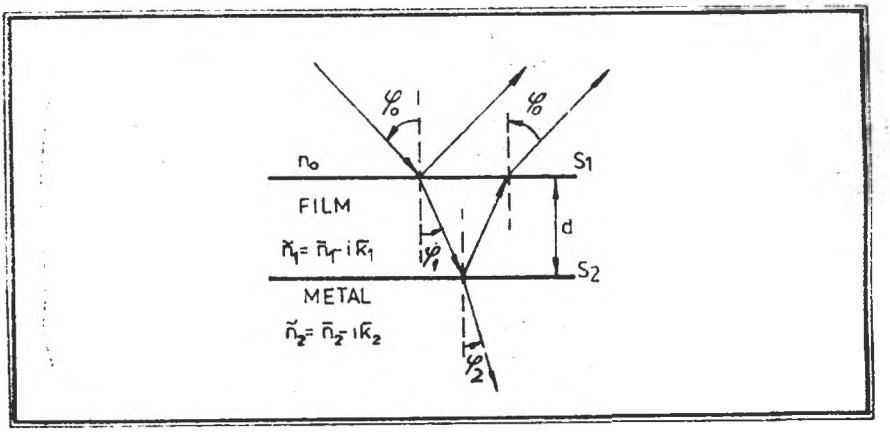

Fig. 2. Radiation reflection on the interface between air and an absorbing medium covered with a homogeneous and isotropic film.

where: — $\tilde{r}_{p1}$ and $\tilde{r}_{s1}$ are the reflection coefficients at the interface medium film, corresponding to the two radiation components:

$$\tilde{r}_{p1} = \frac{\tilde{n}_1 \cos \varphi_0 - n_0 \cos \tilde{\varphi}_1}{\tilde{n}_1 \cos \varphi_0 + n_0 \cos \tilde{\varphi}_1}; \quad \tilde{r}_{s1} = \frac{n_0 \cos \varphi_0 - \tilde{n}_1 \cos \tilde{\varphi}_1}{n_0 \cos \varphi_0 + \tilde{n}_1 \cos \tilde{\varphi}_1} \tag{6}$$

— $\tilde{r}_{p2}$ and $\tilde{r}_{s2}$ are the reflection coefficients at the interface film-underlayer (substrate), corresponding to the radiation components:

$$\tilde{r}_{p2} = \frac{\tilde{n}_2 \cos \tilde{\varphi}_1 - \tilde{n}_1 \cos \tilde{\varphi}_2}{\tilde{n}_2 \cos \tilde{\varphi}_1 + \tilde{n}_1 \cos \tilde{\varphi}_2}; \quad \tilde{r}_{s2} = \frac{\tilde{n}_1 \cos \tilde{\varphi}_1 - \tilde{n}_2 \cos \tilde{\varphi}_2}{\tilde{n}_1 \cos \tilde{\varphi}_1 + n_2 \cos \tilde{\varphi}_2} \tag{7}$$

— $\tilde{\varphi}_1$ and $\tilde{\varphi}_2$ are the complex angle of incidence at the interface medium-film and at the interface film-underlayer, respectively, defined by Snellius's refraction law.

These angles have been used as mathematical artificial means so that, for optical absorbing media, the relationship given by Snellius' law is observed; they should not be confused with the real refractive angles φ, φ_1 and φ_2 in Figs. 1 and 2.

$$n_0 \sin \varphi_0 = \tilde{n}_1 \sin \tilde{\varphi}_1; \quad \tilde{n}_1 \sin \tilde{\varphi}_1 = \tilde{n}_2 \sin \tilde{\varphi}_2 \tag{8}$$

$\tilde{n}_1 = \bar{n}_1 - i\bar{k}_1$ is the film complex refractive index;

$n_2 = \bar{n}_2 - i\bar{k}_2$ is the underlayer complex refractive index;

The complex parameter $\tilde{D}$ is expressed in terms of the wavelength of the incident radiation λ and film thickness d by the relationship:

$$\tilde{D} = 2 \frac{\pi}{\lambda} d(\tilde{n}_1^2 - n_0^2 \sin^2 \varphi_0)^{\frac{1}{2}} \tag{9}$$

The general form of the fundamental ellipsometric equation is as such:

$$\tan \psi \, e^{i\Delta} = f(n_0, \varphi_0, \lambda, \bar{n}_1, \bar{k}_1, \bar{n}_2, \bar{k}_2, d) \tag{10}$$

In case of transparent films ($\bar{k}_1 = 0$) the film thickness d and refractive index $\bar{n}_1$ can be determined through a single ellipsometric measurement (Δ, ψ). For optical absorbing films ($\bar{k}_1 \neq 0$), the three unknown values $\bar{n}_1$, $\bar{k}_1$ and d referring to the surface film can be determined through at least two ellipsometric measurements made either at two different angles of incidence φ_{01} and φ_{02} or using two different incidence media with the refractive indices n_{01} and n_{02}. It is very important that the optical constants $\bar{n}_2$ and $\bar{k}_2$ of the underlayer are exactly known each time.

Calculation of the film characteristics on the basis of the relationships (5÷9) needs either difficult graphical methods [1,2] or the use of electronic computers [3,4]. For thin transparent films under 100 Å mainly deposited on optical absorbing underlayers, the methods of approximation [5, 6, 7] could be used with quite good accuracy.

Experimental. The copper, nickel and OLC—45 steel samples, on which the polymeric films were deposited, had been cut from massive metallic parts to the dimensions $45 \times 22 \times 5$ (mm) then ground and polished with abrasive paper to grain 12. The surface to be studied had been further smothed with metallographic paper to grain M 14 and No. 2 Presi—Italia metallographic aluminium oxide powder. The samples were washed in distilled water and absolute ethanol.

In order to determine the optical constants of the metals ellipsometric measurements of the metallic samples immediately after polishing were performed. The time from polishing to completion of the ellipsometric measurement was less than 15 minutes so that the variations of Δ and ψ are within their measuring error limit. The metallic surface covered with the polymer film could be considered with quite enough accuracy as being free from oxides.

The polymer film was settled down on every sample immediately after the ellipsometric measurement lest it should form oxide films on the metallic surface. The polystyren (PS) and polymethyl methacrylate films (PMMA) were deposited from 1% solutions in benzene and trichloromethane during centrifuging the metallic samples up to 2000 r.p.m. under conditions similar to those used by other authors [8, 9].

The ellipsometric measurements of the newly polished metallic surfaces and of those covered with polymer film were made by an IFTAR—București photoelectrical ellipsometer, with PCSA arrangement using the radiation with the wavelength $\lambda = 5625$ Å at 60° and 70° incidence angles.

All the calculations have been performed by FELIX C-256 electronic computer on the programme worked out by McCrackin, in Fortran IV [4].

Results and Discussions. The optical constants of the metallic surfaces free from surface films have been found after having processed on the computer the ellipsometric measurements made on newly polished metallic samples, before the settling down of polymeric films. The values thus found are shown in Tables 1 and 2 and range among the optical constants of these metals reported by other authors [10, 11, 12, 13].

We considered the polymer films on metals as being optical nonabsorbing ($\bar{k}_1 = 0$) so that the thicknesses d and the refractive indices $\bar{n}_1$ of the polymeric films could be found from a single ellipsometric measurement, based on the optical constants $\bar{n}_2$ and $\bar{k}_2$ of the metallic underlayers.

It is useful to plot the set of curves $\Delta = f(\psi)$ for every separate metal, for different possible values of the film refractive index. Figure 3 shows such a

Table 1

Refractive indices and thicknesses of PS films on metals ellipsometrically found using the radiation of $\lambda = 5625$ Å and 60° incidence.

Metal	SUBSTRATE				POLYMER FILM					
	Δ	ψ	$\bar{n}_2$	$\bar{k}_2$	Δ	ψ	d	$\bar{n}_1$	$\bar{n}_1$ average	
	deg.	deg.	—	—	deg.	deg.	Å	—		—
OLC—45 STEEL	147.15	33.18	2.67	3.17	214.76	35.19	1600	1.54	1.56	1.57 ± 0.03
					121.99	35.03	248	1.59		
					122.49	35.13	258	1.54		
NICKEL	138.44	38.33	1.96	2.83	133.12	57.70	746	1.60	1.60	
COPPER	124.28	32.59	1.36	2.18	136.21	59.11	729	1.56	1.56	

Table 2

Refractive indices and thicknesses of PMMA films on metals ellipsometrically found using the radiation of $\lambda = 5625$ Å and 60° incidence.

SUBSTRATE					POLYMER FILM					
Metal	Δ	ψ	$\bar{n}_2$	$\bar{k}_2$	Δ	ψ	d	$\bar{n}_1$	$\bar{n}_1$ average	
	deg.	deg.	—	—	deg.	deg.	Å	—	—	
OLC—45 STEEL	147.15	33.18	2.67	3.17	113.46	42.48	691	1.43	1.49	1.49 ± 0.05
					224.80	41.79	1334	1.50		
					224.76	40.66	1380	1.49		
					219.47	36.50	1545	1.50		
					221.37	36.69	1500	1.51		
NICKEL	138.44	33.33	1.96	2.83	122.01	50.88	755	1.51	1.50	
					119.30	50.19	734	1.52		
					118.88	35.07	212	1.53		
					119.48	35.21	232	1.45		
COPPER	124.28	32.59	1.36	2.18	130.15	55.22	760	1.50	1.49	
					210.46	45.30	1135	1.48		
					213.57	42.33	1200	1.48		

set of curves for the OLC—45 steel surface covered with films having the refractive indices within 1.4 ÷ 1.6 and thicknesses within 1200 ÷ 1500 Å. The curves have been given by computer, based on the programme worked out by Mc-Crackin [4]. The thicknesses and refractive indices of polymer films corresponding to one ellipsometric measurement (Δ, ψ) performed for a film covered underlayer can be approximately read out of these curves.

The accurate calculation of the refractive index and thickness of each polymer film on the metal surface is performed on the basis of the respective programme showing a narrow range for the film thickness and refractive index values. Tables 1 and 2 show the thicknesses and refractive indices of the PS and PMMA films on different metals. It is found that the refractive indices of polymeric films are close to those of the bulk polymers given in the tables for physical constants. This gives support for the accuracy of our measurements, calculations and assumptions.

As concerns the thickness of the transparent polymer films it may still remain ellipsometrically undetermined due to the periodical feature of the function $e^{-i2\tilde{D}}$ in the relation (5). The curves $\Delta = f(\psi)$ are also periodical, giving

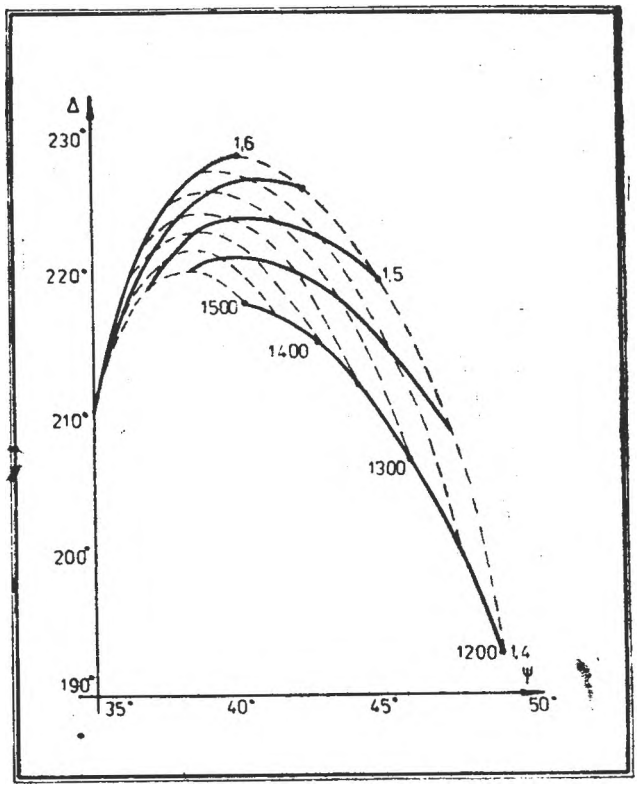

Fig. 3. Curves $\Delta = f(\psi)$ for transparent films on OLC—45 steel.

different thicknesses of the film for the same ellipsometric measurement (Δ, ψ):

$$d_m = d + m \cdot \frac{\lambda}{2} (\tilde{n}_1^2 - n_0^2 \sin^2 \varphi_0)^{-\frac{1}{2}} \quad (11)$$

where: $m = 0, 1, 2 \ldots$ gives the order of periodicity. The minimum thickness of the film for which Δ and ψ repeat is of the order of 2000 Å for the studied polymer films. Hence the ellipsometry can correctly give the film thickness value only if this is less than 2000 Å. The films we settled down on the metal surface meet this condition, hence the film thickness values given in Tables 1 and 2 are actual. As the polymer films have been obtained by settling down a polymer solution in solvents that evaporated afterwards the order of magnitude of the film thickness may be estimated according to the polymeric solution amount settled down per unit area of the metal and according to the polymeric solution concentration. The thickness uniformity of the film on the sample surface has been ensured by centrifuging the sample during evaporation of the solvent.

The film thickness and refractive index values could be more accurate if, for the same sample, measurements at two or more incidence angles are performed.

The results found by the ellipsometric measurements at two incidence angles for several metallic samples covered with polymer films are given in Table 3. The values found for the refractive indices of the polymeric films are in compliance with the refractive index values of the bulk polymers.

Conclusions. The preparation of the metallic surfaces before the polymeric films have settled down is good enough in order to get correct values for the refractive indices of the polymer film thickness.

The refractive indices of the polymer films having thicknesses ranging between 200 and 1600 Å have a value close to that of the bulk polymers.

The ellipsometric determination of the transparent film thickness on metals may only be performed for films thinner than 2000 Å. In case of thicker films it is necessary to specify the order of magnitude of the film thickness to the accuracy of 0.2 μm from another measurement different from the ellipsometric one.

Table 3

Refractive indices and thicknesses of polymer films on metals, ellipsometrically found using the radiation of $\lambda = 5625$ Å.

SUBSTRATE			POLYMER FILM								
METAL	$\bar{n}_2$	$\bar{k}_2$	POLYMER	φ_0	Δ	ψ	d	$\bar{n}_1$	$d_{aver.}$	$\bar{n}_1$ average	
	—	—		deg.	deg.	deg.	Å	—	Å	—	
OLC—45 STEEL	2.67	3.17	PMMA	60	219.47	36.50	1545	1.50	1523	1.50	1.48 ± 0.02
				70	256.84	37.42	1500	1.51			
NICKEL	1.96	2.83		60	119.48	35.21	232	1.45	231	1.46	
				70	87.54	34.09	230	1.46			
OLC—45 STEEL	2.67	3.17	PS	60	121.99	35.03	248	1.58	247.5	1.58	1.59 ± 0.02
				70	90.88	33.51	247	1.58			
NICKEL	1.96	2,83		60	133.12	57.70	746	1.60	735	1.61	
				70	92.22	61.62	725	1.63			
COPPER	1.36	2.18		60	136.21	59.11	729	1.56	705	1.59	
				70	91.45	66.26	681	1.62			

REFERENCES

1. S. S. So. and K. Vedam, *J. Opt. Soc. Amer.* **62,** 16 (1972).
2. J. Kucirek, *Czech. J. Phys.*, **198,** 537 (1969).
3. F. L. McCrackin, E. Passaglia, R. Stromberg and H. L. Steinberg, *J. Res. Nat. Bur. Stand.* **67A,** 363 (1963).
4. F. L. McCrackin, Nat. Bur. Stands. Tech. Note 479, U.S. Gov't Printing Office, Washington, 1969.
5. L. S. Bartell and D. Churchill *J. Phys. Chem*, **65,** 2242 (1961).
6. Archer, R. J., Manual on Ellipsometry, Gaertner Sci. Corp., Chicago, 1968.
7. A. Vašiček, in „The Symposium on the Ellipsometry and its Use in the Measurement of Surfaces and Thin Films", ed. Passaglia E., Stromberg R. R., Kruger J., Natl. Bur. Stand. Misc. Publ., 256, p. 25, U. S. Govn't. Printing Office, Washington, 1964.
8. J. F. Rabolt, M. Jurich, and J. D. Swalen, *Appl. Spectroscopy*, **39,** 269 (1985).
9. D. A. Saucy, S. J. Simko, and R. W. Linton, *Analyt. Chem.*, **57,** 871 (1985).
10. F. C. Schouten, E. W. Kaleveld, and G. A. Bootsma, *Surf. Sci.*, **63,** 460 (1977).
11. J. Mieluch, *Roczniki Chem.*, **49,** 365 (1975).
12. D. Moisil, D. Angheleschu, and D. Mitan, *Rev. Chim.* (Bucureşti), **29,** 63 (1978).
13. S. Matsuda, K. Sugimoto, and Y. Sawada, *Trans. Japan Inst. Metals.*, **18,** 66 (1977).

STUDIA UNIV. BABEŞ—BOLYAI, CHEMIA, XXXI, 2, 1986

POTASSIUM BIS-(PHOSPHO-DIMOLIBDO-9-TUNGSTO) URANATE AND POTASSIUM BIS-(DIPHOSPHO-MOLIBDO-16-TUNGSTO) URANATE

GH. MARCU*, MARIANA RUSU* and ALEXANDRU BOTAR**

Received: October 15, 1986

ABSTRACT. — The U(IV) ion reacts rapidly with unsaturated heteropolyanions, forming complexes of the UL_2 type, where $L = PW_9Mo_2O_{39}^{-7}$ and $P_2W_{16}MoO_{61}^{-10}$ The potassium salts of the heteropoly anions $[U(PW_9Mo_2O_{39})_2]^{-10}$ and $[U(P_2W_{16}MoO_{61})_2]^{-10}$ were isolated. The chemical individualyty and the oxidation state of uranium in these heteropoly compounds were analysed.

The $K_7PW_9Mo_2O_{39} \cdot 13\,H_2O$ and $K_{10}P_2W_{16}MoO_{61} \cdot 19\,H_2O$ heteropoly compounds [1, 2] reacts rapidly with U(IV) ion.

Our investigations indicate that the U(IV) ion forms UL_2 heteropoly compounds, where $L = PW_9Mo_2O_{39}^{-7}$ and $P_2W_{16}MoO_{61}^{-10}$

Experimental. *Synthesis of Potassium Salt of the Bis-(Plospho-dimolibdo-9-tungsto) Uranate*: to a solution containing 6,044 g (0,002 mol) $K_7PMo_2W_9O_{39} \cdot 13H_2O$ in 75 ml water was added stepwise under continuous stirring, a solution containing 0,502 g (0,001 mol)$U(CH_3COO)_4$. The mixture pH was established at 2,5—3. Then the mixture was refluxing 30 minutes at 80°. Finally the solution was filtered and was added 150 ml C_2H_5—OH absolute. Deep brown-red microcrystals were obtained after 48 hours of resting at 5° and were purified by repeated recrystallization from distilled water (80°, pH = 2,5—3).

Synthesis of potassium salt of bis-(diphospho-molibdo-16-tungsto) uranate: to a solution containing 5 g (0,002 mol) $K_{10}P_2MoW_{16}O_{61} \cdot 19H_2O$ in 75 distilled water was added stepwise under continuous stirring a solution containing 0,502 g (0,001 mol) $U(CH_3COO)_4$ in 25 ml distilled water. The mixture pH was established at 2,5—3. Then mixture was refluxing 30 minutes at 80°. Finally the solution was filtered and 150 ml C_2H_5—OH absolute was added. The violete microcrystals were obtained after 48 hours of resting at 5° and were purified by repeated recrystallization from distilled water (80°, pH = 2,5—3).

Chemical Analysis: The potassium salts of the $[U(PMo_2W_9O_{39})_2]^{-10}$ and $[U(P_2MoW_{16}O_{61})_2]^{-16}$ heteropoly anions were chemically analysed according to the general procedure [3]. The amount of tungsten was determined by precipitation with cinchonine, followed by an ignition to WO_3 at 800° [4]. Uranium was photocolorimetrically analysed with Arsenazo III reagent [5]. The molybdenum was determined by precipitation with α-Benzol-oxine [6]. Phosphorus was determined by precipitation as magnesium and ammonium phosphate and calcination at $Mg_2P_2O_7$ [7]. Potassium was determined with tetraphenylborate [8]. The water content of the complexes was determined by ignition at 550° for 1 hour. The results of the chemical analysis are presented in Table 1.

The conductometric study of the reaction betwen the $PMo_2W_9P_{39}^{-7}$, respectivly $P_2MoW_{16}O_{61}^{-10}$ heteropoly anions and the U(IV) ion has been performed by measuring the conductivity of the 50 ml solutions 10^{-2} M containing $K_7PMo_2W_9O_{39}$, respectivelly $K_{10}P_2MoW_{16}O_{61}$ by titring with U(IV)

* *University of Cluj-Napoca, Faculty of Chemical Technology, 3400 Cluj-Napoca, Romania*
** *Institute of Chemistry, 3400 Cluj-Napoca, Romania*

Table 1

Results of chemical analysis.

Compound	K %		U %		P %		Mo %		W %		H_2O %	
	calcn.	found	calcn.	found	calcn.	found	calcn	found	calcn.	found	calcn.	found
$K_{10}[U(PMo_2W_9O_{39})]\cdot 24H_2O$	6.53	5.47	3.97	4.02	1.03	1.00	6.41	6.25	55.31	54.98	7.22	7.15
$K_{16}[U(P_2MoW_{16}O_{61})_2]\,30H_2O$	6.54	6.42	2.49	2.45	1.29	1.18	2.00	1.86	61.58	61.25	5.65	5.48

solution having $T_{U(IV)} = 0.006005$, respectivelly $T_{U(IV)} = 0.005551$. Measurements have been carried out by means of a Radelkis OK—102 type conductometer. Titration curves are given in Figure 1.

The UV electronic spectra : the chemical individuality of $K_{10}[U(PMo_2W_9O_{39})_2]$ and $K_{16}[U(P_2MoW_{16}O_{61})_2$ salts was controlled by recording the UV spectra of compounds having a tungsten concentration of $5 \cdot 10^{-5}$ M (see Fig. 2).

The electronic visible spectra : the oxydation state of uranium in these heteropoly compounds was stablished using the absorption spectra in the visible domain of the solutions with a tungsten concentration of 10^{-2} M (see Fig. 3).

The UV and visible spectra were recorded on a „Specord —UV-Viss" spectrophotometer.

I R. spectra : the IR spectra of solid salts of synthesysed heteropoly compounds in KBr pellets were recorded on a „UR—10—Zeiss Jena" spectrophotometer. The spectral analysis dates are shown Table 2.

Results and Discussion. The following formulas were attributed to the new synthetised heteropoly compounds: $K_{10}[U(PMo_2W_9O_{39})_2]\cdot 24H_2O$ and $[U(P_2MoW_{16}O_{61})_2]\cdot 30\,H_2O$. The conductometric study of the reactions between $PMo_2W_9O_{39}^{-7}$ and $P_2MoW_{16}O_{61}^{-10}$ heteropolyanions and the U(IV) ion shown that the U : Heteropolyanion combination ratio is 1 : 2.

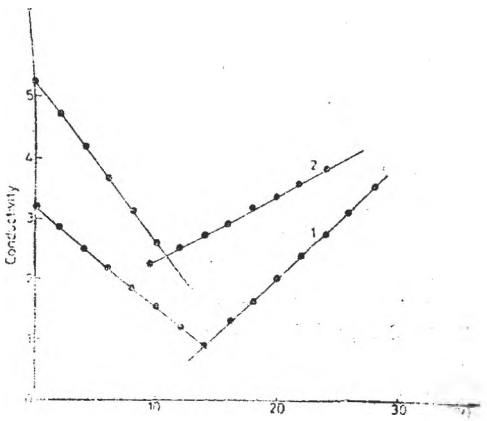

Fig. 1. Conductometric titration curves for :
1 — $K_7PMo_2W_9O_{39}$ with U(IV) ion.
2 — $K_{10}P_2Mo_2W_{16}O_{61}$ with U(IV) ion.

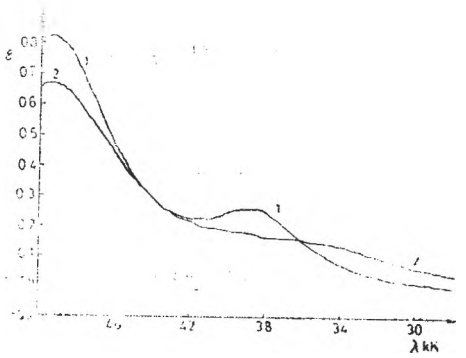

Fig. 2. UV spectra of :
1 — $K_{10}U(PMo_2W\,O_{39})_2$
2 — $K_{16}U(PMoW_{16}O_{61})_2$.

The experimental analytical results are in good agreement with calculated dates. The absorption spectra of the potassium salts of heteropolyanions $[U(PMo_2W_9O_{39})_2]^{-10}$ and $[U(P_2MoW_{16}O_{61})_2]^{-16}$ have a characteristic band between 50.000—48.850 cm^{-1}, that could be assigned to a $p_\pi - d_\pi$ transition in the W = 0 bond [9]. The characteristic band at 38.910 cm^{-1} for $K_{10}[U(PMo_2W_9O_{39})_2]$ is atributed to the electron transition in the three central W—O—W bonds [10]. From spectra recorded by us in visible domain, the L band at 14,490 cm^{-1} is well resolved, which indicates a stronger crystalline field in the studied compounds than that determined by the 6 chlorine atoms in Cs_2UCl_6 [11]. The broad absorption at 25.000—20.000 cm^{-1}, with superimposed f — f peaks, results from the U(IV) to W(VI) change transfer. These bands according to Bagnall [12], suggest an octacoordinated configuration for U(IV) in the studied heteropoly compounds.

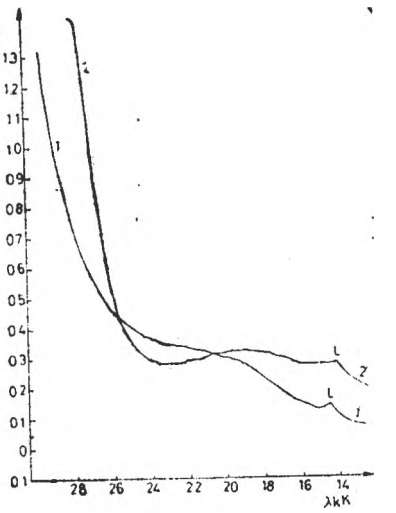

Fig. 3. Electronic absorption spectra of:
1 — $K_{10}U(PMo_2W_9O_{39})_2$
2 — $K_{16}U(P_2MoW_{16}O_{61})_2$
compounds in the visible range.

Table 2

Results of absorption IR spectral analysis.

Compound	ν cm⁻¹	Assigning
$K_{10}[U(PMo_2W_9O_{39})_2]\cdot 24\,H_2O$	765	W-O-W (ν sim) W=O (ν)
	890	W-O-W (ν sim) W=O (ν)
	965	W-O-W (ν sim) W=O (ν)
	1035	P-O (ν)
	1085	
	1120	U-O (ν)
	1640	H-O-H (δ)
$K_{16}[U(P_2MoW_{16}O_{61})_2]\cdot 30\,H_2O$	758	W-O-W (ν sim) W=O (ν)
	875	W-O-W (ν sim) W=O (ν)
	980	W-O-W (ν sim) W=O (ν)
	1060	P-O (ν)
	1085	
	1120	U-O (ν)
	1640	H-O-H (δ)

The IR spectra of the $K_{10}[U(PMo_2W_9O_{39})_2] \cdot 24\ H_2O$ and $K_{16}[U(P_2MoW_{16}O_{61})_2 \cdot$ $\cdot /30\ H_2O$ showed three absorption bands from 1000—700 cm^{-1}, which are due to stretching vibration of the W—O bands. The absorption bands maxima are found at 765, 890 and 965 cm^{-1}, respectively 758, 875 and 980 cm^{-1}. The absorption bands in the above mentioned domain are also characteristic to the heteropoly tungstates, particularly to 1 : 1 : 11 and 1 : 2 : 17 series and allow to identify these compounds based on IR spectra [12]. The four absorption bands located at 1035, 1085, 1240 and 1640, respectively 1060, 1085, 1120 and 1640 cm^{-1}, seen in the IR spectra, are due to P—O, U—O and H—O—H bending vibration.

The conductometric study of the reaction between $PMo_2W_9O_{39}^{-7}$, respectively $P_2MoW_{16}O_{61}^{-10}$ and the U(IV) ion, as well as the analysis of the obtained potassium salts of $[U(PMo_2W_9O_{39})_2]^{-10}$ and $[U(P_2MoW_{16}O_{61})_2]^{-16}$ heteropolyanions showed that the U : hpa ratio is 1 : 2.

The chemical individuality of these compounds was established by recording the UV, visible and IR spectra, and oxidation state of uranium in these compounds was determined by recording the electronic absorption spectra in the visible range. The experimental results suggest an octahedral configuration of the U(IV) ion and an oxidation state of +4 in these compounds.

REFERENCES

1. R. Contant, J. M. Fruchart, G. Hervé and A. Tezé, *Compt. rend., C.* **273**, 195 (1974).
2. R. Contant, J. P. Ciabrini, *J. Chem. Res.*, (S), **222**, 2601 (1977).
3. V. E. Simmons, *Ph. D. Thesis*, Boston University, 1963.
4. A. I. Vogel, *"A Textbook of Quantitative Inorganic Analysis"* 2-nd, edn. London, 1951, p. 418.
5. B. S. Savvin, *Talanta*, **8**, 673 (1961).
6. H. P. Knowles, *J. Res. Nat. Bur. STDS*, **9**, 1 (1932).
7. A. I. Vogel, *"Quantitative Inorganic Analysis"*, 3-nd, edn. London, 1961, p. 575.
8. G. H. Glass, *Chemist Analyst*, **42**, 50 (1953).
9. HynsooSo and M. T. Pope, *Inorg. Chem.*, **11**, 1441 (1972).
10. V. I. Spitsyn, E. A. Torcenkova, L. P. Kazanski, and B. Baidala, *Z. Chem.*, **1**, 1 (1974).
11. C. K. Jorgensen, *Dan. Mat. Fys. Medd.*, **29**, 7 (1955).
12. K. W. Bagnall, D. Brown, P. J. Jones and P. S. Robinson, *J. Chem. Soc.* (A)., *1964*, 2527.

STUDIA UNIV. BABEŞ—BOLYAI, CHEMIA, XXXI, 2, 1986

XANTHOPHYLL FILMS

III. Two-Component Monolayers of Some Xanthophylls and L-α-Dipalmitoyl- Lecithin at the Air/Water Interface

MARIA TOMOAIA-COTIŞEL*, EMIL CHIFU* and JÁNOS ZSAKÓ*

Received: November 6, 1986

ABSTRACT. — Compression isotherms (surface pressure *versus* mean molecular area) are recorded for some two-component films of L-α-dipalmitoyl-lecithin (DPL) and xanthophylls, *viz.* β-cryptoxanthin, lutein and zeaxanthin at air/water interface. With all studied systems the collapse pressure is dependent on monolayer composition, indicating complete miscibility of the surfactants in monolayer — in accord to the surface phase rule. The experimental values of collapse pressure point to positive deviations from the calculated ones, assuming perfect surface solutions in two-component monolayers. Maximum deviation from the perfect behaviour is found with molar fractions of DPL below 0.5, especially in presence of zeaxanthin or lutein, what suggests occurrence in their monolayer of DPL-xanthophyll molecular associations. The obtained results are in agreement with the observed condensing effect of xanthophylls upon DPL, taking into account the excess free energies of mixing of the components in the monomolecular film. The characteristics of DPL-xanthophyll mixed films are discussed in terms of the packing of the two-components in surface solution, according to the molecular structures of the three investigated xanthophylls.

Introduction. In the first paper of the series [1] the monolayer characteristics were investigated for some all-*trans* xanthophyll derivatives at the air/water interface, by using compression isotherms. The results were interpreted considering molecular structures by means of a geometric model proposed by us. The influence of some xanthophylls (β-cryptoxanthin, zeaxanthin or lutein) upon insoluble films of egg lecithin (EL) at air/water interface was the object of investigation in the second paper [2]. The obtained results, generally, pointed to a condensing effect of the xanthophylls upon egg lecithin in mixed monolayers. Maximum condensing effect was found with zeaxanthin or lutein, at EL molar fractions below 0.5.

This paper deals with two-component mixtures of the above mentioned all-*trans* xanthophylls with a saturated lecithin, namely L—α—dipalmitoyl lecithin (DPL).

The performed experiments, too, revealed a condensing effect of the xanthophylls upon DPL at air/water interface, particularly in expanded-liquid state of DPL. Comparing the results obtained on DPL-xanthophyll systems to those previously published by us for EL-xanthophyll [2], the role is evidenced of the physical state of the pure phospholipid film upon behaviour of the mixed films, the lipid molecular structure being important in so far as it determins the physical state of the monolayer.

* *University of Cluj-Napoca, Faculty of Chemical Technology, 3400 Cluj-Napoca, Romania*

The three studied xanthophylls (β-cryptoxanthin: 3-hydroxy-β-carotene; zeaxanthin: 3,3'-dihydroxy-β-carotene; lutein: 3,3'-dihydroxy-α, β-carotene) are all-*trans* carotenoids widespread in the living world [3] and they differ among themselves by both their number of hydroxyl groups and the conformation of ionone rings.

The interest for such researches lies in that both xanthophylls and lecithins are structural and functional components of certain biological membranes [3], and it is precisely the study on mixed films that provides for quantitative information upon interactions likely to appear between various membrane components.

Experimental. Monolayers of pure components as well as of mixtures were studied, at the air/water interface by means of compression isotherms employing the Wilhelmy method. The experimental conditions used for measuring surface pressure (π, $mN \cdot m^{-1}$) as function of molecular area (A, $nm^2 \cdot molecule^{-1}$) relative to single-component xanthophyll films, as were for pure L-α-dipalmitoyl lecithin (DPL) films, have already been described [1, 4].

The monolayer-forming substances: xanthophylls (β-cryptoxanthin, zeaxanthin and lutein) and DPL were supplied by the same source [1, 4], used without further purification. With two component films, the given composition mixtures were prepared from stock solutions of pure components and then spread at air/water interface at the same initial area namely 1.20 nm^2/molecule, avoiding thus artefacts owed to spreading kinetics [5].

Benzene was used as solvent for β-cryptoxanthin, while mixtures of benzene and absolute ethanol (containing 2–4% ethanol) were used for zeaxanthin and lutein [1]. In what regards DPL, it was dissolved in a mixture of *n*-hexane with (2%) absolute ethanol [4]. As is well known, xanthophylls are light-sensitive substances, so their purity had to be checked during the experiments by thin layer cromatography and spectrophotometrically. No degradation of substances was detected.

With each system series of at least ten isotherms were recorded, for 0.02–0.08 $nm^2 \cdot molecule^{-1} \cdot min^{-1}$ compression rates. In these conditions, surface pressure accuracy varies by ± 0.5 $mN \cdot m^{-1}$, while molecular areas are determined to within ± 0.02 $nm^2 \cdot molecule^{-1}$, and reproducibility of the compression isotherms was taken as criterion for acceptable results. For solvent evaporation 5–10 min were allowed and complete compression isotherms were recorded within 20–40 min from onset of compression. Freshly twice-distilled water was used and the measurements were performed at room temperature (22 ± 2 °C).

Results and Discussion. *Surface Pressure-Area Curves.* Compression curves are experimentally recorded for some two-component films of DPL and xanthophylls, *viz.* β-cryptoxanthin, lutein and zeaxanthin. As exemplification, the compression curves are given for DPL-zeaxanthin system of some compositions (Fig. 1). For clarity, the isotherms for the aditionally studied concentrations are not plotted.

We mention that the physico-chemical characteristics of the monocomponent films of xanthophyll and DPL at the air/water interface are similar to the previously published ones [1,4]. Table 1 displays the monolayer characteristics of monocomponent films, given by compression isotherms.

The values A_0 stand for the limiting molecular area obtained by extrapolation of the high pressure linear portion of the compression isotherm, at zero-tending surface pressures. By using the high pressure linear portion slope, the surface compressional modulus $C_s^{-1} = -A_0 \left(\frac{\partial \pi}{\partial A}\right)_T$ was estimated, a magnitude which points to the physical state of the film at high pressures.

In fine, the collapse pressure π_c was obtained as highest surface pressure [5] to which the monolayer can be compressed without detectable ejection of

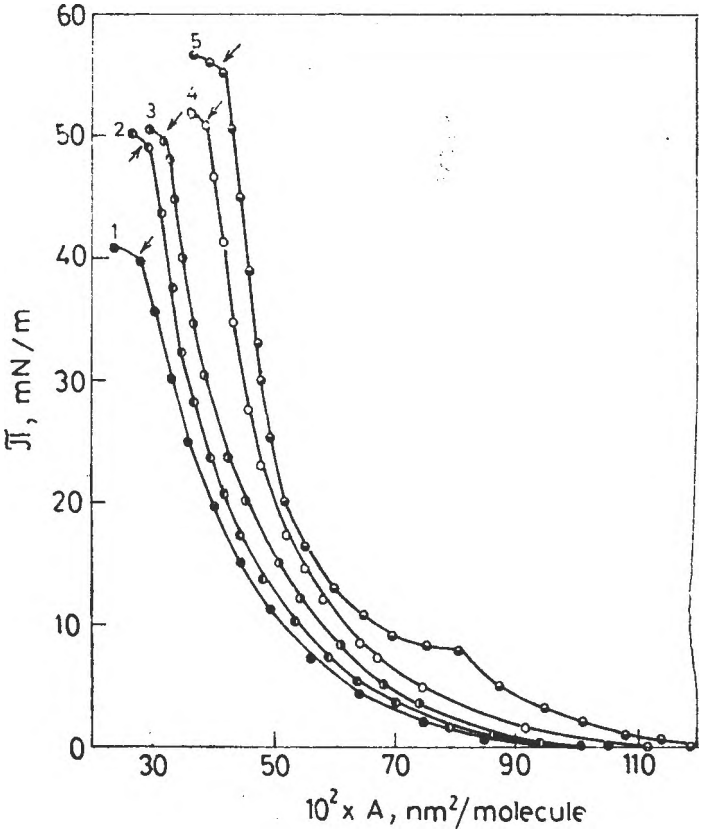

Fig. 1. Surface pressure versus mean molecular area curves for mixed L-α-dipalmitoyl lecithin (DPL) and zeaxanthin monolayers on water at various mole fractions of DPL, x_{DPL}: 0.00 (curve 1); 0.25 (2); 0.50 (3); 0.75 (4); 1.00 (5).

Table 1

Surface characteristics of single component film of xanthophylls, DPL and EL

Compound	A_0 Å²	A_c Å²	π_c mN/m	C_s^{-1} mN/m
β-Cryptoxanthin	42	23	37	82
Zeaxanthin	49	30	40	103
Lutein	63	38	38	96
DPL	55	42	55	229
EL	92	54	42.5	102

the molecules from two-dimension to form a collapsed bulk phase (see arrows, Fig. 1) and the corresponding collapse molecular area as A_c value.

Of the C_s^{-1} values given in Table 1 one can see that the xanthophyll films at high pressures display the features of a condensed-liquid [6] and they are more compressible than the condensed-liquid film of DPL.

It is to be noticed that DPL has the highest collapse pressure from the surfactants studied.

Coming back to curve 5 in Fig. 1, it is observed that the DPL film undergoes a phase transition (at a surface pressure of approximately 8 mN/m) from expanded-liquid to condensed-liquid [4]. To put it differently, a change develops from the orientation possibly governed by intramolecular interactions in a state of expanded-liquid to an orientation prevailed by intermolecular interactions likely to occur in the condensed-liquid state [4,7].

The conformation of a phospholipid in a monolayer is an outcome of the interactions between the hydrocarbon chains, polar groups, hydrocarbon chains and polar groups, and polar groups with aqueous subphase. The conjunction of these interactions in monolayers can also entail polar group conformational transitions affecting/altering the interaction between the hydrocarbon chains. Thus, the DPL head-group can principally reach two different orientations — namely, the plane determined by the atoms P and N of the phosphocholine group can be either parallel (in condensed-liquid) or perpendicular to the hydrocarbon chains (in expanded-liquid film).

Our previous study [4] revealed that in a nonionic environment at low surface pressures the phosphocholine group conformation determined by domination of intramolecular interactions is parallel to water surface, that is perpendicular to the hydrocarbon chains. The parallel to interface DPL head-group orientation could be due to some intermolecular interaction balance between the phosphate group of a molecule and the choline group of an adjacent molecule, and their intramolecular interaction in which the phosphate and choline groups of the same molecules interact electrostatically.

Following on Fig. 1 the sequence of the isotherms for the various compositions of the DPL-zeaxanthin monolayers one can see that the phase transition existent in the DPL pure film is abolished, and the collapse-pressure (see the arrows indicating that the monolayer starts to collapse) varies continuously from one pure component to the other, depending on the composition of the mixed film.

These phenomena have also been found experimentally with the other two systems: DPL-lutein, and DPL-β-cryptoxanthin.

The Mean Molecular Area and the Additivity Rule. Fig. 2 gives the graph of the mean molecular areas as function of composition for the DPL-zeaxanthin system at some constant surface pressures. The mean molecular areas have been obtained by interpolation of the experimental curves plotted in Fig. 1 at the chosen surface pressures. It is to be noticed in Fig. 2 that the mean molecular areas exhibit negative deviations from the perfect behaviour given by means of the additivity rule (dashed line, Eq. (1)) at low surface pressures corresponding to expanded-liquid state for the DPL pure film, deviations that decay by increasing surface pressure.

The additivity rule is given by

$$A = x_1 A_1 + x_2 A_2 \qquad (1)$$

where A stands for the mean molecular area in the two-component film, A_1 and A_2 are the molecular areas in the two monocomponent films at one and the same given surface pressure, while x_1 and x_2 are the molar fractions of the components in monolayer.

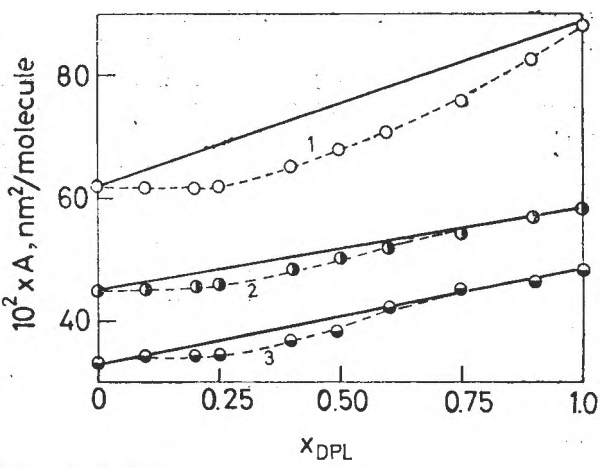

Fig. 2. Variation of mean molecular area with composition for DPL-zeaxanthin monolayers at three values of the surface pressure: 5 mN/m (curve 1), 15 mN/m (2) and 30 mN/m (3). The dashed lines represent the additivity rule.

The condensing effect of zeaxanthin upon DPL in mixed monolayers depends on the physical state of the phospholipid pure film and its maximum is reached with the expanded-liquid state and phospholipid molar fractions below 0.5. The fact that at high surface pressures, namely with condensed-liquid state of both components, the condensing effect is diminished, points to the importance of zeaxanthin in abolishing the phase transition observed in pure DPL monolayers.

This condensing effect was also found with the other two systems: DPL-lutein and DPL-β-cryptoxanthin.

The xanthophyll could affect the DPL phase transition in some ways, namely: by special mechanisms for the packing of the components [8], taking into account the geometric accomodation or "space filling" possibilities [9] through a reduction of the hydrocarbon chain mobility, filling the intermolecular cavities created by the thermic movement of the fatty acid chains in the molecules of lecithins, decreased concentration of DPL by dilution, a local interaction between the hydroxyl group of xanthophyll and the phosphocholine group of DPL resulting in enhanced intermolecular hydrophobic interactions [9]. All these intermolecular effects might reduce the intermolecular electrostatic interactions between the DPL molecules and, probably, they actually operate in a mixed monolayer of DPL and xanthophyll.

However, the mechanisms by which xanthophylls (β-cryptoxanthin, zeaxanthin and lutein) disturb the transition region might be slightly different from one another because of their different chemical structures, the condensing effect upon DPL being more reduced in presence of β-cryptoxanthin.

A similar condensing effect of xanthophylls upon the EL films has been previously evidenced by us [2].

It is worth mentioning that the condensing effect of zeaxanthin, and particularly of lutein upon the EL films is maintained even at high surface pressures

of 35 mN/m. For mere comparison, we resort to the EL monolayer characteristics in Table 1. It is observed that EL forms a liquid-condensed films, however the compressional modulus is smaller, the monolayer being more compressible than that of DPL what might explain the maintaining of the condensing effect even at high surface pressures.

Comparing the effects of the xanthophylls upon EL [2] or DPL, it has been found that the condensing effect of the xanthophyll on phospholipid depends on unsaturation of the fatty acid constituents what points to prevalence of hydrophobic interactions.

Thus, the negative deviation from the additivity of areas could be accounted for by the molecular arrangements of the components that allow the molecules to adopt a more compact packing in film, as compared to the one of the pure components, eventually leading to enhanced dispersion interactions accompanied by specific interactions between the hydroxyl group of the xanthophyll and the polar group of the lecithin.

Miscibility and the Two-Dimensional Phase Rule. The surface phase rule in the case of plane interfaces [10—12] is as follows:

$$w = (c - \varphi) - (\psi - s) - r + 2. \tag{2}$$

where w is system variance, c — number of components, φ — number of bulk phases, ψ — number of surface phases in equilibrium one with the other, s — number of types of surface, r — number of independent chemical reactions likely to evolve in a system. At constant temperature and external pressure and in the absence of chemical reactions ($r = 0$), Eq. (2) turns:

$$w = (c - \varphi) - (\psi - s) \tag{3}$$

Generally, the two components can form either two surface phases if immiscible, or one single surface phase when their miscibility is complete in monolayer.

To the end of obtaining information on the monolayer miscibility the surface phase rule was applied at collapse pressure, i.e. at the equilibrium between the surface film and the collapsed bulk phase.

When the DPL was miscible with the xanthophyll, in both the surface phase and collapsed bulk phase, all the surface types (air/water, collapsed phase/water, collapsed phase/air) would carry but one surface phase. It follows that $s = 3$ and $\psi = 3$. As $c=4$ (water, xanthophyll, DPL, air — presumed to be monocomponent for brevity [11]) and $\varphi = 3$ (water, air, collapsed phase), in accord to Eq. (2) in the absence of chemical reactions ($r = 0$) one obtains $w = 3$, what denotes that T, p and the collapse pressure π_c can be set arbitrarily. At T constant and P constant, according to Eq. (3) the system variance is $w = 1$ and consequently the collapse surface pressure varies with composition — x_{DPL} (the molar fraction of lecithin) — of the monolayer:

$$\pi_c = \pi_c(x_{DPL}) \tag{4}$$

We further discuss on the monolayer isotherms of the studied systems, i.e. variation of the collapse pressure π_c of the mixed films of DPL — zeaxan-

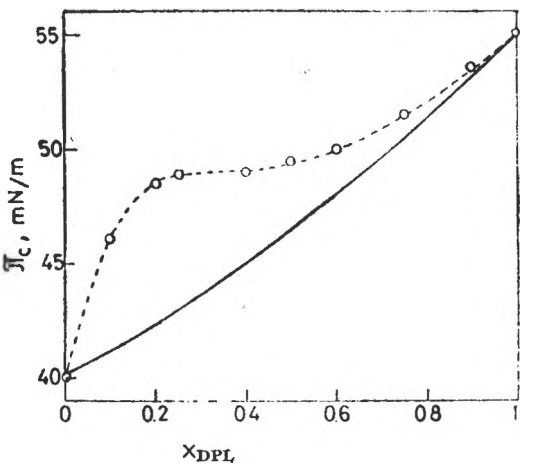

Fig. 3. The relation between collapse pressure and mole fraction of DPL for monolayers of DPL and zeaxanthin. Full line calculated for perfect behaviour of mixed monolayers.

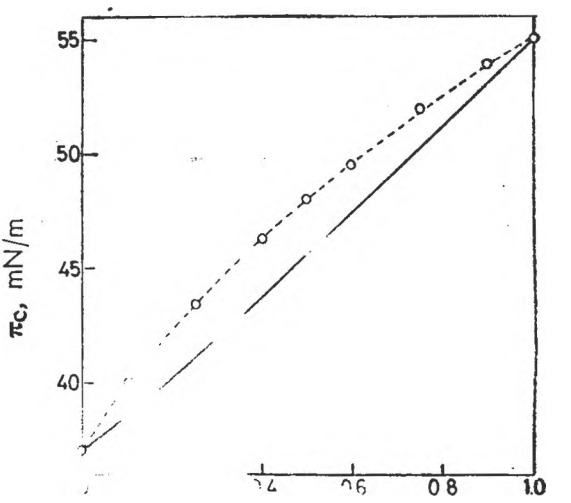

Fig. 4. Collapse surface pressures as a function of composition for the system DPL-β-cryptoxanthin. (Symbols as in Fig. 3).

thin (Fig. 3; some experimental data taken from Fig. 1), DPL — β-cryptoxanthin (Fig. 4) and DPL — lutein (Fig. 5) as function of the composition of phospholipid in monolayer. Of Figs. 3—5, it appears a certain dependence of the experimental π_c on film composition (monolayer curve, see dashed curves), what is in accord to Eq. (4) and points to a complete miscibility of the components in system. The Equation of the monolayer curve can be described by employing various simplifying approximations.

The simplest approximation assumes both the monolayer phase (M) and the collapsed bulk phase (C) as perfect solutions in a metastable thermodynamic equilibrium [13, 14], what implies equality of the chemical potentials of the components (xanthophyll (1) and DPL (2)) present in both phases. In these circumstances the monolayer curve equation is

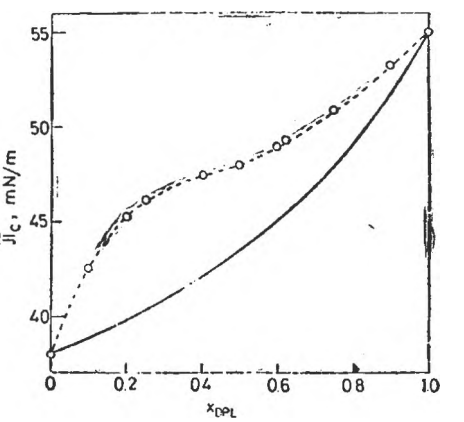

Fig. 5. Collapse surface pressure plots as a function of the DPL-lutein film composition.(Symbols as in Fig. 3).

given by:

$$x_1 \exp\left[\frac{(\pi_c - \pi_{c1})A_{c1}}{kT}\right] + x_2 \exp\left[\frac{(\pi_c - \pi_{c2})A_{c2}}{kT}\right] = 1 \quad (5)$$

where, π_{ci} is the collapse pressure of component i in the pure film, while A_{ci} stands for the corresponding collapse molecular area, k and T are Boltzmann constant and absolute temperature, respectively.

The full line curves in Figs. 3—5 stand for the theoretic isotherms of the collapse pressure as function of DPL content ($x_{DPL} = x_2$) for perfect mixtures in both M and C calculated by Eq. (5), by using the collapse characteristics (Table 1) of the pure monolayers.

The experimental results given in Figs. 3—5 display positive deviation from perfect behaviour, what points to an enhanced stability of the mixed films — an expression of the interactions ensuing between DPL and each of the studied xanthophylls. This observation is in accord with the results obtained by applying both the mean molecular area method and that of the free energy of mixing.

Excess Free Energy of Mixing. The excess free molar energy of mixing ΔG_M^E at the air/water interface [15—17] was calculated by:

$$\Delta G_M^E = N \int_{\pi^*}^{\pi} (A - x_1 A_1 - x_2 A_2) d\pi \quad (6)$$

where N is Avogadro's constant, π^* is a surface pressure beyond which the surface binary mixtures can be treated as a perfect two-dimensional solution and conventionally $\pi^* \simeq 0$ [16, 17], while the other magnitudes have known significance. The upper limit for the integrations may be arbitrarily selected, however it must be smaller than the one corresponding to the collapse of each pure component. The values ΔG_M^E were outright graphically determined from the compression isotherms for the pure and mixed monolayers, taking as superior integration limit the same values of surface pressure for all the three systems investigated, namely, DPL — zeaxanthin (Fig. 6), DPL — β-cryptoxanthin (Fig. 7) and DPL — lutein (Fig. 8).

It is found from Figs. 6—8 that the ΔG_M^E values are negative in all the investigated DPL—xanthophyll systems and their absolute value increases with enhancing surface pressure, being approximately twice higher in presence of zeaxanthin (Fig. 6) or lutein (Fig. 8) than the corresponding values in presence of β-cryptoxanthin (Fig. 7). The $|\Delta G_M^E|$ values as function of the film composition show a maximum at DPL molar fractions ranging between 0.25—0.5. These results are in general accord to the previously obtained ones by collapse pressure method (Fig. 3, 5). The enhanced collapse pressures in mixed monolayers of DPL: zeaxanthin and DPL: lutein as well as the negative values of the excess free energy of mixing point to a high stability of the mixed films and to stronger interactions than in a perfect mixture.

The three xanthophylls gave qualitatively similar results, the differences in behaviour of the mixtures of DPL and xanthophyll are owed to the dif-

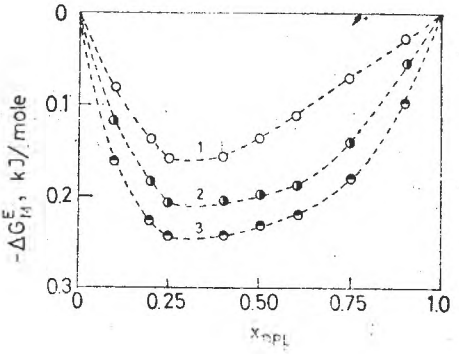

Fig. 6. Excess free energy of mixing, ΔG_M^E, for the DPL-zeaxanthin mixtures, at three values of the surface pressure: 5 mN/m (Curve 1), 15 mN/m (curve 2) and 30 mN/m (Curve 3).

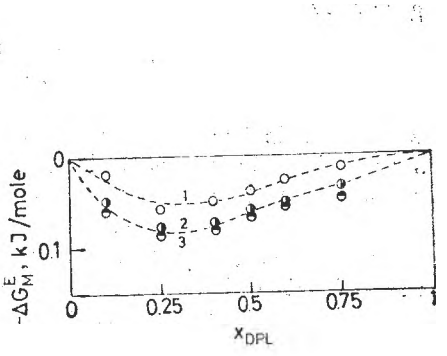

Fig. 7. Excess free energy of mixing for DPL- β-cryptoxanthin mixtures (Symbols as in Fig. 6).

ferent chemical structures of xanthophylls namely the bipolar nature of zeaxanthin and lutein as well as to the presence of an α-ionone ring in the xanthophyll structure of lutein.

In a first approximation the deviation of the surface DPL and xanthophyll solution from perfect behaviour could be interpreted in terms of certain special molecular mechanisms of packing in the mixed films of DPL — β-cryptoxanthin, DPL — zeaxanthin and DPL — lutein, which entail enhanced dispersive interactions.

Besides these hydrophobic interactions the rôle of specific polar interactions, such as ion-dipole interaction between hydroxyl group of xanthophyll and the phosphate group of DPL, probably leading even to formation of hydrogen bridges, seems to be very likely. The idea of hydrogen bridge formation between the air phase hydroxyl groups of two xanthophyll molecules is also suggested by the above mentioned difference between the behaviour of the bipolar xanthophylls, as compared to β-cryptoxanthin. This dimerization may be imaged in two different ways, namely a "head-to-head" association, with a common molecular plane for both molecules, and a "lateral" association, with

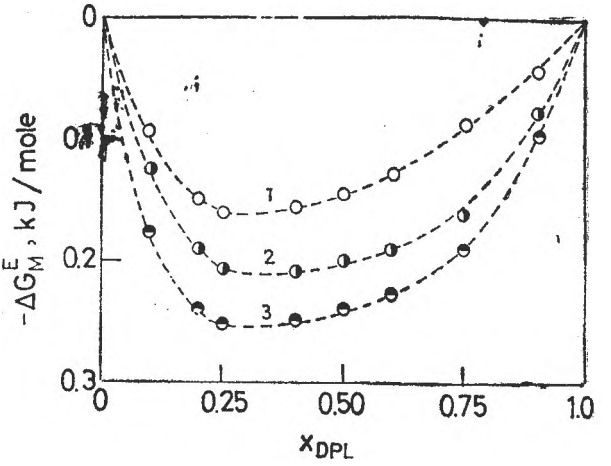

Fig. 8. Excess free energy of mixing for DPL-lutein mixtures (Symbols as in Fig. 6).

molecular planes in parallel, involving enhanced dispersive interactions. The former leads to the expansion of the film, the latter to a condension. It is worth mentioning, that in our previours paper [1] higher A_0 values were obtained in pure monolayers of bipolar xanthophylls than expected on the basis of molecular models and this behaviour was attributed to a dimerization (of the type "head-to-head"). Results presented in the present paper suggest a "lateral" dimerization. One might presume, that the prevalence of the "lateral" dimerization could be due to the presence of the phospholipid since with this kind of association two adjacent hydroxyl groups appear, allowing the dimer and phosphatidyl group of the lipid to interact more strongly. This could account for the higher condensing effect, higher excess free energies and higher deviations from the perfect behaviour in the case of both zeaxanthin and lutein, as compared to β-cryptoxanthin, having no air phase hydroxyl group.

REFERENCES

1. E. Chifu, J. Zsakó, and M. Tomoaia-Cotişel, *J. Colloid Interface Sci.*, **95**, 346 (1983).
2. M. Tomoaia-Cotişel, and E. Chifu, *J. Colloid Interface Sci.*, **95**, 355 (1983).
3. O. Isler, *„Carotenoids"*, Birkhäuser Verlag, Basel-Stuttgart, 1971.
4. M. Tomoaia-Cotişel, J. Zsakó, and E. Chifu, *Ann. Chim. (Rome)*, **71**, 189 (1981).
5. G. L. Gaines, Jr., *„Insoluble Monolayers at Liquid-Gas Interfaces"*, Interscience, New York, 1966.
6. J. T. Davies, and E. K. Rideal, „Interfacial Phenomena", 2nd. ed. Academic Press, New York, 1963.
7. R. Almog, and D. S. Berns, *J. Colloid Interface Sci.*, **81**, 332 (1981).
8. D. O. Shah, *J. Colloid Interface Sci.*, **32**, 577 (1970), **37**, 744 (1971).
9. D. A. Cadenhead, and F. Müller-Landau, *J. Colloid Interface Sci.*, **78**, 269 (1980).
10. R. Defay, I. Prigogine, A. Bellemans, and D. H. Everett, *„Surface Tension and Adsorption"*, Longmans, Green, London, 1966.
11. M. C. Phillips, and P. Joos, *Kolloid-Z. Z. Polym.*, **238**, 499 (1970).
12. M. Nakagaki, and N. Funasaki, *Bull. Chem. Soc. Japan.*, **47**, 2094 (1974).
13. P. Joos, *Bull. Soc. Chim. Belg.*, **78**, 207 (1969).
14. M. Tomoaia-Cotişel, E. Chifu, and J. Zsakó, *Colloids and Surfaces*, **14**, 239 (1985).
15. F. C. Goodrich, *„Proceedings Second International Congress Surface Activity"*, vol. 1, Butterworths, London, 1957, p. 85.
16. I. S. Costin, and G. T., Barnes, *J. Colloid Interface Sci.*, **51**, 106 (1975).
17. K. Fukuda, T. Kato, S. Machida, and Y. Shimizu, *J. Colloid Interface Sci.*, **68**, 82 (1979).

STUDIA UNIV. BABEŞ—BOLYAI, CHEMIA, XXXI, 2, 1986

INSOLUBLE MIXED MONOLAYERS

IV. Ejection Curves of β-Cryptoxanthin Palmitate — Egg Lecithin Films at the Air/Water Interface

EMIL CHIFU*, JÁNOS ZSAKÓ* and MARIA TOMOAIA-COTIŞEL*

Received: November 10, 1986

ABSTRACT. — Ejection curve, i.e. collapse pressure *vs.* A/x_1 plots are given for β-cryptoxanthin palmitate (CP) — egg lecithin (EL) binary mixed monolayers, spread at the air/water interface (x_1 stands for the molar fraction in the monolayer, before collapse, for the surfactant with higher collapse pressure and A is mean molecular area.). Theoretical ejection curves are constructed, by using the regular solution approximation and the phase diagram calculated from interaction parameters derived earlier for the studied surfactants. These curves are compared with the experimental ones and conclusions are drawn concerning: miscibility of the surfactants in the collapsed bulk phase, nature of collapse equilibria and area necessity of the collapsed bulk phase.

Introduction. By spreading a mixture of two insoluble surfactants at a gas/liquid interface, a monolayer (M) is obtained, which may consist of one or two phases, depending on the miscibility of the surfactants in the monolayer. If they are completely miscible, a single monolayer phase results, if they are immiscible, two pure monolayer phases appear. In the case of partial miscibility, one or two mixed monolayer phases are formed, depending on the composition of the mixture.

The compression of the monolayer/monolayers leads to a given surface pressure (π), which will be referred to as collapse pressure (π_c), to the ejection of a collapsed bulk phase (C) forming or a polylayer, or a lens floating on the liquid surface, if the surfactant is liquid at the working temperature, or a crystalline aggregate if it is solid. C may consist of a pure component, or it can be a mixture, depending on the miscibility of the surfactants in C. Consequently, the ejected material may form a single collapsed bulk phase (pure or mixed one), and in the case of immiscibility or partial miscibility two C phases (pure or mixed ones).

Generally, at the collapse of monolayers a thermodynamic equilibrium between the monolayer/monolayers and the collapsed bulk phase/phases is presumed, or at least a metastable equilibrium of the monolayer/monolayers with the freshly collapsed bulk phase/phases.

By taking into account the "two-dimensional phase rule" [1—3], one can give the possible types of phase diagrams, representing at constant temperature and external pressure the composition of the equilibrium phases (M and C ones) as function of the surface pressure. These diagrams were given in our previous paper [4].

* *University of Cluj-Napoca, Faculty of Chemical Technology, 3400 Cluj-Napoca, Romania*

The main experimental method in determining these phase diagrams is the measurement of π as function of the mean molecular area $A = \mathbf{A}/(N_1 + N_2)$, where **A** stands for the area of the surface, N_1 and N_2 represent the number of molecules of surfactants 1 and 2, respectively. The graphical plot of π *vs.* A, calles compression isotherm, allows us to determine π_c and the collapse area (A_c) as the co-ordinates of the point where a sudden slope change of the curve is observed at high surface pressures, marking the appearance of the collapsed bulk phase. The compression isotherms recorded for different compositions of the monolayer are very close to each other and even may be partially overlapped. Therefore, it seems to be useful to make a plot of π *vs.* $A/x_1^{oM} = \mathbf{A}/N_1$, where x_1 stands for the molar fraction of surfactant 1 in the initially spread M, by presuming component 2 to be more easily collapsable than 1, i.e. if $\pi_{2c} < \pi_{1c}$ where π_{1c} and π_{2c} stand for the collapse pressure of the pure monolayers, containing only surfactants 1 and 2, respectively [1]. These π *vs.* A/x_1^{oM} plots will be referred to as ejection curves.

In the present paper the ejection curves of β-cryptoxanthin palmitate (CP) — egg lecithin (EL) monolayers are recorded and discussed.

Materials and Methods. The monolayers of the pure components and of the mixtures were studied at the air/water interface by means of compression isotherms. The surface pressures were determined by the Wilhelmy method, as reported earlier [5, 6].

Commercial benzene of p.a. purity (Reactivul, Bucharest) was used as spreading solvent. Bidistilled water served as subphase.

The compression of the monolayer was begun after a waiting time of about 2—10 min, with a compression speed of about 0.02—0.09 nm^2 molecule^{-1} min^{-1}. Measurements were carried out at room temperature (22 ± 2°C). The experimental points given in Fig. 1 are the arithmetical mean obtained from at least 10 isotherms recorded under identical conditions.

All monolayers were spread at the same initial molecular area of about 1.3 nm^2 molecule^{-1}.

CP was a natural product [6] and EL a natural commercial product [7]. During the experiments the purity of the surfactants was tested by means of thin-layer chromatography and by spectrophotometry and no degradation was observed.

Results and Discussion. Since $\pi_{EL} > \pi_{CP}$, EL is taken for component 1. The ejection curves are visualized in Fig. 1. The main characteristic of the system studied is the dependence of π_c on composition, i.e. $\pi_c = \pi_c(x_1^{oM})$, indicating the miscibility of surfactants in M. At high π values, all curves have a linear portion up to π_c, corresponding to a liquid condensed state. The dashed straight lines in Fig. 1 have been calculated from the surface characteristics of the pure components, given in Tab. 1.

Table 1

Surface characteristics of the pure components

Surfactant	i	π_c mN/m	A_{ic} nm²/molec.	A_{i0} nm²/molec.
EL	1	42.5	0.54	0.92
CP	2	28.0	0.44	0.83

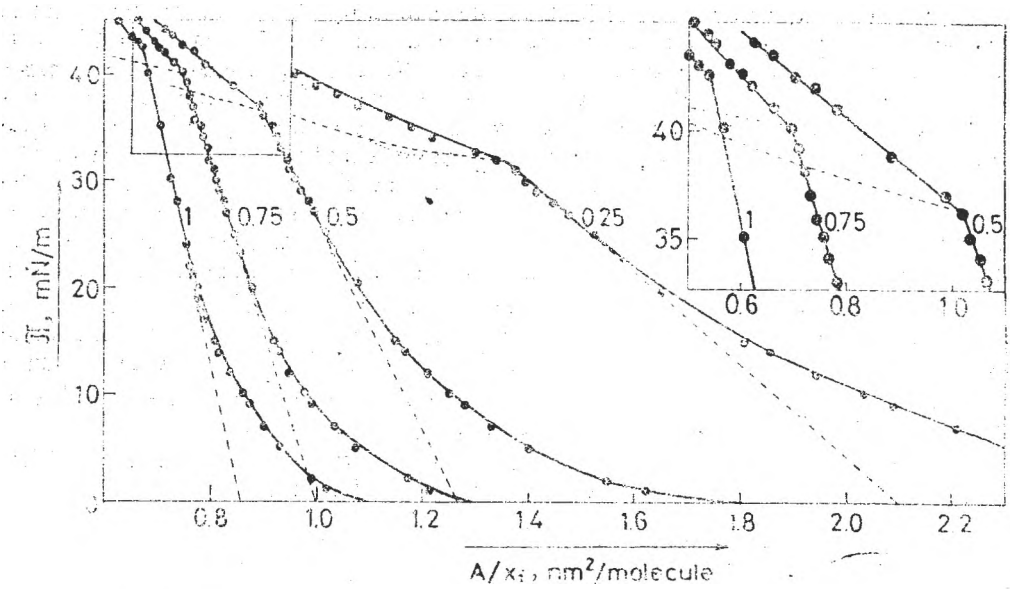

Fig. 1. Ejection curves of CP—EL mixed monolayers. The figures beneath the curves indicate x_1^{oM}, denoted on the abscissa simply by x_1. Full line curves: obtained experimentally. Dashed line curves: Calculated by means of Eqs. (2) and (12) for mM—mC system. Dotted line curves: Calculated by means of Eq. (19) for mM - iC system.

Since the limiting molecular areas A_{i0} are obtained by extrapolating the linear portion of the isotherm to $\pi = 0$, the equation of the straight line can be given as

$$A_i = A_{i0} - \pi \frac{A_{i0} - A_{ic}}{\pi_{ic}} \tag{1}$$

By presuming for the mixed films the additivity of areas, the equation of the linear portion will be

$$A = x_1^{oM}\left[A_{10} - \pi\frac{A_{10} - A_{1c}}{\pi_{1c}}\right] + (1 - x_1^{oM})\left[A_{2c} - \pi\frac{A_{20} - A_{2c}}{\pi_{2c}}\right] \tag{2}$$

The dashed straight lines in Fig. 1, extrapolated to $\pi = 0$, have been calculated by means of Eq.(2) and by using the characteristics given in Tab. 1. As seen, in the surface pressure region between 21 mN/m and π_c, practically the experimental points are situated on these straight lines.

At the collapse of the mixed film, the ejected bulk phase may be a pure component (mM-iC system, the surfactants being miscible in M and immiscible in C), or a mixed phase (mM—mC system, the surfactants being completely miscible both in M and in C). In the latter case the ejected phase must be richer in the more easily collapsable component than the remaining M. In both cases the gradual increase of the equilibrium pressure is expected, in agreement with the experimental results. If the components were immiscible in the bulk, there would be mixed monolayers having a collapse pressure greater than

π_{1c}. In this case the maximum collapse pressure (corresponding to the concollapse, i. e. to the equilibrium of M with two pure C phases), could reach even 44 mN/m, as calculated from the surface characteristics of the pure components and by using the relation given for perfect systems for mM — iC in our previous paper [4]. According to our compression isotherms, at all compositions one has $\pi_{1c} > \pi_c > \pi_{2c}$, i.e. the components seem to be totally miscible both in M and C.

The experimental π_c *vs.* x_1 curve of the studied system can be well described by means of the theory of regular solutions, as shown earlier [8]. The hypothesis that the surfactants form regular solutions in both M and C, allowed us to derive interaction parameters, equal to $\xi^C = -1.73$ and $\xi^M = -2.65$, respectively. By using these interaction parameters, a phase diagram can be given, containing π_c as function of x_1^M(monolayer curve) and π_c as function of x_1^C(bulk curve). Both curves calculated are given in Fig. 2.b. For the sake of comparison, the same figure also contains the equilibrium curves calculated for a perfect system ($\xi^M = \xi^C = 0$), having the surface characteristics of the substances studied.

Concerning the collapse equilibria during the ejection of the new phase, we used the following model:

At the compression of the monolayer corresponding to $x_1^M = x_1^{oM}$, the $\pi_c(x_1^{oM})$ being reached, the collapsed bulk phase appears and an equilibrium is established at $\pi = \pi_c(x_1^{oM}) + \Delta\pi$. The composition of the equilibrium phases can be characterized by the mole fractions x_1^{1C} and x_1^{1M} corresponding to $\pi_c + \Delta\pi$ on the phase diagram, respectively. According to the lever rule:

$$N^C(x_1^{oM} - x_1^{1C}) = (N - N^M)(x_1^{oM} - x_1^{1C}) = N^M(x_1^{1M} - x_1^{oM}) \qquad (3)$$

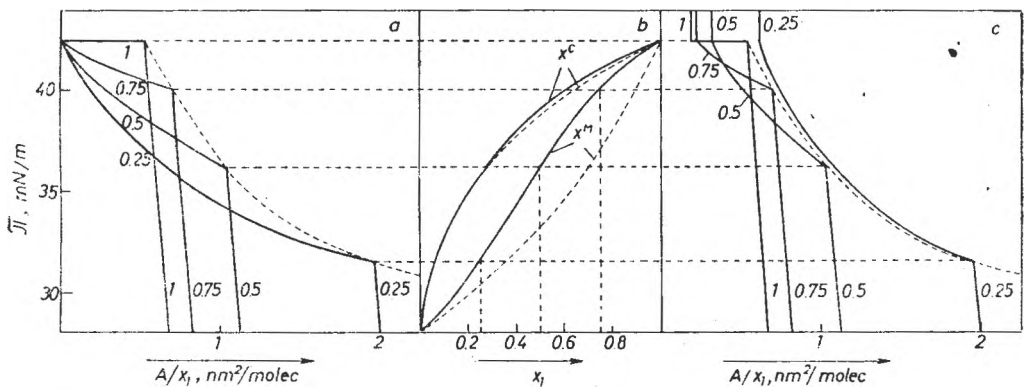

Fig. 2. Theoretical ejection curves and phase diagrams for CP—EL mixed monolayers: a — Ejection curves calculated in aproach 1, by means of Eqs. (2) and (11) for regular solutions; b — Phase diagrams. Full lines: calculated for regular solutions with $\xi^C = -1.73$ and $\xi^M = -2.65$. Dashed lines: calculated for perfect solutions; c — Ejection curves calculated in approach 2, by means of Eqs. (2) and (12) for regular solutions. In *a* and *c*: Figures beneath the curves indicate x_1^{oM}, denoted on the abscissa simply x_1. Dashed line curves are the collapse pressure curves, calculated by means of Eq. (15).

where N^C and N^M stand for the overall number of surfactant molecules in C and M respectively, i.e.

$$N^M/N = (x_1^{oM} - x_1^{1C})/(x_1^{1M} - x_1^{1C}) \tag{4}$$

As the area necessity of the collapsed bulk phase, A^C, is concerned, two approximations will be used, viz.

Approach 1: A^C is neglectingly small as compared to A^M. Consequently, the mean molecular area can be given as

$$A^{(1)} = AN^M/N \tag{5}$$

Concerning the partial molecular areas, we shall presume $A_2 = A_{2c}$, since $\pi > \pi_{2c}$, and for the component 1, we shall use a relation, analogous with Eq. (1), viz.

$$A_1^0 = A_{10} - \pi \frac{A_{10} - A_{1c}}{\pi_{1c}} \tag{6}$$

From Eqs. (4), (5) and by expliciting A one obtains

$$A^{(1)} = \frac{x_1^{oM} - x_1^{1C}}{x_1^{1M} - x_1^{1C}} [x_1^{1M} A_1^0 + (1 - x_1^{1M}) A_{2c}] \tag{7}$$

Approach 2: at the collapse the formation of a trilayer is presumed. This hypothesis corresponds to a collapse mechanism proposed in the literature [9] and its validity seemes to be proved by our earlier studies concerning the kinetics of relaxation phenomena observed in apocarotenoid monolayers [10]. In this approach the mean molecular area will be equal to

$$A^{(1)'} = A^{(1)} + (A - A^{(1)})/3 \tag{8}$$

where A — means

$$A = x_1^{oM} A_1^0 + (1 - x_1^{oM}) A_{2c} \tag{9}$$

i.e. the mean molecular area which the surfactants would have at the corresponding π if the collapse did not occur.

Further, the already collapsed M is presumed not to participate to the phase equilibria and the next equilibrium is presumed to be established at $\pi = \pi_c(x_1^{oM}) + 2\Delta\pi$. In approach 1, the mean molecular area becomes

$$A^{(2)} = \frac{x_1^{oM} - x_1^{1C}}{x_1^{1M} - x_1^{1C}} \frac{x_1^{1M} - x_1^{2C}}{x_1^{2M} - x_1^{2C}} [x_1^{2M} A_1^0 + (1 - x_1^{2M}) A_{2c}] \tag{10}$$

By presuming the phase equilibrium to be established at each step equal to $\Delta\pi$, after n such steps the mean molecular area will be

$$A^{(n)} = \prod_{i=1}^{n} \frac{x_1^{(i-1)M} - x_1^{iC}}{x_1^{iM} - x_1^{iC}} [x_1^{nM} A_1^0 + (1 - x_1^{nM}) A_{2c}] \tag{11}$$

In approach 2 one has always

$$A^{(n)'} = A^{(n)} + (A - A^{(n)})/3 \tag{12}$$

The equations of the ejection curves are

$$A^{(n)}/x_1^{oM} = \prod_{i=1}^{n} \frac{x_1^{(i-1)M} - x_1^{iC}}{x_1^{iM} - x_1^{iC}} \left[\frac{x_1^{nM}}{x_1^{oM}} A_1^0 + \frac{1 - x_1^{nM}}{x_1^{oM}} A_{2c} \right] \tag{13}$$

and

$$A^{(n)'}/x_1^{oM} = A^{(n)}/x_1^{oM} + (A - A^{(n)})/3x_1^{oM} \tag{14}$$

in approaches 1 and 2, respectively.

The ejection curves constructed for $x_1^{oM} = 0.25$, 0.5, 0.75 and 1.00 by performing stepwise calculations of $\Delta\pi = 0.1$ mN/m, are given in approach 1 in Fig. 2. a, and in approach 2 in Fig. 2.c.

In these figures the dashed line curve gives the collapse pressure curve for all possible compositions, if $0.05 < x_1^{oM} < 1$. Its equation can be obtained from Eq. (7), by taking $x_1^{1M} = x_1^{oM}$ and by dividing the equation with x_1^{oM}. One obtains

$$A^{(0)}/x_1^{oM} = A_1^o - \frac{1 - x_1^{oM}}{x_1^{oM}} A_{2c} \tag{15}$$

where A_1^o is calculated by means of Eq. (6), by using instead of π the π_c value corresponding to x_1^{oM} chosen. The theoretical ejection curves obtained by means of approach 2, are also given in Fig. 1, marked by dashed lines. As seen, from the beginning of the collapse, the experimental π values are greater than the theoretical ones, but the shape of both curves is the same. Although by taking smaller $\Delta\pi$ values, the theoretical π would have a little higher values, the possibility of the overcompression of the monolayers seems to be obvious.

Since the variation of π_c with composition can also be expected if the surfactants are immiscible in C, an attempt was made to describe the π_c *vs.* x^M curve given in [8], by using the regular solution approximation for mM-iC systems [4]. The standard deviation of the experimental points from the theoretical ones was found to be minimum for $\xi^M = -0.008$, but its value is very high viz. $\Delta_m = 0.866$ mN/m, as compared to $\Delta_m = 0.169$ mN/m, obtained in the mM-mC approximation mentioned above. This argues for the miscibility of the surfactants in C. Nevertheless, the ejection curves were calculated even for the hypothetic mM-iC system. Since ξ^M has a neglectingly small value, calculations have been performed for the perfect system. At the collapse the pure surfactant 2 is ejected at the compositions considered above. Thus, one has $x_1^C = 0$ (for $x_1^{oM} < 0.8226$, the value corresponding to the concollapse) and for all $\pi > \pi_c\,(x_1^{oM})$ values the lever rule gives:

$$N^M/N = x_1^{oM}/x_1^M \tag{16}$$

where x_1^M is the value corresponding to the chosen π value in the phase diagram.

Consequently, in approach 1, the mean molecular area will be

$$A_{(i)} = \frac{x_1^{oM}}{x_1^M}\,[x_1^M A_1^0 + (1 - x_1^M)A_{2c}] \tag{17}$$

where A_1^0 is given by the same Eq. (6) up to π_{1c}, and for higher π values it is presumed to become equal to A_{1c}.

The equation of the ejection curve can be written as

$$A_{(i)}/x_1^{oM} = A_1^0 + \frac{1 - x_1^M}{x_1^M} A_{2c} \tag{18}$$

i.e. it is independent of x_1^{oM}. This means that, from the incipient collapse on, a unique curve is obtained irrespective of the initial composition of the monolayer.

By using approach 2, one obtains

$$A'_{(i)}/x_1^{oM} = A_{(i)}/x_1^{oM} + (A - A_{(i)})/3x_1^{oM} \qquad (19)$$

A having the same meaning given by Eq. (9).

The curves calculated by using Eq. (19) are given in Fig. 1 with dotted lines. As seen, the shape of these curves differ essentially both from the experimental curves and from the theoretical ones, calculated for regular mM-mC systems.

The comparison of the experimental ejection curves with the theoretical ones suggests the following main conclusions:

1. The system studied is of mM-mC type, i.e. the surfactants are totally micsible in both M and C;

2. At the compression of the monolayers the ejected phase C is not a homogeneous one, but it consists of portions of different compositions, i.e. the thermodynamic equilibrium can be presumed only between M and the just ejected portion of C;

3. The area necessity of the ejected C cannot be completely neglected and the presumption that only trilayers are actually formed seems to be reasonable as a first approach;

4. At the collapse the momentary thermodynamic equilibrium is not reached completely and slight overcompression of the monolayer occurs.

REFERENCES

1. R. Defay, I. Prigogine, A. Bellemans, and D. H. Everett, in *"Surface Tension and Adsorption"*, Longmans, Green, London, 1966, p. 81.
2. D. J. Crisp, in *"Surface Chemistry"*, Supplement to Research, London, 1949, p. 17.
3. M. C. Phillips, and P. Joos, *Kolloid–Z. Z. Polym.*, **238**, 499 (1970).
4. J. Zsakó, M. Tomoaia-Cotișel, and E. Chifu, *J. Colloid Interface Sci.*, **102**, 186 (1984).
5. M. Tomoaia-Cotișel, and E. Chifu, *Gazz. Chim. Ital.*, **109**, 371 (1979); *J. Colloid Interface Sci.*, **95**, 355 (1983).
6. E. Chifu, J. Zsakó and M. Tomoaia-Cotișel, *J. Colloid Interface Sci.* **95**, 346 (1983).
7. M. Tomoaia-Cotișel, J. Zsakó, and E. Chifu, *Ann. Chim.* (Rome), **71**, 189 (1981).
8. M. Tomoaia-Cotișel, E. Chifu, and J. Zsakó, *Colloids and Surfaces*, **14**, 239 (1985).
9. H. E. Ries, *Jr., Nature*, **281**, 287 (1979).
10. J. Zsakó, M. Tomoaia-Cotișel, I. Stan, V. Coman, V. Tămaș, and E. Chifu, *Proc. 3rd National Conference on Biophysics*, Jassy (Romania), 1985, p. 63.

ÎNTREPRINDEREA POLIGRAFICĂ CLUJ, Municipiul Cluj-Napoca, Cd. nr. 581/1987

Revista științifică a Universității din Cluj-Napoca, **STUDIA UNIVERSITATIS BABEȘ-BOLYAI,** apare începînd cu anul 1986 în următoarele condiții:

matematică — trimestrial

fizică — semestrial

chimie — semestrial

geologie-geografie — semestrial pentru geologie și anual pentru geografie

biologie — semestrial

filosofie — semestrial

științe economice — semestrial

științe juridice — semestrial

istorie — semestrial

filologie — semestrial

STUDIA UNIVERSITATIS BABEȘ-BOLYAI, the scientific journal of the University of Cluj-Napoca, starting with 1986 is issued as follows:

mathematics: quarterly

physics: biannually

chemistry: biannually

geology-geography: biannualy on geology and yearly on geography

biology: biannually

philosophy: biannually

economic sciences: biannually

juridical sciences: biannually

history: biannually

philology: biannually

43 870

Abonamentele se fac la oficiile poştale, prin factorii poştali şi prin difuzorii de presă, iar pentru străinătate prin „ROMPRESFILATELIA“, sectorul export-import presă, P. O. Box 12—201, telex. 10376 prsfir, Bucureşti, Calea Griviţei nr. 64—66.

Lei 35